IEEE Access
Multidisciplinary | Rapid Review | Open Access Journal

Received December 14, 2021, accepted January 3, 2022, date of publication January 6, 2022, date of current version January 20, 2022.

Digital Object Identifier 10.1109/ACCESS.2022.3140587

Analysis of Microgrid's Operation Integrated to Renewable Energy and Electric Vehicles in View of Multiple Demand Response Programs

HABIB UR RAHMAN HABIB[1], (Member, IEEE), ASAD WAQAR[2], MOHAMED G. HUSSIEN[3], (Member, IEEE), ABDUL KHALIQUE JUNEJO[4], (Member, IEEE), MEHDI JAHANGIRI[5], RASOOL M. IMRAN[6], YUN-SU KIM[7], (Senior Member, IEEE), AND JUN-HYEOK KIM[7], (Student Member, IEEE)

[1]Department of Electrical Engineering, Faculty of Electrical and Electronics Engineering, University of Engineering and Technology Taxila, Taxila 47050, Pakistan
[2]Department of Electrical Engineering, Bahria University, Islamabad 44000, Pakistan
[3]Department of Electrical Power and Machines Engineering, Faculty of Engineering, Tanta University, Tanta 31512, Egypt
[4]Department of Electrical Engineering, Qaid-e-Awam University of Engineering, Science and Technology, Nawabshah 67450, Pakistan
[5]Department of Mechanical Engineering, Shahrekord Branch, Islamic Azad University, Shahrekord 8816765714, Iran
[6]School of Artificial Intelligence, Wuchang University of Technology, Wuhan 430223, China
[7]Graduate School of Energy Convergence, Gwangju Institute of Science and Technology (GIST), Gwangju 61005, South Korea

Corresponding author: Yun-Su Kim (yunsukim@gist.ac.kr)

This work was supported by the Institute of Information & communications Technology Planning & Evaluation (IITP) grant funded by the Korea government Ministry of Science and Information & Communication Technology (MSIT) (2021-0-02068, Artificial Intelligence Innovation Hub) and the Korea Institute of Energy Technology Evaluation and Planning (KETEP) and the Ministry of Trade, Industry & Energy (MOTIE) of the Republic of Korea (No. 20204010600340).

ABSTRACT A suitable energy management scheme and integrating renewable energy resources (RERs) can significantly increase energy efficiency and the stability of future grids operation. This work modeled a household energy management comprising a microgrid (MG) system and demand response programs (DRPs). Residential loads with price-based tariffs are introduced to reduce peak load demands and energy costs. For incorporating the uncertainties in RERs, their stochastic nature is modeled with a probabilistic method. This paper proposes a joint optimization approach for the optimal planning and operation of grid-connected residential, rural MG integrated into renewable energy and electric vehicles (EVs) in view of DRPs. The investigation focuses on energy saving of residential homes under different DRPs and RERs integration. The EVs are integrated into MG by including photovoltaic (PV), wind turbine (WT), fuel cell (FC), and diesel engines (DEs). A multi-objective optimization problem has been formulated to minimize the operating cost, pollutant treatment cost, and carbon emissions cost defined as C1, C2, and C3, respectively. The load demand has been rescheduled because of three DRPs, i.e., critical peak pricing (CPP), real-time electricity pricing (RTEP), and time of use (TOU). Further, the EV load has also been analyzed in autonomous and coordinated charging strategies. Using a judgement matrix, the proposed multi-objective problem is transformed into a single-objective problem. The results of an artificial bee colony (ABC) algorithm are compared with the particle swarm optimization (PSO) algorithm. The simulation analysis was accomplished by employing ABC and PSO in MATLAB. The mathematical model of MG was implemented, and the effects of DRPs based MG were investigated under different numbers of EVs and load data to reduce different costs. To analyze the impact of DRPs, the residential, rural MG is implemented for 50 homes with a peak load of 5 kW each and EV load with 80 EVs and 700 EVs, respectively. The simulation results with different test cases are formulated while analyzing the tradeoff between ABC and PSO algorithms. The simulation analysis shows that multiple DRPs, EVs, and RERs offered a substantial trade-off.

INDEX TERMS Demand response programs (DRPs), distributed generations (DG), electric vehicles (EVs), joint sequential optimization, multi-objective optimization, residential microgrids.

The associate editor coordinating the review of this manuscript and approving it for publication was Alexander Micallef.

NOMENCLATURE

Subscripts:

ABC	Artificial bee colony.
BBSA	Binary BSA.
BSA	Backtracking search algorithm.
BSS	Battery storage system.
CCP	Chance constraints programming.
CPP	Critical peak pricing.
DEs	Diesel engines.
DERs	Distributed energy resources.
DG	Diesel generator.
DGs	Distributed energy generations.
DOD	Depth of discharge.
DRPs	Demand response programs.
DSM	Demand-side management.
EMA	Exchange market algorithm.
EMS	Energy management system.
ESRMC	Energy and spinning reserve market clearing.
ESS	Energy storage system.
EVs	Electric vehicles.
FC	Fuel cell.
GA	Genetic algorithm.
GAMS	General algebraic modeling system.
GHG	Greenhouse gas.
GSA	Gravitational search algorithm.
HES	Hybrid energy system.
HOMER	Hybrid optimization of multiple energy resources.
LCOE	Levelized cost of energy.
LPSP	Loss of power supply probability.
LSA	Lightning search algorithm.
MBAT	Modified bat algorithm.
MILP	Mixed integer linear programming.
MIP	Mixed-integer programming.
MOPSO	Multi-objective PSO.
MPGSA	Multi-period GSA.
MPSO	Modified PSO.
MT	Micro-turbine.
NPC	Net present cost.
NREL	National renewable energy laboratory.
OPF	Optimal power flow.
PDFs	Probability density functions.
PFs	Participation factors.
PQ	Power quality.
PSO	Particle swarm optimization.
PV	Photovoltaic.
RERs	Renewable energy resources.
RO	Robust optimization.
RTED	Real-time economic dispatch.
RTEP	Real-time electricity pricing.
SA	Simulated annealing.
SG	Smart grid.
SNO	Social network optimization.
SPEA	Strength Pareto evolutionary algorithm.
TOU	Time of use.
TS	Tabu search.
V2G	Vehicle-to-grid.
WGA	Wild goat algorithm.
WT	Wind turbine.

Superscripts:

m	Type of DER.
t	Index for a time interval.
x	Type of dispatch-able DG (MT, DE).

Parameters and Constants:

C_{gas}	Gas price in PKR/m^3.
L_{gas}	Low-hot value of gas in kWh/m^3.
C_D	Diesel price in PKR/litre.
$k_{OM,x}$	Maintenance cost of x^{th} DG unit in PKR/kWh.
$C_s(t)$	Selling price in PKR/kWh at time t.
$C_b(t)$	Buying price in PKR/kWh at time t.
ρ_m	Initial investment cost of m^{th} DG in PKR/kW.
ζ_x (min)	Minimum power limit of x DG.
ζ_x (max)	Maximum power limit of x DG.
γ_C (max)	Maximum charging rate coefficient of BSS.
γ_D (max)	Maximum discharging rate coefficient of BSS.
SOC	State of charge.
η_C	Charging efficiency of BSS.
η_D	discharging efficiency of BSS.
Δt	Time interval of 1 hour.
γ_x	Emission coefficient of pollutant from x^{th} DG.
γ_g	Emission coefficient of pollutant from the grid

Functions and Variables:

P_{PVr}	PV rated power output.
I_{cp}	Certain solar irradiation point.
I_{sv}	Standard solar irradiation value.
A, B, C	Windpower constants.
V_i	Cut-in wind speed.
V_o	Cut-out wind speed.
V_{Wr}	Rated wind speed.
P_{WTr}	Wind turbine rated power output.
P_{MT}	Rated power capacity of MT.
$P_{DG}(t)$	Power capacity of DE generator at t.
$\sigma_L(t)$	Standard deviation.
$\mu_L(t)$	Average load demand.
L(t)	Total load for all consumers during time interval t.
F_0, F_1	Coefficients of fuel consumption curve fitting.
F_C, C_E	Objective functions for total annualized cost and emission.
ω_w	Weighting factor.
λ_s	Scaling factor.

C_C	Total annual capital cost of all DERs.
C_{OM}	Total annual operation & maintenance cost of all DERs.
$C_O(t)$	Total operation cost of a microgrid at time t.
$C_x(t)$	Power generation cost of x^{th} DG unit at time t.
$P_x(t)$	Power generation of x^{th} DG unit at time t.
$P_s(t)$	Selling power at time t.
$P_b(t)$	Buying power at time t.
Ω_m	Total capacity of m^{th} DG.
$P_{PV}(t)$	Solar power generation at time t.
$P_{WT}(t)$	Wind power generation at time t.
$P_{Ld}(t)$	Total load demand at time t.
$P_B(t)$	Battery charging power at time t.
$P_D(t)$	Battery discharging power at time t.
n_m	Actual number of m^{th} DER.
n_x	Actual number of x^{th} DER.
Ω_{BSS}	Total capacity of BSS.

I. INTRODUCTION

A rapid increase in global energy demand requires further distributed energy generation with the existing fossil fuels-based conventional generation. Fossil fuel-based generation leads to other acute challenges in terms of global warming and environmental pollution. However, microgrid (MG) based distributed and hybrid energy generation systems are less dependent on fossil fuels based power generations. MG can partially handle the environmental issues to fulfill the increasing load demand locally with different distributed generations (DGs). These DGs include solar photovoltaic (PV), wind turbines, fuel cells, micro-turbines, and diesel generators [1], [2].

MG modes for power generations play a prominent role in a smart grid (SG) environment. In general, there are two modes of MG, namely grid-tied and standalone. MG power generation is mostly dependent on intermittent-based renewable energy resources (RERs). The MG central control system effectively handles the uncertain nature of load demands and RERs power generation by managing and controlling all MG unit operations. Various benefits can be achieved with the help of optimal MG operations under SG environment, such as improved reliability, higher operation flexibility, peak shaving, lower energy cost, load balancing, auto control operation, protection, integrated EMS operation, matching load-generation capacity, minimum pollution, and improved power quality (PQ) [3]–[5]. Due to the inclusion of shiftable loads, MGs can apply demand response programs (DRPs) for balancing the system loads [6], [7]. Therefore, optimal scheduling and sizing problems are taken as critical issues. Moreover, the availability of RERs and their operation uncertainty have placed complex challenges for optimal operation [8], [9], which must be considered at the designing stage; so that the overall system can work properly. Different research articles with different strategies have been published on different scenarios of the problem with DRPs. Table 1 shows the comparison of different methods with related literature.

Various articles have been published on new heuristic methods. A discrete harmony searching technique was proposed in [20] to manage a PV-WT-BSS-DG hybrid model. A hybrid SA-TS algorithm was implemented in [21] to handle optimal configuration challenges. Reference [22] utilized MPSO to optimize the hybrid energy system (HES). A new two-layer iterative algorithm implemented the optimal allocation of grid-tied HES [23]. The first layer was implemented for RERs optimization, and the second layer was considered for optimal BSS capacity. In [24], SNO for optimal controller training of rule-based standalone HES was obtained. The authors in [25] introduced a double loop two-level hybrid technique with multiple heuristic optimization techniques for optimally allocated switching capacitors and reactive power managing. The multi-objective adaptive evolutionary technique is proposed in [26] for optimal allocation of hybrid PV-WT-BSS-DG system. Moreover, WGA-EMA with parallel processing quality is implemented in [27] for dynamically reconfiguring the MGs and distribution networks. In [28], novel multi-layer optimization with a time-dependent price algorithm is proposed for optimal sizing and planning of residential MGs to minimize energy costs.

Different software tools were used for MG optimization and EMS. HOMER was utilized in [29] for optimal allocation and size optimization of MG components. Moreover, techno-economic size optimization of islanded MG was implemented in [30] with the help of HOMER and GAMS software tools. Some articles used deterministic and mathematical methods rather than heuristic algorithms. The authors in [31] proposed a novel deterministic optimization technique for size optimization of hybrid PV-WT-DG model. In [32], the MIP-based optimization method for MG planning was implemented to minimize risk in profit. Reference [33] used a new deterministic method by incorporating LCOE and LPSP for size optimization of the standalone PV-WT model. The authors in [34] proposed two-level predictive EMS with MILP for standalone MG. The first level was used for unit commitment, and the second level was implemented to regulate real-time MG operation.

The objective function selection is another critical problem that must be efficient and suitable to optimize sizes and allocation. Reference [21] uses size optimization's objective function to minimize the total MG energy cost. The objective function of hybrid MG is to minimize LCOE and LPSP while maximizing the RERs penetration [26]. The authors in [33] claimed optimal sizing to minimize investment costs with higher reliability. The authors in [35] introduced a novel smart scheme for size optimization and energy trading of standalone MGs clusters. Significant profit allocation for MG owners with enhanced overall system reliability are the main objectives of this study.

Various factors influence the MG performance in size optimization and allocation, such as DRPs, ESS, major uncertainties, and environmental challenges. Few articles have discussed the impact of these factors on MGs size optimization. The authors in [21] introduced RERs intermittency

TABLE 1. Comparative analysis of different methods with related literature studies.

Ref.	Algorithm	MG components	Contributions	Limitations
[10]	PSO	PV-WT-BSS	Optimal allocation and DERs capacity with ESS.	More computation time, premature convergence to a local optimum solution.
[11]	MOPSO	PV-WT-BSS	Reduction in operating cost with maximum MG revenue.	A bidirectional operation to ensure higher reliability.
[12]	GA	PV-WT-CHP	GA in energy management improved the ability for MG optimal scheduling.	Multiple sets of the parameter are required for GA.
[13]	MPGSA	PV-WT-BSS	MPGSA with EMS addressed the optimal operation of standalone MG while minimizing the production cost and enhancing efficiency.	Higher DOD causes fast ESS degradation with reduced life.
[14]	MBAT	PV-WT-MT-FC-BSS	Grid-tied MG with EMS and different PV irradiances for the optimal scheduling with lower computation time than GA/PSO.	Single loads are investigated without DE emission cost.
[15]	CCP	PV-WT-DE-BSS	Day-ahead scheduling with a three-level system for MG clusters was considered with ESS degradation cost.	DE emission cost and uncertain nature of load are not included.
[16]	MPSO	PV-WT-CHP	Optimal power-sharing with minimum LCOE and uncertain nature of load are considered.	BSS and DE are not included.
[17]	BBSA	PV-WT-DE-FC-BSS	Optimal scheduling with reduced power generation cost/losses and improved power-saving and reliability.	BSS charging and discharging scenarios are not investigated.
[18]	RO-GAMS	PV-WT-BSS	Optimal sizing of standalone MG with shiftable DRPs. RERs uncertainty was applied with RO.	Grid-connected operation and EVs load are not considered. Only one DRP is considered.
[19]	LSA	PV-WT-DE-BSS	LSA to design an optimized controller for handling MG uncertainties with optimum power delivery and minimum cost. A modified IEEE 14-bus test system is used. More effective as compared to recently developed BSA. Minimum operating cost and solution of complicated constraints are considered.	DRPs and EVs load are not considered.

with sensitivity study on different case scenarios. In [36], optimization of a single objective function was used to find the optimal sizes of the MG components. Probability density functions (PDFs) were also used to incorporate RERs intermittency while finding the optimal sizes of the DGs. Reference [37] used deterministic uncertainty sets rather than PDFs to optimize MG sizes and placement. HES with a new techno-economic approach is implemented in [38] for the MG system designing. Load shifting scheme with priority load scenarios was used, and their impact on MG sizing was investigated. Reference [30] used DRPs for the cost reduction and improvement of the MG sizing method. In [39], the impact of DRPs and environment on optimal sizing was analyzed. This paper's uncertain nature of RERs and loads was not investigated. Moreover, twenty-four (24) hours' time steps were considered with yearly samples of RERs and loads. The authors in [29] investigated DERs combinations by utilizing the HOMER tool. Moreover, GHG emission was also considered in this study. Similarly, reference [31] investigated the impact of ESS on MG sizing. It was shown that BSS installation to a standalone HES reduced the investment cost.

In [40], the authors replaced the conventional method, which employed RTED with 5 to 15 minutes static snapshot forecasted data, including each minute variation data of RERs and load. DGs manage power unbalancing based on "best-fit" PFs obtained from previous ED, keeping the same objective dimension by evaluating only PFs at the start. This approach is applicable for both sequential and dynamic variability. Two test systems are used for the verification of the proposed scheme. The authors in [41] proposed SPEA 2+ for bi-objective (total cost and system risk) ESRMC scheme for wind-thermal systems with two market models: thermal alone and thermal DGs with demand. Weibull PDF is employed for handling the stochastic nature of wind, while normal PDF is used for load. IEEE 30 bus system is validated with the proposed scheme. In [42], stochastic optimization technique is proposed for voltage and VAR control with OPF under variable loads and uncertainty of RERs. The proposed method is validated on a 24 bus system. In [43], the authors proposed an integrated optimal and dynamic fast and slow reserve action plan during emergency conditions of line interruption or/and load demand increment. The three sources of reserves are considered: conventional DGs, hydro, and load. The proposed schemes are tested on IEEE 30, 57, and 300 bus systems while implementing GA, MATLAB, and GAMS.

By summarizing the above literature work, the following observations regarding limitations in literature studies are observed:

- Grid-connected operation and EVs load are not considered. Only one DRP is considered [18].
- DRPs and EVs load are not considered [19].
- BSS charging and discharging scenarios of EVs are not investigated [17].
- BSS of EVs and DE are not included [16].
- DE emission cost and uncertain nature of load are not included [15].
- Single loads are investigated without DE emission cost [14].

This paper proposes a joint optimization approach for the optimal planning and operation of grid-connected residential PV-WT-FC-DE based community rural microgrid (MG) integrated into EVs in view of multiple DRPs. A multi-objective

optimization problem has been formulated to minimize the operating cost (C1), pollutant treatment cost (C2), and carbon emissions cost (C3). The load demand has been rescheduled in view of three DRPs such as CPP, RTEP, and TOU. Moreover, the EV load has also been analyzed in autonomous and coordinated charging strategies. The suggested multi-objective optimization problem is transformed into a single objective problem using a judgement matrix, and the results of the ABC algorithm are compared with the PSO algorithm. To analyze the impact of DRPs, the residential community rural MG is implemented for 50 homes with a peak load of 5 kW each and EV load of 80 EVs and 700 EVs, respectively. The main contributions of this paper can be summarized as:

- Comparison of two heuristic algorithms under three DRPs.
- Analysis in grid-connected MG increases the complexity of the optimization problem. However, the authors in recent literature mostly considered the islanded MG cases.
- Consideration of RERs uncertainty and DRPs by employing ABC and PSO algorithms. However, literature studies lack: (1) the consideration of RERs uncertainty and DRPs, (2) grid-connected EVs integrated residential PV-WT-MT-DE based community rural microgrid (MG) by employing single-objective problem using ABC and PSO algorithms [44]–[57].
- Analyzing tradeoff perspectives between two heuristic algorithms with load rescheduling as the major part of three DRPs.
- Investigating EVs load with autonomous and coordinated charging scenarios.
- Rescheduling the load demand based on different tariffs as DRPs and economic dispatch (ED) by considering optimal sizing as DSM.
- For incorporating the uncertainties in RERs, their stochastic nature is modeled with a probabilistic method.

The rest of the paper is organized as follows. Section II involves modeling of the studied MG system, in which the role of ABC and PSO algorithms is explained. The solution steps for applying ABC and PSO algorithms are also explained. Modeling of RERs uncertainty, WT, PV, load demand, fuel cell, and the diesel generator is also part of this section. Problem formulation is explained in Section III, which includes objective functions, and constraints. Section IV highlights all test cases which are analyzed in this paper. Simulation data for the study system is mentioned in Section V which includes unscheduled summer load, scheduled (summer and winter) loads with (CPP, RTEP, and TOU) tariffs. Section VI analyzes the results with discussion. Comparison between PSO and ABC for (summer and winter) loads with (unscheduled, CPP, RTEP, and TOU) tariffs during autonomous and coordinated modes of 80 EVs and 700 EVs, respectively are explained in detail. Section VII presents critical analysis and discussion. The conclusion is given in Section VIII.

II. MODELING OF THE STUDIED MICROGRID SYSTEM

Fig. 1 shows the schematic configuration of the rural community microgrid under study. The initial data and components of the microgrid model under study are taken from the base papers [57], [58]. The details of the studied system can be seen from the base papers. ABC and PSO algorithms are not planning tools. They are metaheuristic algorithms used to solve the multi-objective optimization problem. This paper analyzes joint multi-objective optimization problems based on load scheduling and optimal sizing considering demand-side management (DSM). The first step involves DSM, and the second step involves optimal sizing, and it has been analyzed which algorithm (ABC or PSO) performs well for the proposed optimization problem is incorporated in this paper. Future planning also involves deciding the size and type of DG, which was emphasized in this paper. Conversion from multi-objective to single-objective is done with a judgment matrix by assigning weights, which are taken from base papers. ABC and PSO are then used for solving the optimization problem.

Moreover, the diesel generator is the normal tradition in Pakistan as the main generation source for handling the basic load demand. Hence, adding a diesel generator is a reasonable choice for the extension of the MG system by incorporating the existing DGs. The MG model is suggested for the residential, rural community load of Shah Allah Ditta of Islamabad, Pakistan. The authors in [59] used the Indian location, while this paper used the Pakistani location. In this way, we tailored the proposed problem according to our local context.

A community MG is studied in this paper formed by combining the prosumers close to serve multiple customers [49]. It may include residential customers (residential microgrid) or other community servings such as hospitals, public buildings, etc. [60].

The solution steps of applying the ABC algorithm for optimization problem are as follows:

Step1: Initializing the solutions population X, i.e., the maximum number of bees MB, total number of iterations i_{max}, the controlling parameter *limit*, lower ($X_{j,max}$) and upper ($X_{j,min}$) limits of the searching space, and random generated initial population ($X_i i = 1, 2, 3 \ldots, MB$);

Step2: Calculate the nectar value of the population through their fitness function.

Step3: Producing neighbouring solutions for the employed bees through random numbers and validating them according to step 2.

Step4: Applying the selection procedure.

Step5: Go to step 9 for distributed onlooker bees, otherwise, follow next step 6.

Step6: Calculate the probability values for the solutions.

Step7: Producing neighbouring solutions for the nominated onlooker bee, based on the value, through random numbers and applying step 2.

Step8: Applying step 4.

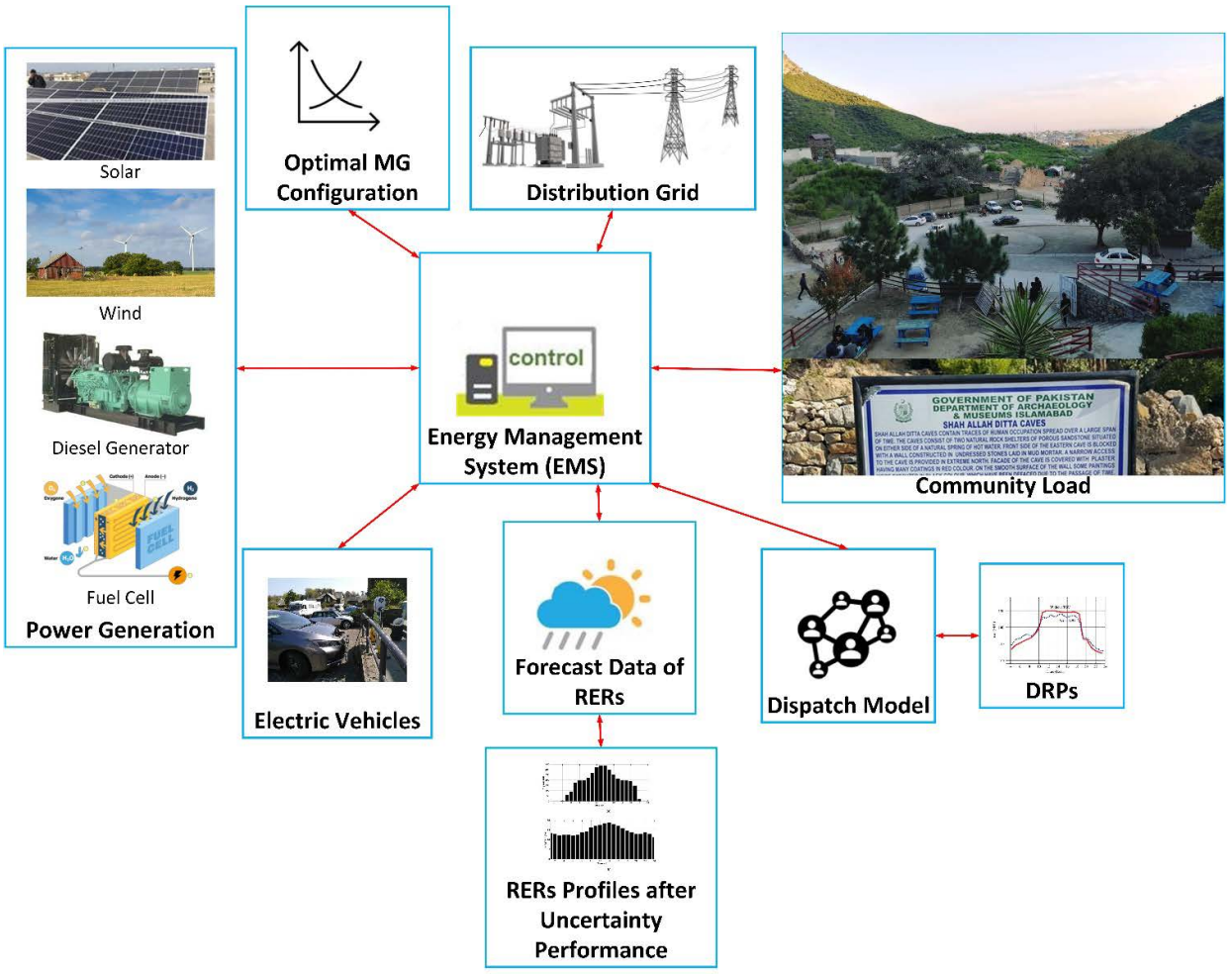

FIGURE 1. Schematic configuration of the studied rural community microgrid.

Step9: Determining the abandoned solution for the scout bees if available, and replacing it with an entirely new solution, and evaluating them according to step 2.

Step10: Save the best solution obtained so far.

Step11: Stopping and printing results if the maximum number of iterations is reached. Otherwise, repeat step 3.

The PSO process for solving the optimization problem is as follows:

Step1: Start initialization of the swarm with its velocity and position, coefficients, and maximum iterations.

Step2: Initialize X and V.

Step3: Set the objective as a fitness value.

Step4: Calculate the fitness of each swarm for personal best P_{best}, while comparing with other swarms for global best G_{best}.

Step5: Modify swarm velocity and position.

Step6: Modify the personal best P_{best} and global best G_{best} solutions accordingly.

Step7: Repetitions of steps 5 and 6 until achieving the limit for maximum iterations t_{max}.

Step8: The end product is global best G_{best}, personal best P_{best}, and its relevant position X.

A. UNCERTAINTY MODELING OF RER

Integrating renewable energy resources (RERs), such as solar and wind, can be an alternative approach to saving the environment from contaminated fossil fuel-based power generation. Nevertheless, the main complexities involve modeling the uncertain and intermittent nature of these RERs worsening the MG planning. Consequently, MG optimal scheduling with the modeling of the uncertain and intermittent nature of RERs is analyzed in this work, considering the scenario in which MG is operating in grid-connected under autonomous and coordinated modes. With optimal scheduling, the proposed MG system can schedule the load and manage the optimal sizing of DGs for optimal power generation. Besides diesel generators, other RERs are used for load scheduling based on variable and unpredictable load demands.

Their stochastic nature is modeled with a probabilistic method for uncertainty modeling MG components, such as solar and wind. The mathematical modeling for these three scenarios can be written as follows [51]:

$$E(x_t) = \sum_{n=1}^{N} P_n(x_t).X_t \tag{1}$$

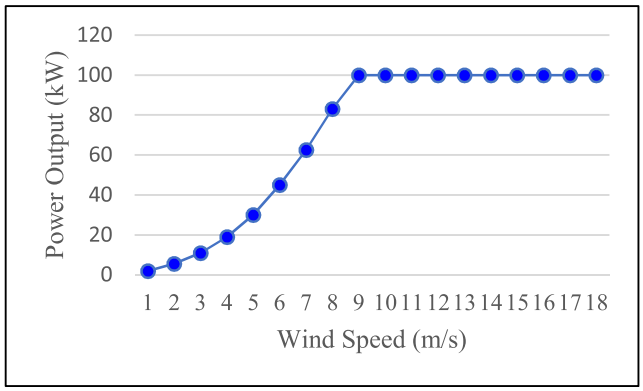

FIGURE 2. The power curve of wind turbine.

where $E(x_t)$ denotes the expectation of variable x_t at time t, $P_n(x_t)$ shows the probability of x_t at scenario n. The E values are calculated, then used in the optimization algorithms, and three cost objectives are obtained.

B. POWER GENERATION MODELING OF PV AND WT

Renewable energy resources such as solar and wind are the best choices abundant in nature and easily accessible. The output power of each PV and WT unit are highly dependent on solar irradiation and wind speed, respectively. The PV output power in [59] is represented as

$$P_{PV}(t) = \begin{cases} P_{PVr} \cdot \dfrac{I^2(t)}{I_{cp}.I_{sv}}; & 0 \le I(t) \le I_{cp} \\ P_{PVr} \cdot \dfrac{I(t)}{I_{sv}}; & I_{cp} \le I(t) \le I_{sv} \\ P_{PVr}; & I(t) \ge I_{sv} \end{cases} \tag{2}$$

I_{cp} and I_{sv} are usually set at 0.15 kW/m^2 and 1 kW/m^2, respectively. The approximation of WT output power is expressed as [59]

$$P_{WT}(t) = \begin{cases} 0; & V(t) \le V_i, V(t) \le V_o \\ \left\{A + BV(t) + CV^2(t)\right\} P_{WTr}; & V_i \le V(t) \le V_{Wr} \\ P_{WTr}; & V_{Wr} \le V(t) \le V_o \end{cases} \tag{3}$$

where cut-in, cut-out, and average rated wind speeds are taken as 3, 25, and 5.71 m/s, respectively.

Average wind speed is mentioned only for the selected site's information, but the authors have used hourly wind speed data. Moreover, the power curve of the selected wind turbine XANT M-21 is also shown in Fig. 2. Hub height is 31.80 m, while rotor diameter is 21 m. This type of wind turbine is easy to transport and can be erected without support from a crane. Their design is based on JEEP (just enough essential parts) to save capital. This WT design is aligned with the IEC 64100-1 and GL standards.

C. MODELING OF LOAD DEMAND

For a practical scenario, hourly load demand varies significantly because of various energy utilization patterns at the consumer's end. The mathematical relationship of the normal distribution function ($f_{nd}(t)$) for load demand is expressed as follows [59]

$$f_{nd}(t) = \frac{1}{\sqrt{2\pi} * \sigma_L(t)} e^{\frac{-[L(t)-\mu_L(t)]^2}{2*[\sigma_L(t)]^2}} \tag{4}$$

D. MODELING OF FUEL CELL (FC)

The mathematical modeling of the FC power is represented as follows [61]

$$P_{FC} = H \times \eta_{FC} \times 37.8 \tag{5}$$

where η_{FC} represents FC efficiency which is 37.8, H represents usage of hydrogen in kg. The mathematical relationship of FC cost is as follows [61]:

$$C_{FC} = I_C \left(N.C_C.C_R.C_{OM}.L.i_r.L_P\right) \tag{6}$$

I_c, N, C_C, C_R, C_{OM}, L, i_r, and R represent cost index, the number of FC units, capital cost, replacement cost, repairing/maintenance cost, life span, interest rate, project lifetime, respectively. For 24-hours simulation, the net cost in one day is represented as follows [61]:

$$C_d = \left(\frac{C_{FC}}{365 \times 20}\right) \tag{7}$$

E. MODELING OF DIESEL GENERATOR

Diesel engine (DE) generators are normally used as backup sources. The fuel consumption (F_{DG} (t)) and generation cost (C_{DG}(t)) of DE generator are expressed as follows [59]

$$F_{DG}(t) = F_0 * P_{DG} + F_1 * P_{DG}(t) \tag{8}$$

$$C_{DG}(t) = C_D * F_{DG}(t) \tag{9}$$

where F_1 and F_2 are taken as 0.08415 and 0.246 in litre/kWh, respectively [21], [62].

III. PROBLEM FORMULATION

The total annualized cost and emission objectives are taken in this combined optimal planning and operation modeling concerning economic and environmental perspectives. The suggested multi-objective problem is devised as follows

$$\min \omega_s F_C + \lambda_w (1 - \omega_s) F_E, \quad 0 \le \omega_s \le 1 \tag{10}$$

The objective functions and their constraints are mathematically modeled as follows [63]–[65].

A. OBJECTIVE FUNCTIONS

1) TOTAL ANNUALIZED COST (TAC)

The minimization of TAC of a grid-connected residential, rural microgrid is formulated as follows [59]

$$\min F_C = C_C + C_{OM} + \sum_{t=1}^{N} C_O(t) \tag{11}$$

where

$$C_O(t) = \sum_{x=1}^{X} \left[C_x(t) + k_{OM,x}.P_x(t) \right] + C_b(t) P_b(t) - C_s(t) P_s(t) \quad (12)$$

$$C_C = \sum_{m=1}^{M} [\rho_m.\Omega_m] \quad (13)$$

2) TOTAL ANNUALIZED EMISSION (TAE)

The TAE is formulated as follows [59]

$$\min C_E = \sum_{t=1}^{N} \sum_{x=1}^{X} \left[\begin{Bmatrix} \gamma_x(CO_2) + \gamma_x(SO_2) \\ +\gamma_x(NO_x) \end{Bmatrix} * P_x(t) \right] + \left[\begin{Bmatrix} \gamma_g(CO_2) + \gamma_g(SO_2) \\ +\gamma_g(NO_x) \end{Bmatrix} * P_b(t) \right] \quad (14)$$

3) OPERATION COST

The OC (OC) of the microgrid is expressed [57]:

$$\min OC = OC \begin{Bmatrix} Fuel + OM + DC + N.GRID \\ +(1-N)LS \end{Bmatrix} \quad (15)$$

where $Fuel$, OM, $GRID$, LS, and N represent costs for fuel; O&M; MG-Grid coordination; compensation cost for load interruption; grid On/Off, respectively. N = 1 indicates MG is connected with the grid, while N = 0 shows an islanded operation.

The depreciation cost ($OC(DC)$) is determined [57]:

$$OC(DC) = \frac{In\,\mathrm{Cos}\,t * \left[\frac{a(1+a)^l}{(1+a)^l - 1} \right]}{P_{\max} * 8760 * bc} * P_i \quad (16)$$

where $P_i, i, bc, In\,\mathrm{Cos}\,t, a, l$ and $P_{\max}$ are output power; capacity factor; installation costs; interest rates (8%); DGs life; and DGs maximum capacity, respectively.

4) POLLUTANT TREATMENT COST

The pollutant treatment cost (PTC) of the microgrid is [57]:

$$\min PTC = \sum_{j=1}^{M} \sum_{m} \left(C_j \gamma_{jm} \right) P_j + \sum_{m} \left(C_m \gamma_{Gridm} \right) P_{Grid} \quad (17)$$

where $M, m, C_m, \gamma_{jm}, \gamma_{Gridm}$, and P_{Grid} represent DGs sum; pollutant emission type; treatments cost; emission coefficient; coefficient of grid pollutant emission; and grid output power, respectively.

B. CONSTRAINTS

1) DER SIZING

The sizing constraint of each MG component is mathematically represented as [59]

$$n_m(\min) \le n_m \le n_m(\max), \quad \forall m \in \{1, 2, 3, \ldots M\} \quad (18)$$

2) POWER BALANCE

At any given time t, the difference of total load demand and total power generation must be equal to zero, which can be represented as follows [59]

$$\sum_{x=1}^{X} P_x(t) + P_{PV}(t) + P_{WT}(t) - P_{Ld}(t) - P_C(t) + P_D(t) + P_b(t) - P_s(t) = 0 \quad (19)$$

3) DG POWER LIMITS

The power limits for DG units can be represented as follows [59]

$$n_x \xi_x(\min) \le P_x(t) \le n_x \xi_x(\max), \quad \forall x \in \{1, 2, 3, \ldots X\} \quad (20)$$

4) EXCHANGING POWER LIMIT

The power exchanging limits between grid and MG can be represented as follows [59]

$$\begin{aligned} &0 \le P_b(t) \le P_b(\max)\, b_b(t), \\ &0 \le P_s(t) \le P_s(\max)\, b_s(t), \\ &b_b(t) + b_s(t) \le 1, \\ &b_b(t), \quad b_s(t) \in \{0, 1\} \end{aligned} \quad (21)$$

5) EV BATTERY CHARGING/DISCHARGING LIMITS

The charging and discharging limits of BSS can be represented as follows [59]

$$\begin{aligned} &0 \le P_C(t) \le \gamma_C(\max)\, \Omega_{BSS}, \\ &0 \le P_D(t) \le \gamma_D(\max)\, \Omega_{BSS}, \\ &P_C(t).P_D(t) = 0, \end{aligned} \quad (22)$$

The SOC constraint of BSS can be represented as follows [59]

$$\begin{aligned} SOC(\min) \le SOC(t) \le SOC(\max), \\ SOC(t) = OC(t-1) + \frac{\left[\eta_C P_C(t)\, \Delta t - P_D(t)\, \Delta t / \eta_D \right]}{\Omega_{BSS}} \end{aligned} \quad (23)$$

At any given time interval t, the sum of total charged energy and initial energy level must be greater than the total discharged energy of the battery. It can be represented as follows [59]

$$\sum_{t=1}^{N} P_D(t)\, \Delta t / \eta_D \le SOC(\min)\, \Omega_{BSS} + \sum_{t=1}^{N} \eta_C P_C(t)\, \Delta t \quad (24)$$

6) RAMP RATE LIMITS

DEs ramp rate can be represented as [57]:

$$|P_{DE}(t) - P_{DE}(t-1)| \le r_{\max} * \Delta t \quad (25)$$

where $P_{DE}(t)$, $P_{DE}(t-1)$, $r_{\max}$ and t are outputs; maximum ramp rate, and time interval, respectively.

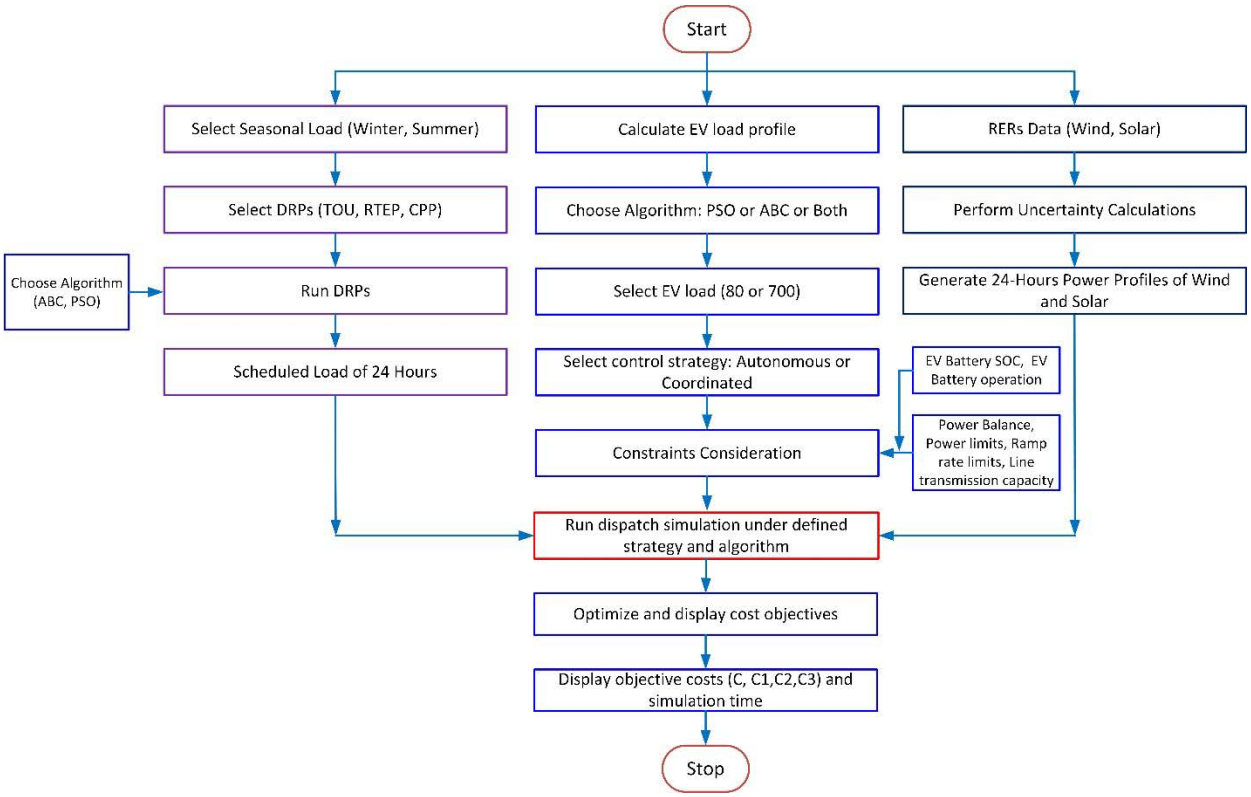

FIGURE 3. Flowchart of proposed optimization methodology to find feasible scheduling for DSM and optimal DGs sizing.

7) LINE TRANSMISSION CAPACITY

Power flow between MG and PG is expressed as [57]:

$$-P_{Line\text{Max}} \leq P_{Grid} \leq P_{Line\text{Max}} \tag{26}$$

where $P_{Line\text{Max}}$ shows the maximum line capacity.

IV. TEST CASES

The grid-connected MG system is analyzed under different scenarios of RERs and DGs. During scheduling strategy-1, EVs are charging in autonomous mode. During scheduling strategy-2, EVs are charging and discharging in coordinated mode. This study's analysis includes 80 EVs and 700 EVs. Performance of ABC and PSO are compared for the following test cases that are analyzed in this paper and explained as follows:

- Test Case 1: Unscheduled summer loads with 80 EVs during autonomous mode and coordinated mode.
- Test Case 1: Unscheduled summer loads with 80 EVs and 700 EVs during autonomous mode and coordinated mode.
- Test Case 2: CPP summer loads with 80 EVs and 700 EVs during autonomous mode and coordinated mode.
- Test Case 3: RTEP summer loads with 80 EVs and 700 EVs during autonomous mode and coordinated mode.
- Test Case 4: TOU summer loads with 80 EVs and 700 EVs during autonomous mode and coordinated mode.
- Test Case 5: Unscheduled winter loads with 80 EVs and 700 EVs during autonomous mode and coordinated mode.
- Test Case 6: CPP winter loads with 80 EVs and 700 EVs during autonomous mode and coordinated mode.
- Test Case 7: RTEP winter loads with 80 EVs and 700 EVs during autonomous mode and coordinated mode.
- Test Case 8: TOU winter loads with 80 EVs and 700 EVs during autonomous mode and coordinated mode.

V. SIMULATION DATA FOR STUDY SYSTEM

Fig. 3 shows the flow chart of the proposed methodology. In this research, hourly data of PV and WT speed for one year is taken from NREL for the rural town (Shah Allah Ditta) in Islamabad, Pakistan (33.7209642 °N 72.9143201 °E). This location's maximum and minimum temperatures are 30.93 °C (June) and 8.61 °C (January), respectively. The annual average temperature is 20.43 °C. The maximum and minimum values of daily solar radiation are 7.063 kWh/m^2 (June) and 2.566 kWh/m^2 (December), respectively. The annual average radiation is 4.89 kWh/m^2. The maximum wind speed of this location is 6.99 m/s (April), while the annual average speed is 5.71 m/s. This rural town is 700 years old and was used

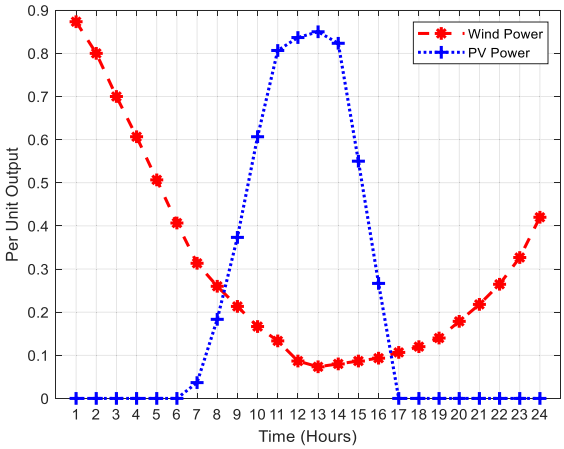

FIGURE 4. The power output (wind & solar).

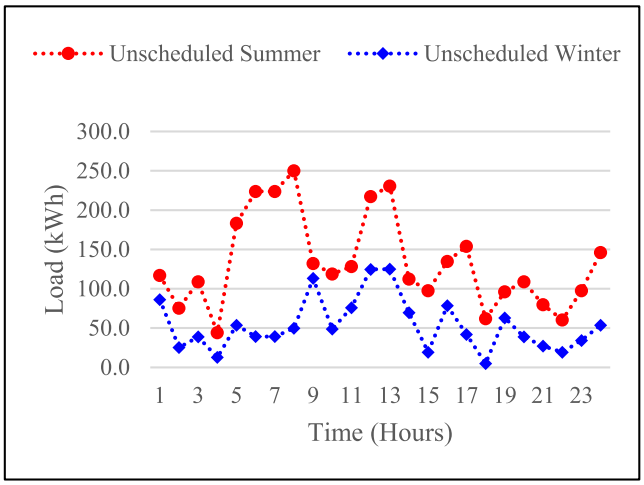

FIGURE 5. Unscheduled load profiles for summer and winter.

to route from Kabul (Afghanistan) to the Gandharan city of Taxila (Hindustan) by Alexander the Great and Sher Shah Suri. Other emperors, including Mughal rulers, frequently travelled from Afghanistan to the Hindustan [52].

The grid-connected residential, rural community MG is analyzed under different RERs and DGs. Different costs (such as annual capital, O&M, and emission coefficients) and other DER parameters are taken from [48], [51], [53], [54]. The power limits of all DGs are adopted from [46]. Home appliances details are taken from [70]–[75]. The total number of 50 smart residential, rural consumers, are considered. Three pricing schemes (CPP, RTEP, and TOU) are used to handle power exchanging costs between the grid, and MG. Fig. 4 shows the power output curves of solar and wind used in this study. The time step of the simulation is based on 24 hours. Therefore, the estimated profile of 24 hours is shown to find cost by solving the optimization problem with 24 hours. The data is taken from the base papers [57], [58], which used 24 hours in their simulation. Fig. 5 shows the total unscheduled load for summer and winter. Fig. 6 shows the

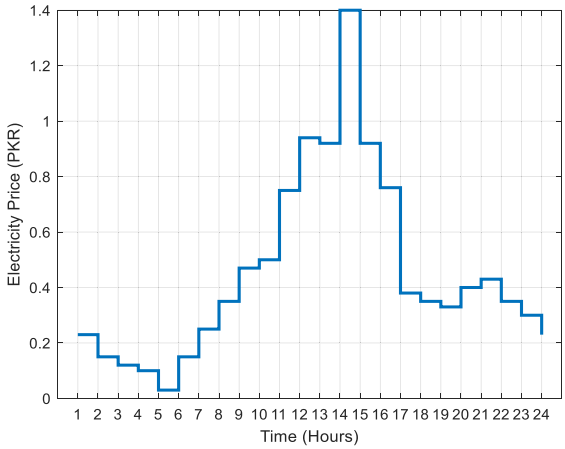

FIGURE 6. TOU tariff.

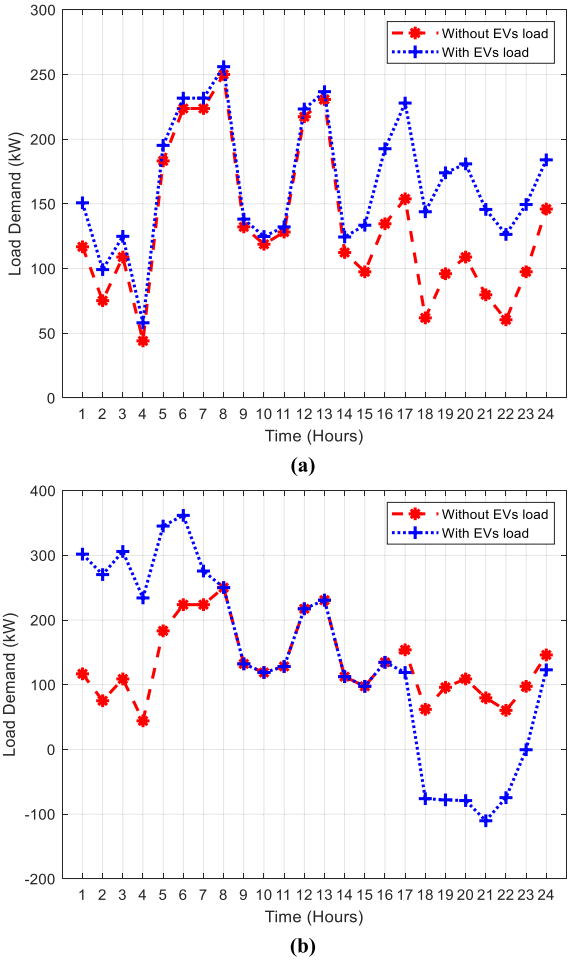

FIGURE 7. Unscheduled load profile of MG for 80 EVs under (a) autonomous mode; (b) coordinated mode.

TOU tariff for an unscheduled load. All other load conditions with CPP and RTEP tariffs are taken from base paper [77].

8) UNSCHEDULED SUMMER LOAD

Fig. 7 and Fig. 8 show the unscheduled load profiles of MG under autonomous mode and coordinated modes for 80 EVs and 700 EVs, respectively. Fig.7a shows unscheduled load

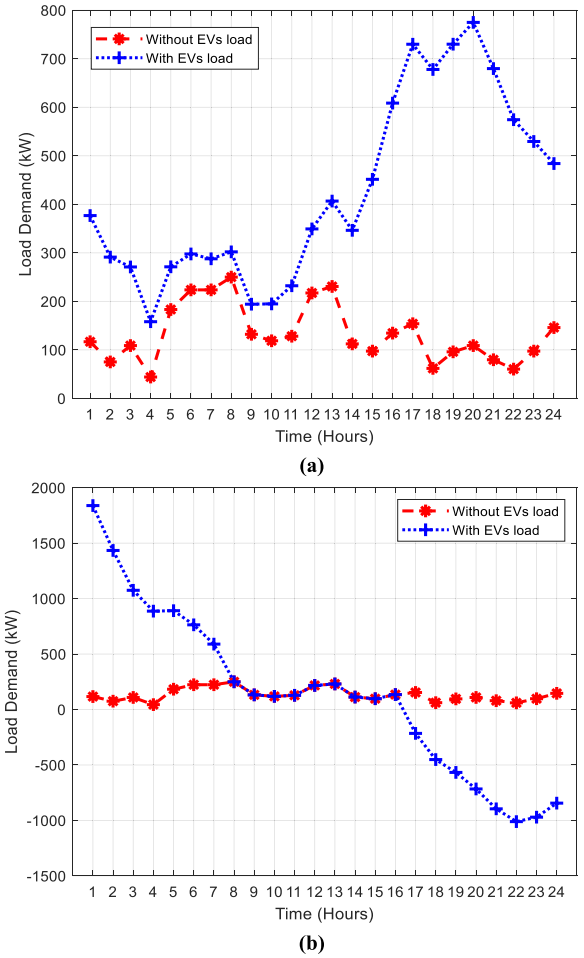

FIGURE 8. Unscheduled load profile of MG for 700 EVs under (a) autonomous mode; (b) coordinated mode.

for an autonomous mode of MG operation with and without EVs load. It is shown that the load with EVs increased from 1400 onward compared to the load without EVs. The peak load is almost 250 kW, the same peak value with and without EVs load. Fig. 7b shows the same procedure for coordinated mode. It is observed that EVs introduced more charging load during the morning (0100 to 0800) while contributing the power in the evening (1700-2400). The peak loads are observed as 370 kW and 250 kW with and without EVs load. In Fig.8a, EVs load absorbs energy throughout the day during autonomous mode with a peak load of 790 kW. The peak load without EVs remained at 250 kW in all summer tariffs. Fig. 8b shows that EVs are in charging mode in the morning (0100-0800) while in discharging mode in the evening (1600-2400). The peak load is recorded as 1800 kW.

9) CPP SCHEDULED SUMMER LOAD

Fig. 9 shows the CPP tariff of summer load with peak pricing at 1200-1600 due to hot weather while maximum usage of cooling load. The peak pricing value of the CPP tariff is 5.5 which is greater than the unscheduled tariff peak of 1.4. Fig. 10a and Fig. 10b show almost the same trend as the relevant graph of unscheduled load but with the

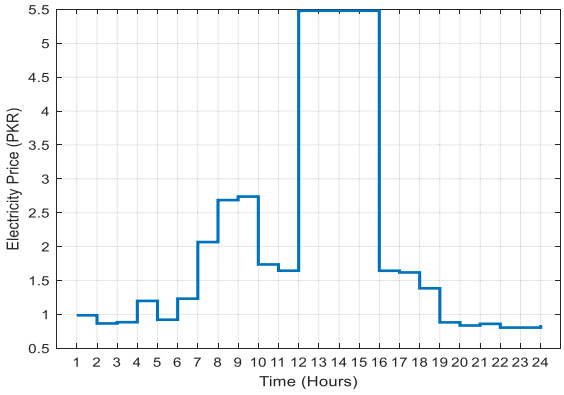

FIGURE 9. CPP tariff for summer load.

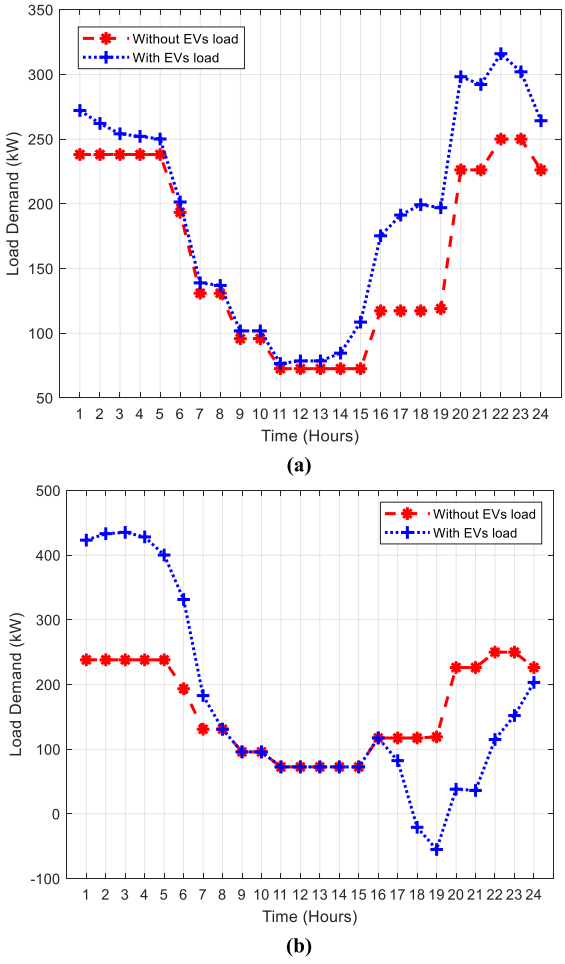

FIGURE 10. CPP summer load profile of MG for 80 EVs under (a) autonomous mode; (b) coordinated mode.

peak value of 320 kW and 440 kW, respectively. Similarly, Fig. 11a and Fig. 11b show a similar profile compared to unscheduled load but with the peak load demand of 900 kW 2000 kW, respectively.

10) RTEP SCHEDULED SUMMER LOAD

Fig. 12 shows the RTEP tariff for the summer load. Load profiles for this tariff are the same as that of unscheduled load,

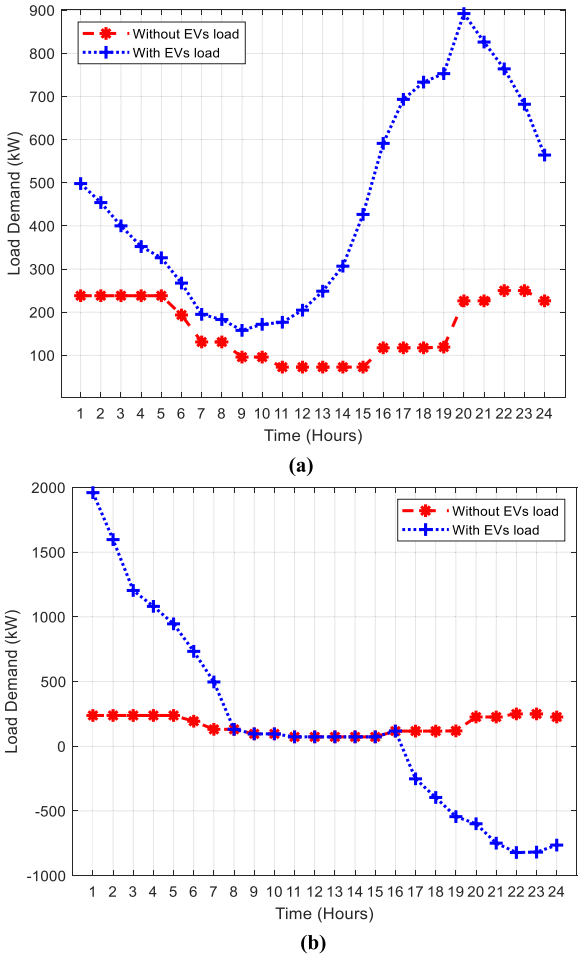

FIGURE 11. CPP summer load profile of MG for 700 EVs under (a) autonomous mode; (b) coordinated mode.

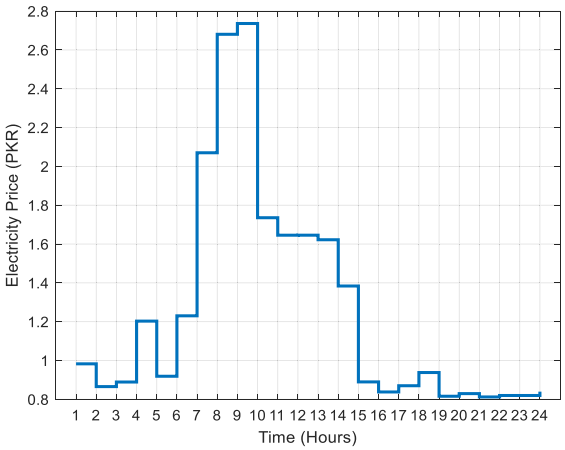

FIGURE 12. Electricity rate for summer load with RTEP tariff.

as shown in the relevant fiures (Fig. 13a, Fig. 13b, Fig. 14a, and Fig. 14b).

11) TOU SCHEDULED SUMMER LOAD

Fig. 15a and Fig. 15b show the TOU load profile for autonomous and coordinated modes with 80 EVs,

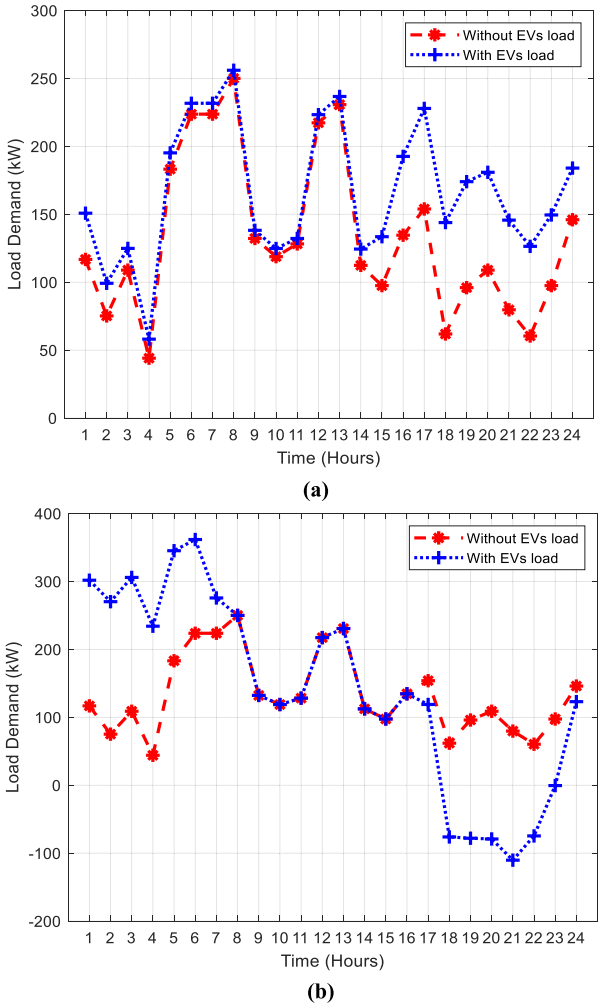

FIGURE 13. RTEP summer load profile of MG for 80 EVs under (a) autonomous mode; (b) coordinated mode.

respectively. Fig. 16a and Fig. 16b show the autonomous and coordinated modes with 700 EVs, respectively.

12) UNSCHEDULED WINTER LOAD

Fig. 17a and Fig. 17b show the unscheduled load profile for autonomous and coordinated modes with 80 EVs, respectively. Fig. 18a and Fig. 18b show the unscheduled load profile for autonomous and coordinated modes with 700 EVs, respectively.

13) CPP SCHEDULED WINTER LOAD

Fig. 19a and Fig. 19b show the scheduled load profile for autonomous and coordinated modes with 80 EVs, respectively. Fig. 20a and Fig. 20b show the scheduled load profile for autonomous and coordinated modes with 700 EVs, respectively.

14) RTEP SCHEDULED WINTER LOAD

Fig. 21a and Fig. 21b show the scheduled load profile for autonomous and coordinated modes with 80 EVs,

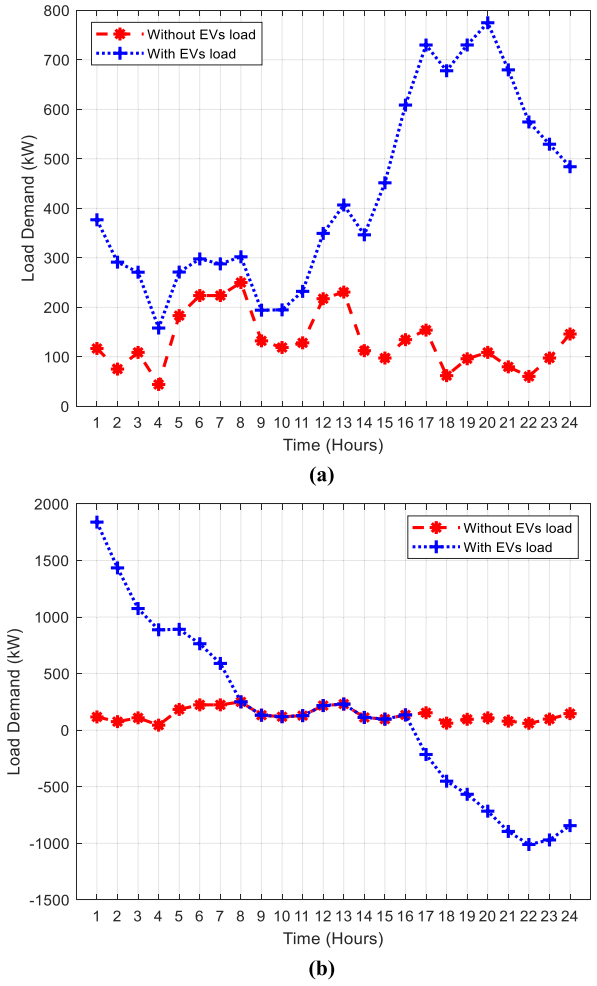

FIGURE 14. RTEP summer load profile of MG for 700 EVs under (a) autonomous mode; (b) coordinated mode.

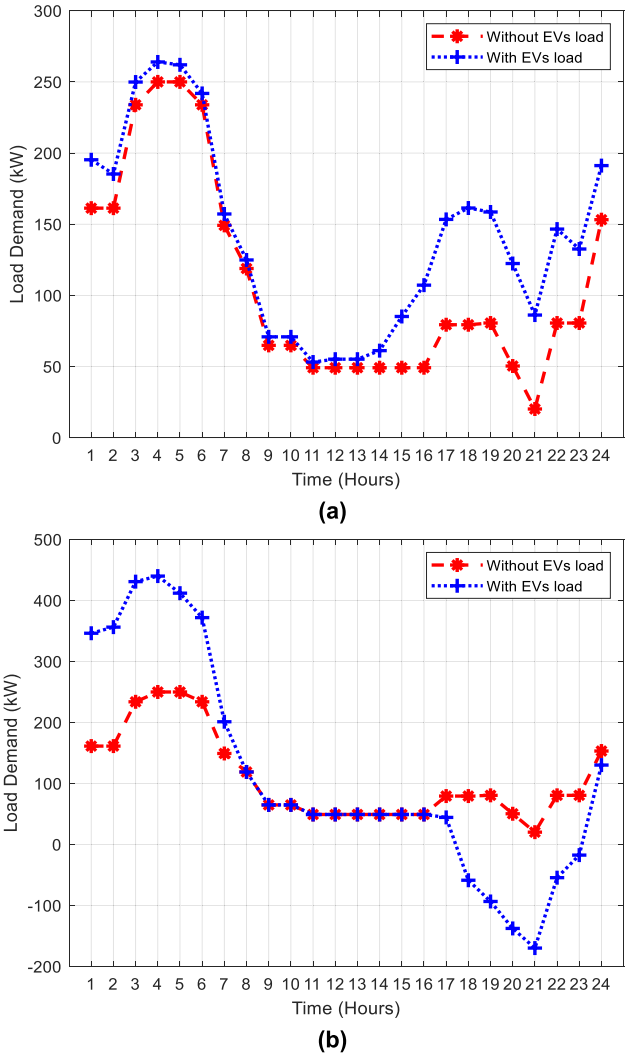

FIGURE 15. TOU summer load profile of MG for 80 EVs under (a) autonomous mode; (b) coordinated mode.

respectively. Fig. 22a and Fig. 22b show the scheduled load profile for autonomous and coordinated modes with 700 EVs, respectively.

15) TOU SCHEDULED WINTER LOAD

Fig. 23a and Fig. 23b show the scheduled load profile for autonomous and coordinated modes with 80 EVs, respectively. Fig. 24a and Fig. 24b show the scheduled load profile for autonomous and coordinated modes with 700 EVs, respectively.

VI. RESULT ANALYSIS AND DISCUSSIONS

Fig. 25 and Fig. 26 show the scheduled load profiles for summer and winter, respectively. Fig. 27a and Fig. 27b show the autonomous and coordinated EVs load profiles with three scenarios of EVs. Still, this study's analysis includes only two scenarios of EVs, such as 80 EVs and 700 EVs.

A. SUMMER LOAD

Fig. 28a and Fig. 28b show the unscheduled convergence curves for 80 EVs during autonomous and coordinated modes, respectively. It is observed that the performance of the ABC algorithm is better in autonomous mode, while PSO performed well in coordinated mode. Table 2 shows the computational burden of unscheduled load under different circumstances. These table values are used as the base values for comparing three DRPs.

Table 3 shows data for the CPP summer tariff. During the CPP summer tariff, a significant reduction of computational burden is observed in the PSO algorithm for 80 EVs in autonomous mode. The simulation time reduction is also observed with ABC and PSO for 80 EVs in autonomous and coordinated modes, respectively. All remaining scenarios show more computational burden as compared to the base case.

Fig. 29a and Fig. 29b show the convergence curves for the RTEP summer tariff. The almost same trend of final convergence is observed for both algorithms during autonomous and coordinated modes. Table 4 shows the data of simulation

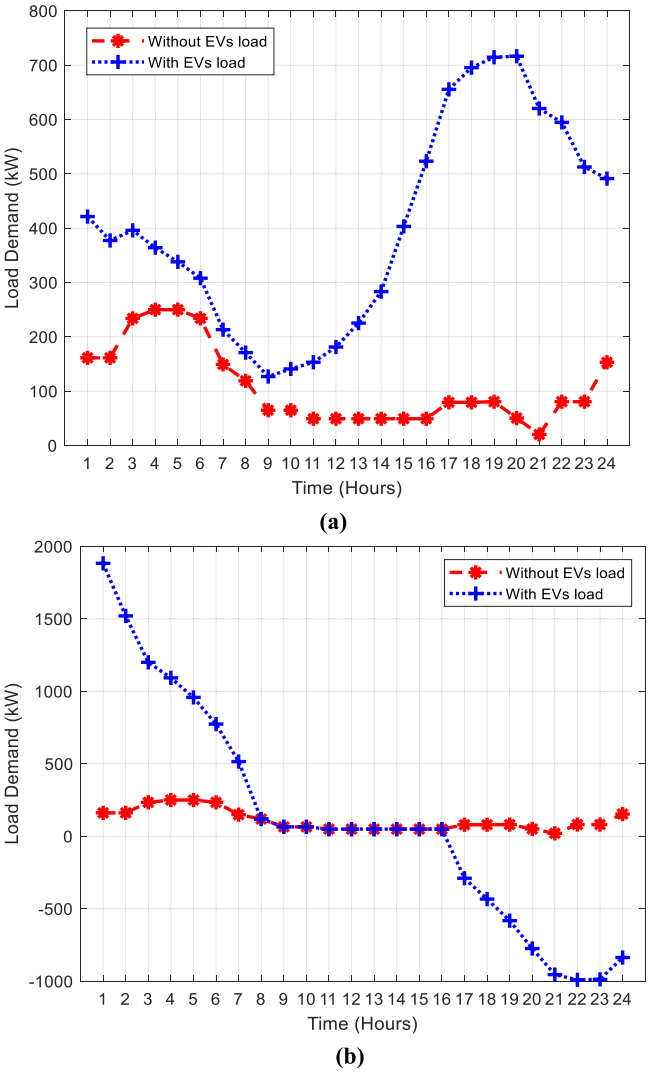

FIGURE 16. TOU summer load profile of MG for 700 EVs under (a) autonomous mode; (b) coordinated mode.

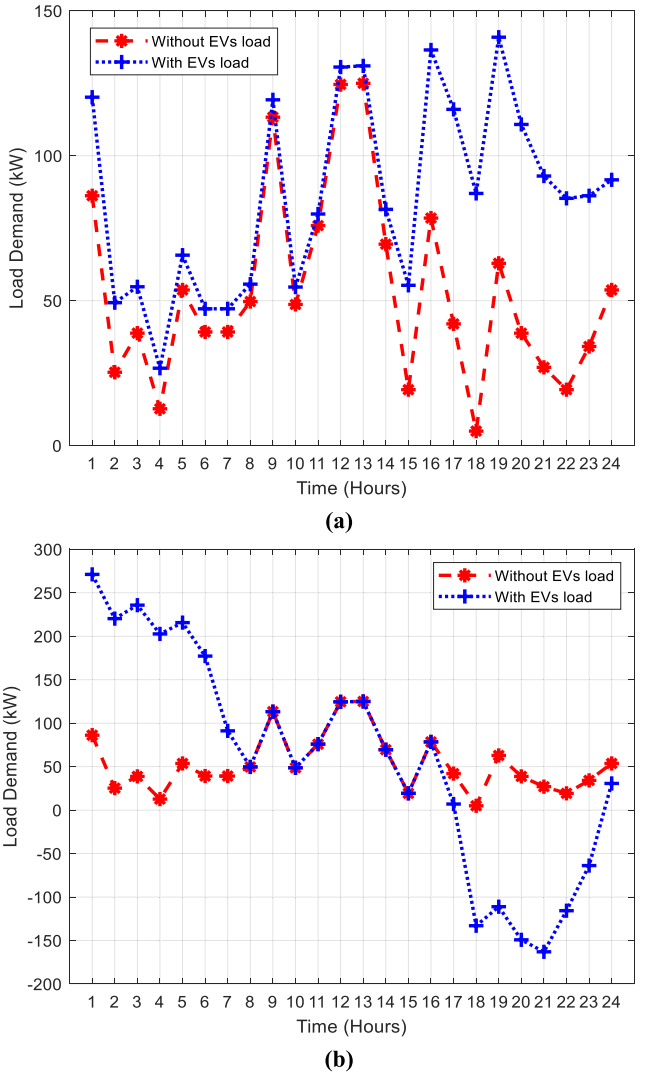

FIGURE 17. Unscheduled load profile of MG for 80 EVs under (a) autonomous mode; (b) coordinated mode.

time for RTEP summer tariff. During the RTEP summer tariff, a significant reduction in computational burden is observed with PSO for 80 EVs in autonomous mode. The simulation time reduction is also observed with PSO for 80 EVs and 700 EVs in coordinated and autonomous modes, respectively. All remaining scenarios show more computational burden as compared to the base case.

Fig. 30 shows the convergence curve for the TOU summer tariff. It is observed that the performance of the PSO algorithm is better in coordinated mode. Table 5 shows the data of simulation time for the TOU summer tariff. During the TOU summer tariff, a significant reduction in computational burden is observed with PSO for 80 EVs in autonomous mode. The simulation time reduction is also observed with PSO and ABC for 80 EVs in coordinated and autonomous modes, respectively. All remaining scenarios show more computational burden as compared to the base case.

TABLE 2. Comparative analysis of computational burden between two algorithms for unscheduled load.

Algorithm	EVs	Mode	Simulation time/s
PSO	80	Autonomous	8.770599
ABC	80	Autonomous	3.006831
PSO	80	Coordinated	2.645057
ABC	80	Coordinated	2.696129
PSO	700	Autonomous	2.147220
ABC	700	Autonomous	2.634880
PSO	700	Coordinated	2.129485
ABC	700	Coordinated	2.614929

1) UNSCHEDULED SUMMER LOAD

Fig. 31a and Fig. 31b show PSO-based unscheduled load scheduling with 80 EVs in autonomous and coordinated modes. During autonomous mode, excess energy from DGs is supplied to the grid for three hours in the early morning (0100-0300) and one hour afternoon (1300). EVs charging

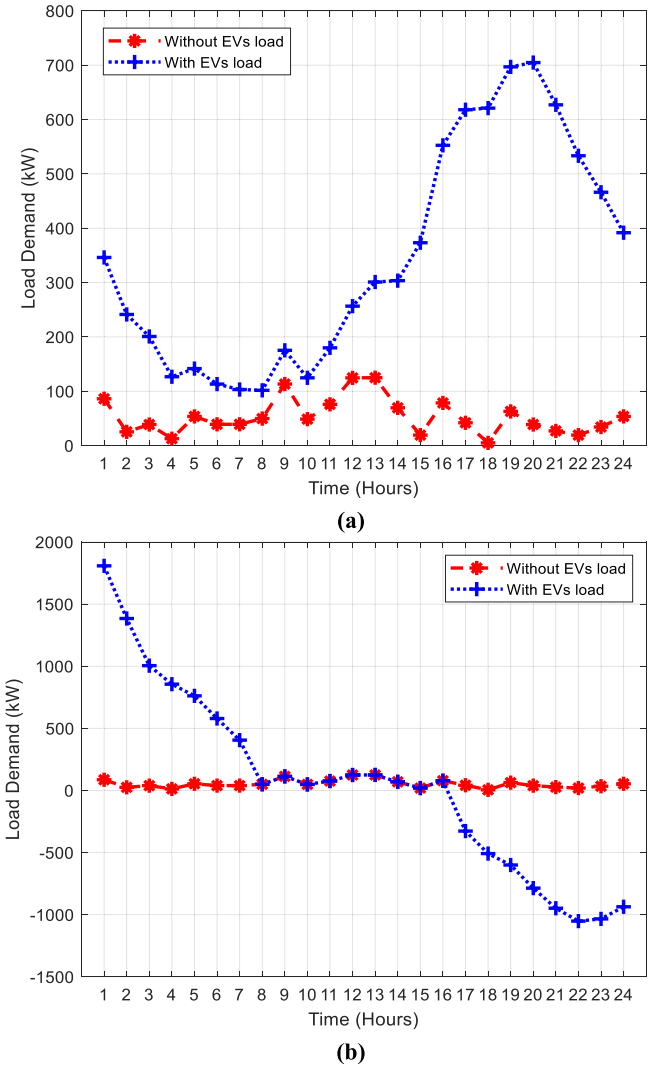

FIGURE 18. Unscheduled load profile of MG for 700 EVs under (a) autonomous mode; (b) coordinated mode.

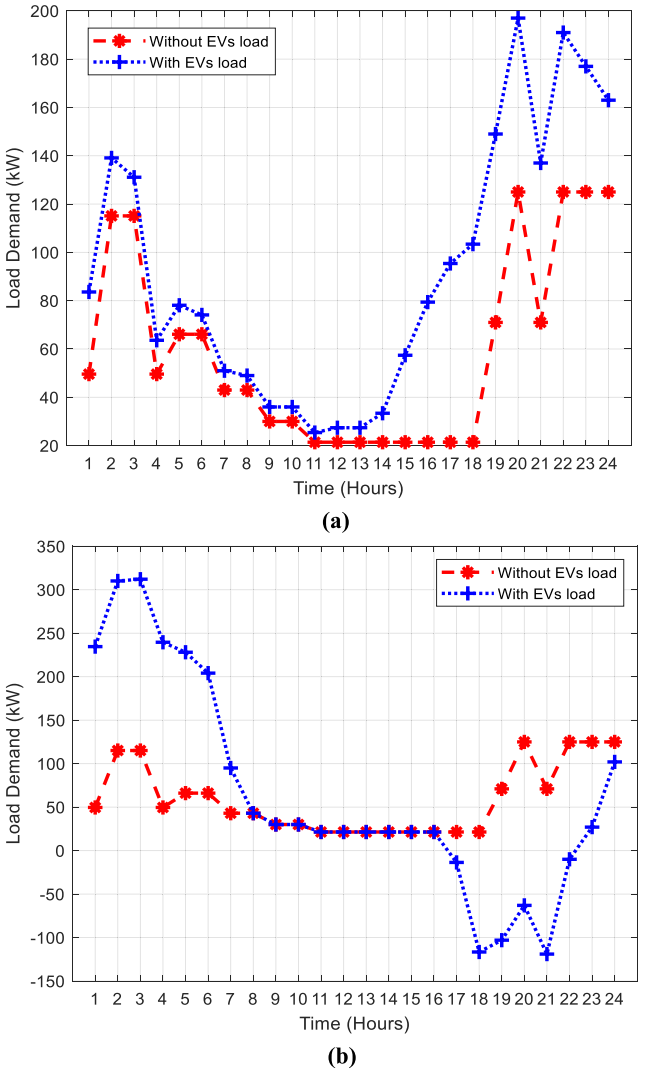

FIGURE 19. CPP summer load profile of MG for 80 EVs under (a) autonomous mode; (b) coordinated mode.

TABLE 3. Comparative analysis of computational burden between two algorithms for summer CPP.

Algorithm	EVs	Mode	Simulation time/s	%Δ
PSO	80	Autonomous	2.192651	-300.00
ABC	80	Autonomous	2.713274	-10.82
PSO	80	Coordinated	2.583831	-2.37
ABC	80	Coordinated	2.880647	6.41
PSO	700	Autonomous	2.169166	1.01
ABC	700	Autonomous	2.840564	7.24
PSO	700	Coordinated	2.188206	2.68
ABC	700	Coordinated	2.790609	6.30

load is negligible during the starting day time (0600-1300), while EVs discharging load is significantly increased (above 50 kW) during the second half-day (1600-2300). DE is supplying power at an almost constant rate, while the main grid handles FC power fluctuations. During coordinated mode, excess energy from DGs is supplied to the grid for the second half-day (1700-2200). EVs discharging load is significant during the start of the day (0100-0700), while EVs charging load is significantly increased during the second half of the day (1700-2400). DE supplies negligible power at an almost constant rate, while the main grid handles EVs power fluctuations. Fig. 32a and Fig. 32b show ABC-based unscheduled load scheduling with 80 EVs in autonomous and coordinated mode. During autonomous mode, excess energy from DGs is supplied to the grid for three hours in the early morning (0100-0300) and at different daytime (0800, 1000, 1300-1400, 2100). EVs charging load is negligible during the starting day time (0600-1400), while EVs charging load is significantly increased (above 50 kW) during the second half-day (1600-2300). DE is supplying power with slightly changing power output, while the main grid handles FC power fluctuations. During coordinated mode, excess energy from DGs is supplied to the grid for the second half-day (1700-2200). EVs discharging load is significant during the

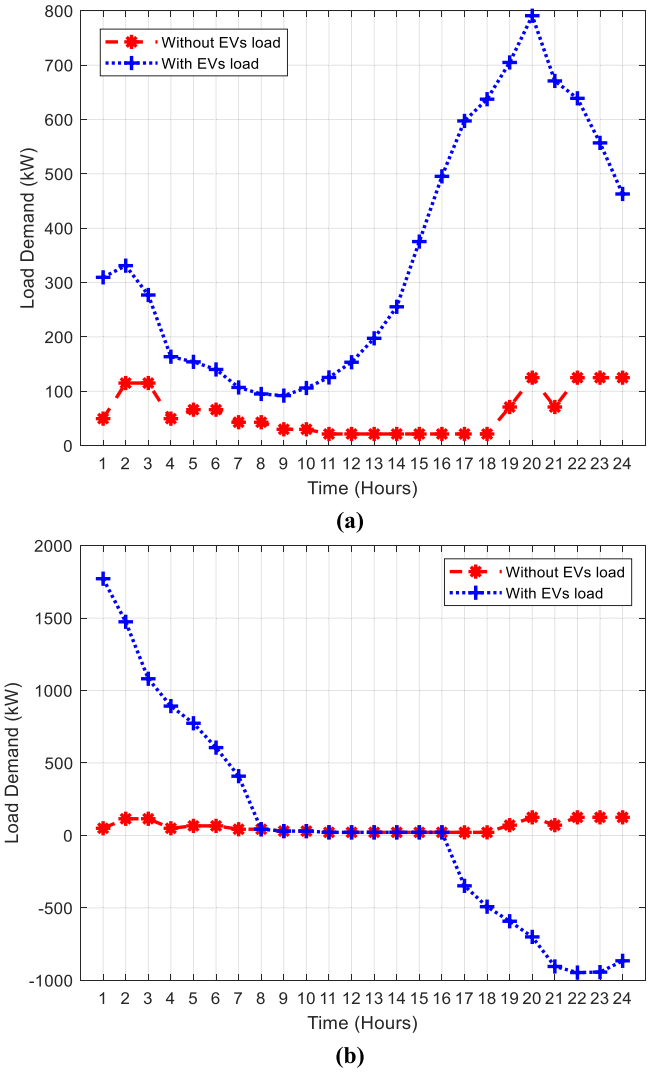

FIGURE 20. CPP summer load profile of MG for 700 EVs under (a) autonomous mode; (b) coordinated mode.

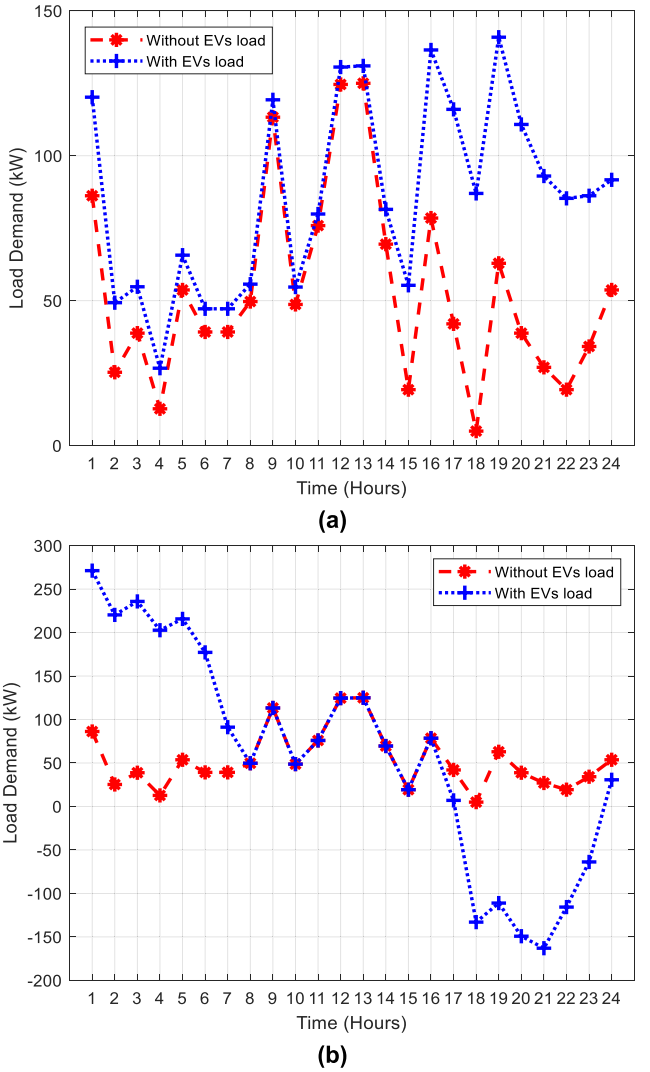

FIGURE 21. RTEP summer load profile of MG for 80 EVs under (a) autonomous mode; (b) coordinated mode.

start of the day (0100-0700), while EVs charging load is significantly increased during the second half of the day (1700-2400). DE is supplying constant power at the start of the day (0100-0700) and almost negligible power during midday (0800-1800), while no power during nighttime (1900-2300). EV excess power is supplied to the main grid (1700-2400). The demand-generation mismatch is supplied by RERs (PV, WT). Fig. 33a and Fig. 33b show unscheduled load scheduling with 700 EVs in autonomous and coordinated modes, respectively. During autonomous mode, EVs charging load is more during the starting day (0100-0700), while EVs charging load is significant throughout the simulation with a 700 kW peak during the night (2000). DE and FC are supplying almost constant power. During coordinated mode, excess energy from DGs is supplied to the grid at night (1600-2400). EVs charging load is more during the starting day (0100-0700), while EVs discharging load is significant at night (1700-2400). DE and FC are supplying almost negligible power.

TABLE 4. Comparative analysis of computational burden between two algorithms for summer RTEP.

Algorithm	EVs	Mode	Simulation time/s	%Δ
PSO	80	Autonomous	2.596207	-237.82
ABC	80	Autonomous	3.226615	6.81
PSO	80	Coordinated	2.211806	-19.59
ABC	80	Coordinated	2.831761	4.79
PSO	700	Autonomous	2.135269	-0.56
ABC	700	Autonomous	2.827750	6.82
PSO	700	Coordinated	2.169600	1.85
ABC	700	Coordinated	2.841320	7.97

Fig. 34a and Fig. 34b show unscheduled load scheduling with 700 EVs in autonomous and coordinated modes, respectively. The almost same trend of PSO-based modes is observed during autonomous and coordinated modes. The demand-generation gap is supplied by RERs (PV, WT).

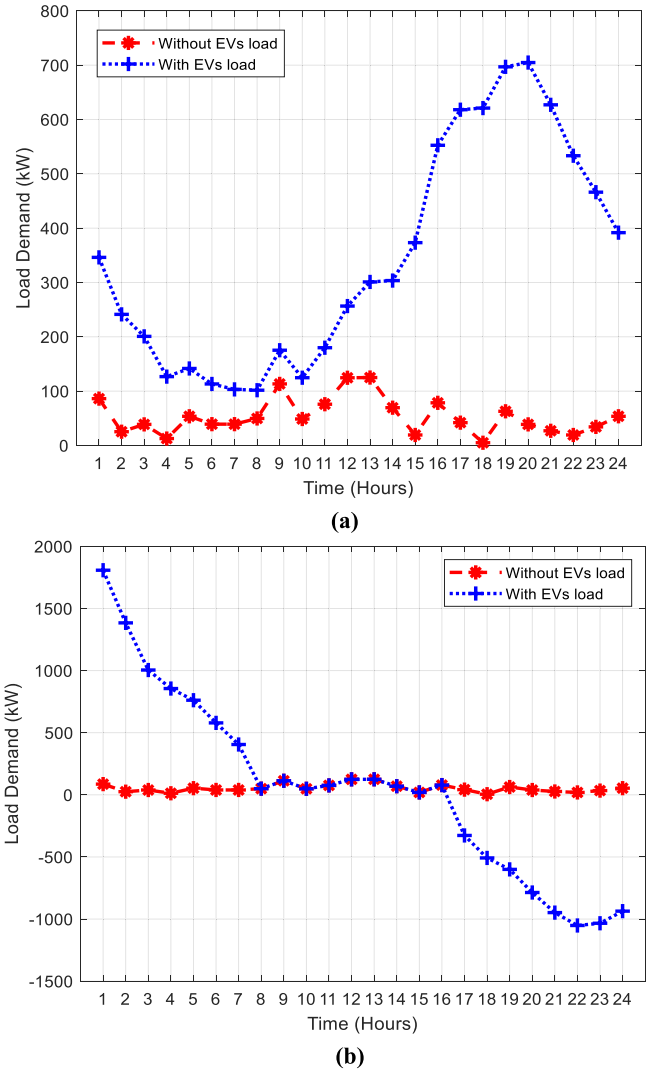

FIGURE 22. RTEP summer load profile of MG for 700 EVs under (a) autonomous mode; (b) coordinated mode.

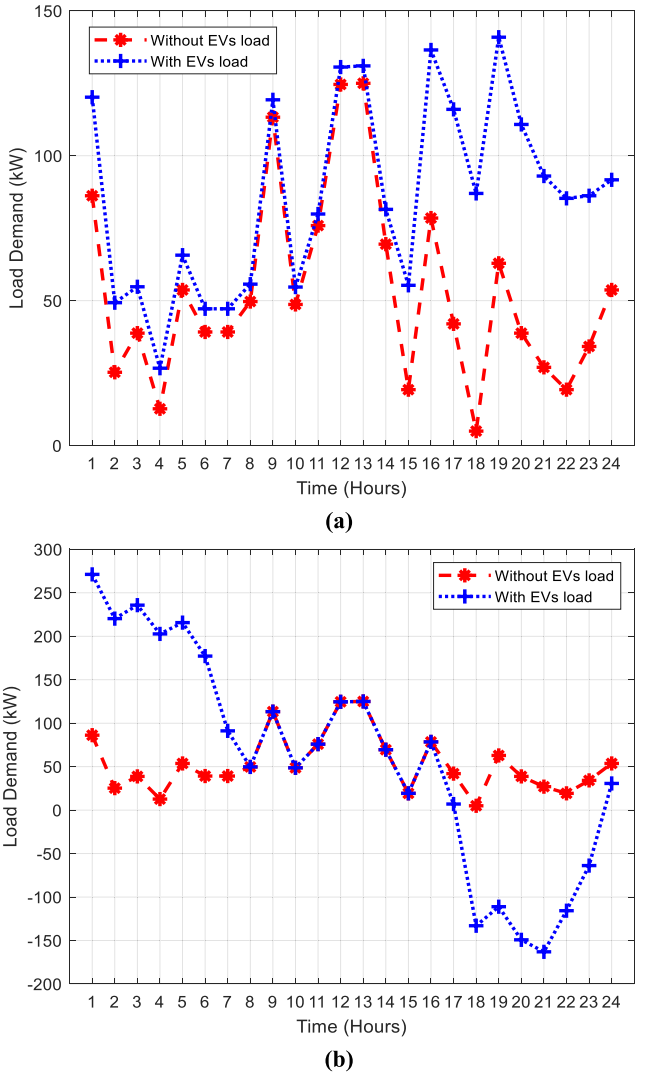

FIGURE 23. TOU summer load profile of MG for 80 EVs under (a) autonomous mode; (b) coordinated mode.

TABLE 5. Comparative analysis of computational burden between two algorithms for summer TOU.

Algorithm	EVs	Mode	Simulation time/s	%Δ
PSO	80	Autonomous	2.213347	-296.26
ABC	80	Autonomous	2.901536	-3.63
PSO	80	Coordinated	2.189551	-20.80
ABC	80	Coordinated	2.880561	6.40
PSO	700	Autonomous	2.188684	1.89
ABC	700	Autonomous	2.953510	10.79
PSO	700	Coordinated	2.643755	19.45
ABC	700	Coordinated	3.139453	16.71

TABLE 6. Dispatch results under scheduling schemes 1 and 2 for 80 EVs.

Algorithm	Cost objective	Scheduling scheme 1	Scheduling scheme 2
PSO	C1	4190.9243	3859.3385
	C2	900.178	225.3876
	C3	386.7902	325.1174
	C	2942.6317	2550.6561
ABC	C1	4227.9033	3628.0037
	C2	859.4718	429.8848
	C3	390.2647	302.3531
	C	2956.0367	2453.734

Table 6 and Table 7 shows unscheduled load results during scheduling scheme 1 (autonomous) and scheduling scheme 2 (coordinated), respectively. The data of these tables are used as the base case for three DRPs.

2) CPP SCHEDULED SUMMER LOAD

Fig. 35a and Fig. 35b show the CPP summer load scheduling with 80 EVs in autonomous and coordinated modes, respectively. Excess energy from DGs is supplied to the grid (0600, 0800-1300). EVs charging load is negligible during the starting day (0100-1400), while EVs' charging load increases during the second half-day (1500-2400). DE supplies power at an almost constant rate, while FC power is variable. Excess energy from DGs is supplied to the grid (0800, 1000-1400,

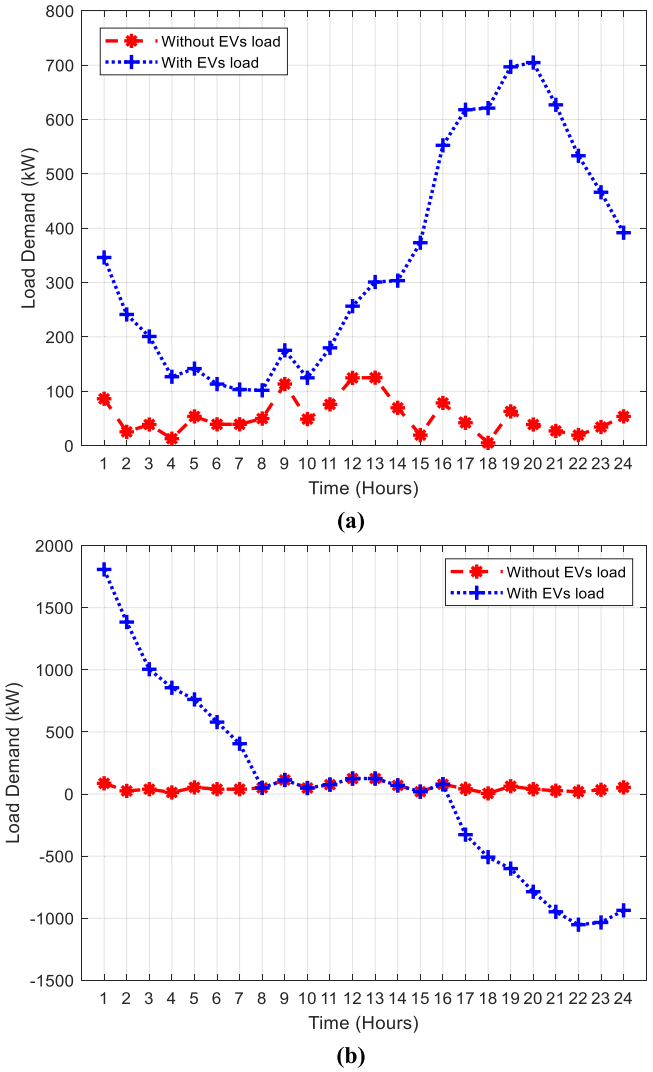

FIGURE 24. TOU summer load profile of MG for 700 EVs under (a) autonomous mode; (b) coordinated mode.

TABLE 7. Dispatch results under scheduling schemes 1 and 2 for 700 EVs.

Algorithm	Cost objective	Scheduling scheme 1	Scheduling scheme 2
PSO	C1	10520.572	2919.9346
	C2	1203.4781	654.9253
	C3	1175.6719	221.2688
	C	7135.5556	2052.3324
ABC	C1	10692.5988	2882.7402
	C2	1276.2611	687.8111
	C3	1192.1855	219.0349
	C	7265.6655	2036.9001

1700-2000). EVs charging load is significant during the start of the day (0100-0700), while EVs discharging load is significantly increased during the second half of the day (1700-2400). DE is supplying almost constant power.

Fig. 36a and Fig. 36b show ABC-based CPP summer load scheduling with 80 EVs in autonomous and coordinated modes. Excess energy from DGs is supplied to the grid (0800-2200). EVs charging load is significant during the starting day (0100-0700), while EVs discharging load is significantly increased during the second half-day (1700-2400). DE supplies power at the start of the day till noon with a slight change in power output afternoon, while FC power fluctuates. Excess energy from DGs is supplied to the grid (0800-2200). EVs discharging load is significant during the start of the day (0100-0700), while EVs discharging load is significantly increased during the second half of the day (1700-2400). DE supplies constant power at the start of the day and almost negligible power at night. EV excess power is supplied to the main grid (1700-2400), while the demand-generation mismatch is supplied by RERs (PV, WT).

Fig. 37a and Fig. 37b show PSO-based summer CPP load scheduling with 700 EVs in autonomous and coordinated modes. EVs charging load is significant during the autonomous mode throughout the daytime with a 700 kW peak at night (2000). DE and FC are supplying almost constant power. During coordinated mode, excess energy from DGs is supplied to the grid at night (1700-2400). EVs charging load is more during the starting day (0100-0700), while EVs discharging load is significant at night (1700-2400). DE and FC are supplying almost negligible power.

Fig. 38a and Fig. 38b show ABC-based summer CPP load scheduling with 700 EVs in autonomous and coordinated modes. The almost same trend of PSO-based modes is observed during autonomous and coordinated modes. The demand-generation gap is supplied by RERs (PV, WT).

Table 8 shows CPP summer load scheduling results for 80 EVs during scheduling scheme 1 (autonomous) and scheduling scheme 2 (coordinated). During autonomous mode, the ABC algorithm outperformed PSO by reducing all four costs, such as the operating cost (C1), pollutant treatment cost (C2), carbon emissions cost (C3), and the overall cost (C). The ABC algorithm also outperformed PSO during coordinated mode by reducing three costs C1, C3, and C.

Table 9 shows the CPP summer load scheduling results for 700 EVs during scheduling scheme 1 (autonomous) and scheduling scheme 2 (coordinated). During autonomous mode, the ABC algorithm performed better by reducing all four costs such as C1, C2, C3, and C. The PSO algorithm performed better by reducing one cost, such as C2. Both ABC and PSO algorithms performed better during coordinated mode by reducing all four costs such as C1, C2, C3, and C. Significant reduction in cost C3 is observed during both ABC and PSO algorithms. However, ABC reduced C3 cost twice as compared to PSO.

3) RTEP SCHEDULED SUMMER LOAD

Fig. 39a and Fig. 39b show PSO-based RTEP summer load scheduling with 80 EVs in autonomous and coordinated modes. Excess energy from DGs is supplied to the grid (0100-0300). EV charging load is negligible during the starting day (0100-1400), while EVs' charging load increases during the second half-day (1500-2400), and Excess energy

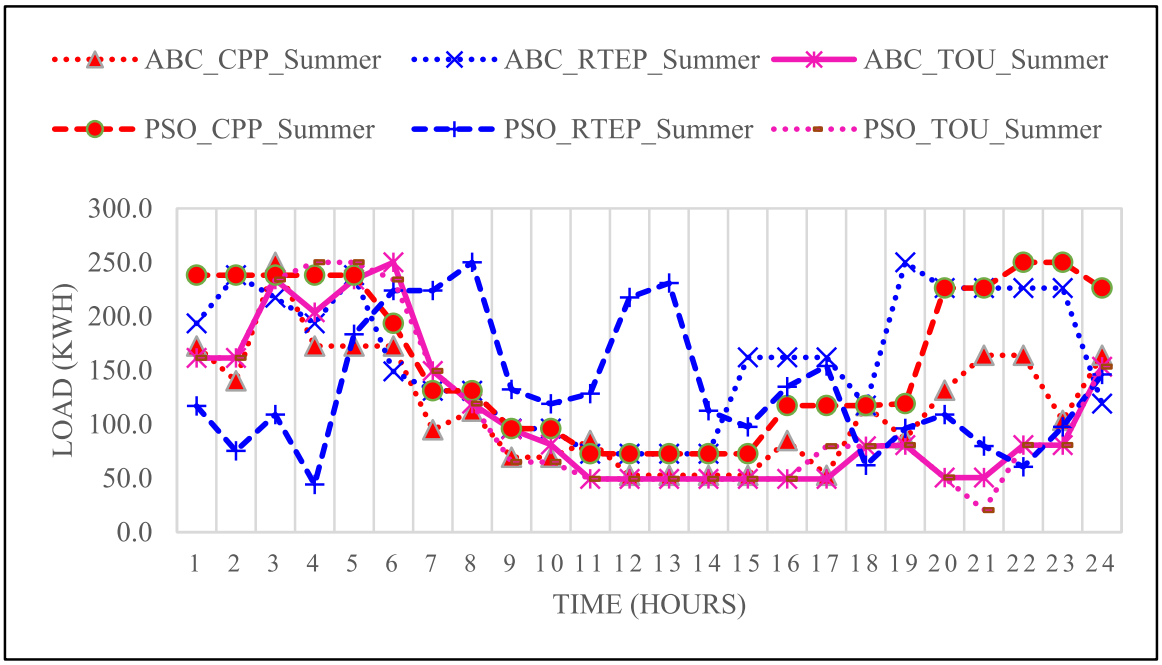

FIGURE 25. Scheduled load profile for summer.

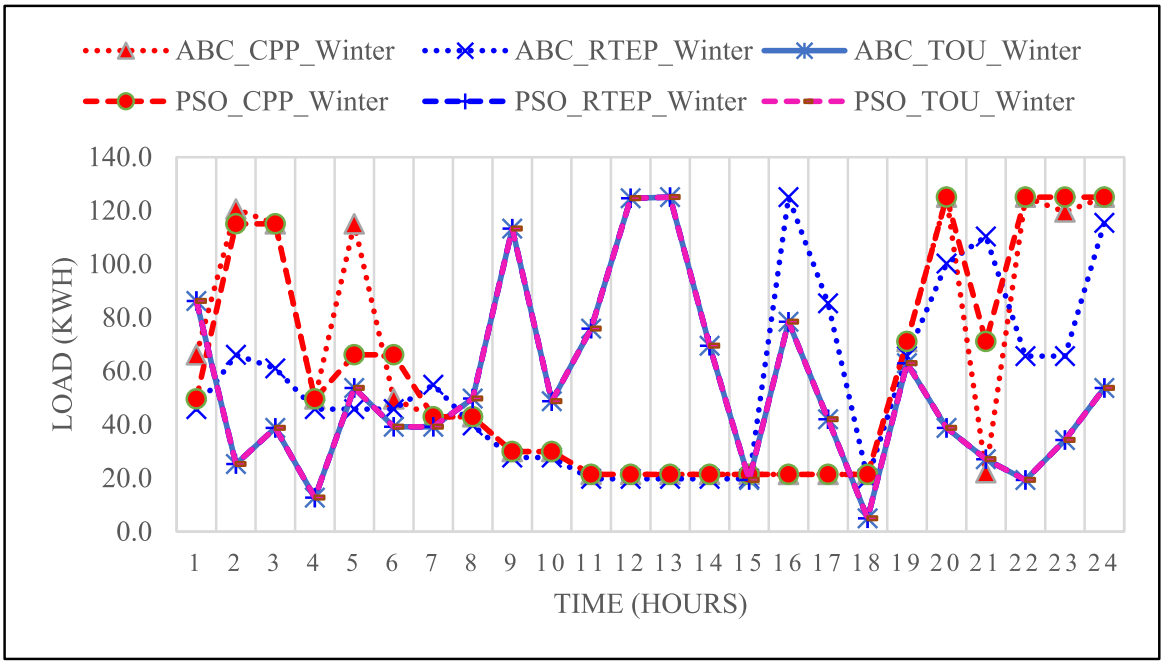

FIGURE 26. Scheduled load profile for winter.

from DGs is supplied to the grid (1700-2200). EVs charging load is significant during the start of the day (0100-0700), while EVs discharging load is significantly increased during the second half of the day (1700-2400). DE is supplying almost constant power.

Fig. 40a and Fig. 40b show ABC-based RTEP summer load scheduling with 80 EVs in autonomous and coordinated modes. Excess energy from DGs is supplied to the grid (0500, 0800, 1000, 1200-1300). EVs charging load is significant during the starting day (0100-1400), while EVs' charging load increases during the second half-day (1500-2400). Excess energy from DGs is supplied to the grid (0800-1000, 1200-1300, 1700-2100, 2300-2400). EVs charging load is significant during the start of the day (0100-0700), while EVs discharging load is significantly increased during the second half of the day (1700-2400).

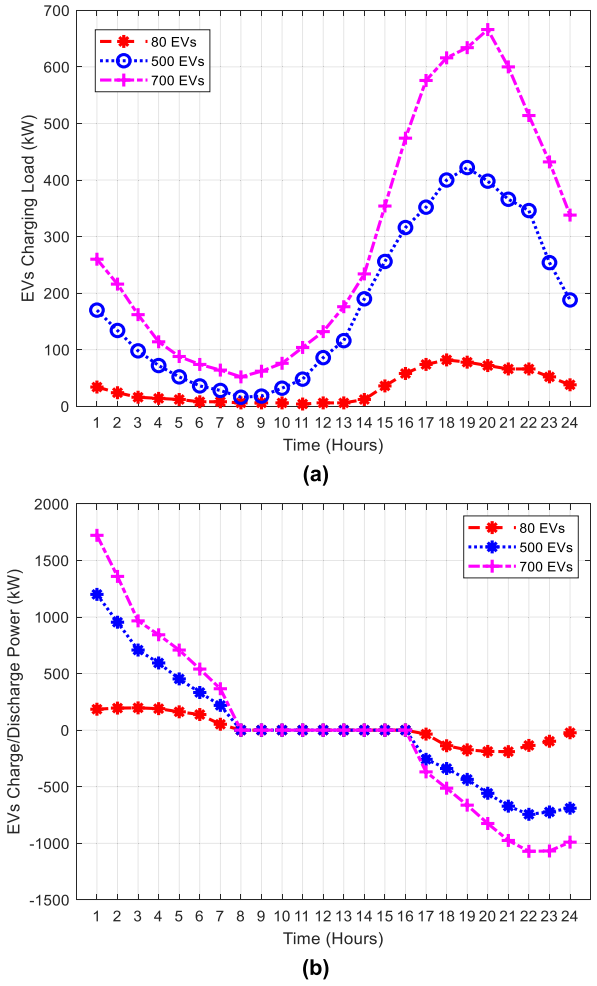

FIGURE 27. The load profile (a) autonomous mode; (b) coordinated mode.

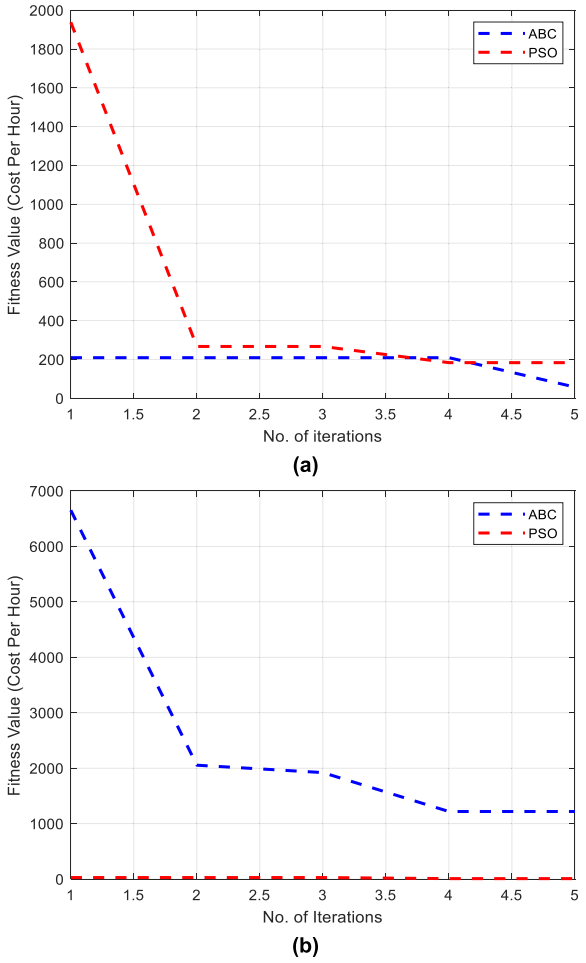

FIGURE 28. Unscheduled convergence value for PSO and ABC with 80 EVs (a) autonomous mode; (b) coordinated mode.

Fig. 41a and Fig. 41b show PSO-based RTEP summer load scheduling with 700 EVs in autonomous and coordinated modes. EVs charging load is significant during the autonomous mode throughout the daytime with a 700 kW peak at night (2000). During coordinated mode, excess energy from DGs is supplied to the grid at night (1600-2400). EVs charging load is more during the starting day (0100-0700), while EVs discharging load is significant at night (1700-2400).

Fig. 42a and Fig. 42b show ABC-based RTEP summer load scheduling with 700 EVs in autonomous and coordinated modes. The almost same trend of PSO-based modes is observed during autonomous and coordinated modes.

Table 10 shows RTEP summer load scheduling results for 80 EVs during autonomous and coordinated modes. The PSO algorithm performed better during autonomous mode by reducing one cost, such as C2. The PSO algorithm performed better during coordinated mode by reducing three costs such as the C1, C3, and C.

Table 11 shows RTEP summer load scheduling results for 700 EVs during autonomous and coordinated, while the

TABLE 8. CPP summer dispatch results under scheduling schemes 1 and 2 for 80 EVs.

Algo	Cost	scheme 1	scheme 2	%Δ1	%Δ2
PSO	C1	5186.1172	4384.167	19.19	11.97
	C2	932.0747	701.9687	3.42	67.89
	C3	513.8481	403.8925	24.73	19.50
	C	3598.1115	3016.3204	18.22	15.44
ABC	C1	3731.6331	2745.6717	-13.30	-32.14
	C2	696.014	660.1927	-23.48	34.88
	C3	324.5822	201.2626	-20.24	-50.23
	C	2590.8145	1940.5928	-14.10	-26.44

TABLE 9. CPP summer dispatch results under scheduling schemes 1 and 2 for 700 EVs.

Algo	Cost	scheme 1	scheme 2	%Δ1	%Δ2
PSO	C1	10595.9371	2003.0116	0.71	-45.78
	C2	1109.505	544.4679	-8.47	-20.29
	C3	1182.8848	104.0419	0.61	-112.7
	C	7160.0451	1427.4476	0.34	-43.78
ABC	C1	9895.6486	1674.6548	-8.05	-72.14
	C2	1203.6935	530.9025	-6.03	-29.56
	C3	1093.5975	63.6757	-9.02	-244.0
	C	6728.9418	1210.5541	-7.98	-68.26

ABC algorithm performed better during autonomous mode by reducing all four costs. Both ABC and PSO algorithms performed better during coordinated mode by reducing all

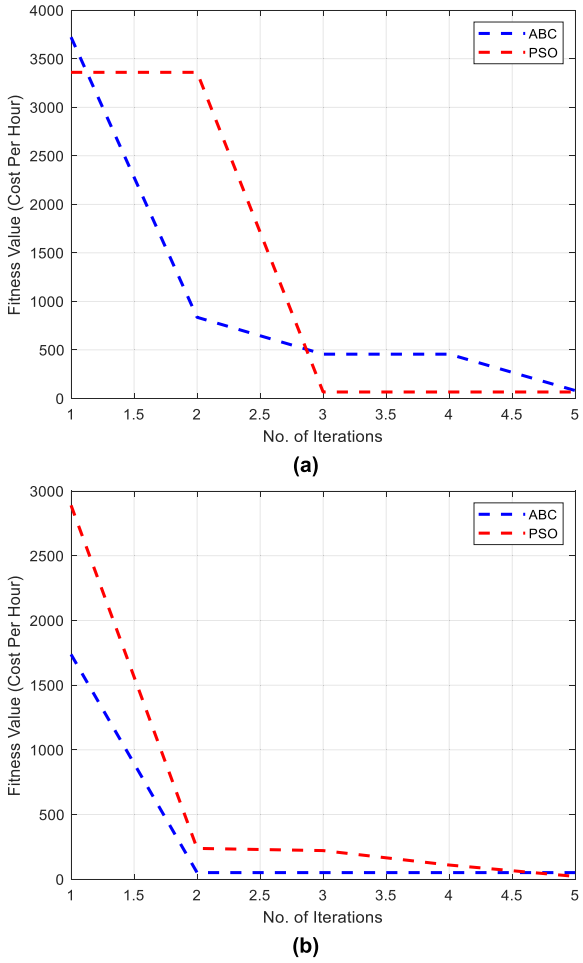

FIGURE 29. Summer RTEP convergence value for PSO and ABC with 80 EVs (a) autonomous mode; (b) coordinated mode.

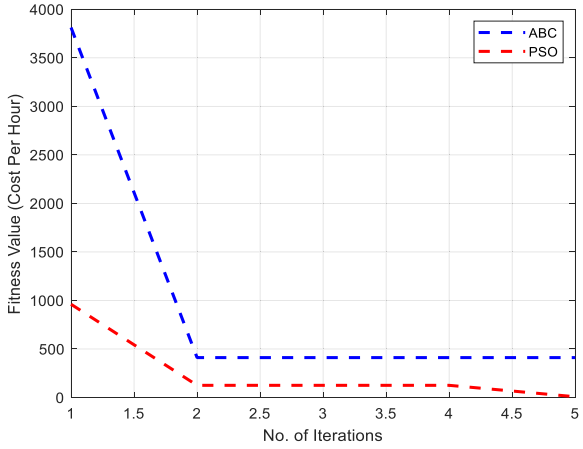

FIGURE 30. Summer RTEP convergence value for PSO and ABC with 80 EVs with coordinated mode.

four costs. A significant reduction in cost C3 is observed during the ABC algorithm.

4) TOU SCHEDULED SUMMER LOAD

Fig. 43a and Fig. 43b show PSO-based TOU summer load scheduling with 80 EVs in autonomous and coordinated

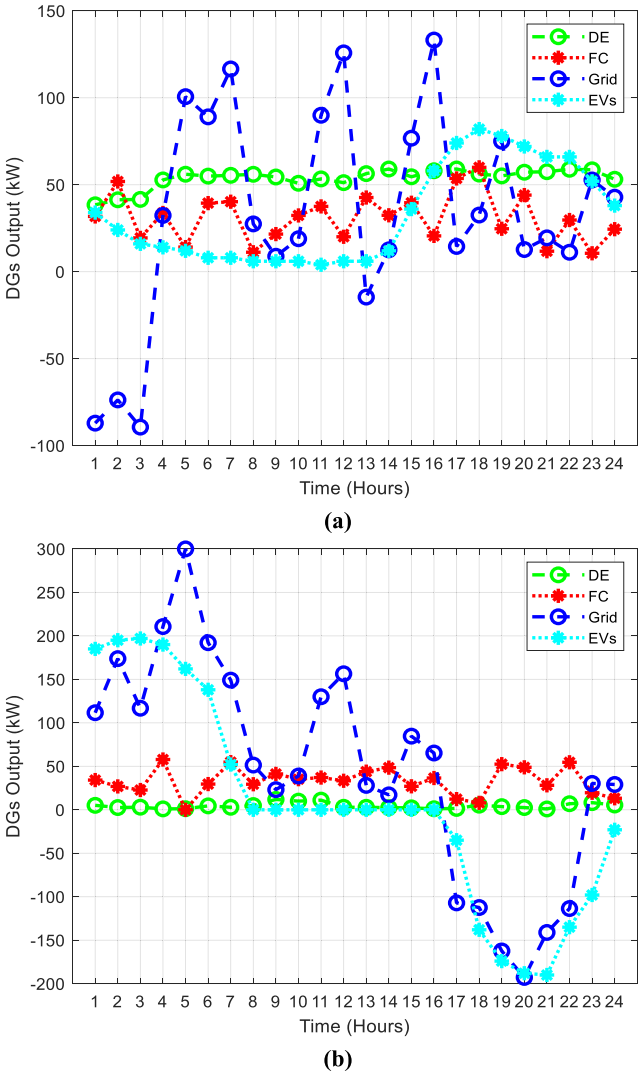

FIGURE 31. PSO-based unscheduled economic dispatch with 80 EVs (a) autonomous mode; (b) coordinated mode.

modes. Excess energy from DGs is supplied to the grid (0800-1300). EV charging load is negligible during the starting day (0100-1400), while EVs' charging load increases during the second half-day (1500-2400), and excess energy from DGs is supplied to the grid (0700-2400). EVs charging load is significant during the start of the day (0100-0700), while EVs discharging load is significantly increased during the second half of the day (1700-2400).

Fig. 44a and Fig. 44b show ABC-based TOU summer load scheduling with 80 EVs in autonomous and coordinated modes. Excess energy from DGs is supplied to the grid (1000-1300). EVs charging load is small during the starting day (0100-1400), while EVs' charging load increases during the second half-day (1500-2400). Excess energy from DGs is supplied to the grid (1000-1300). EVs charging load is small during the starting day (0100-1400), while EVs' charging load increases during the second half-day (1500-2400).

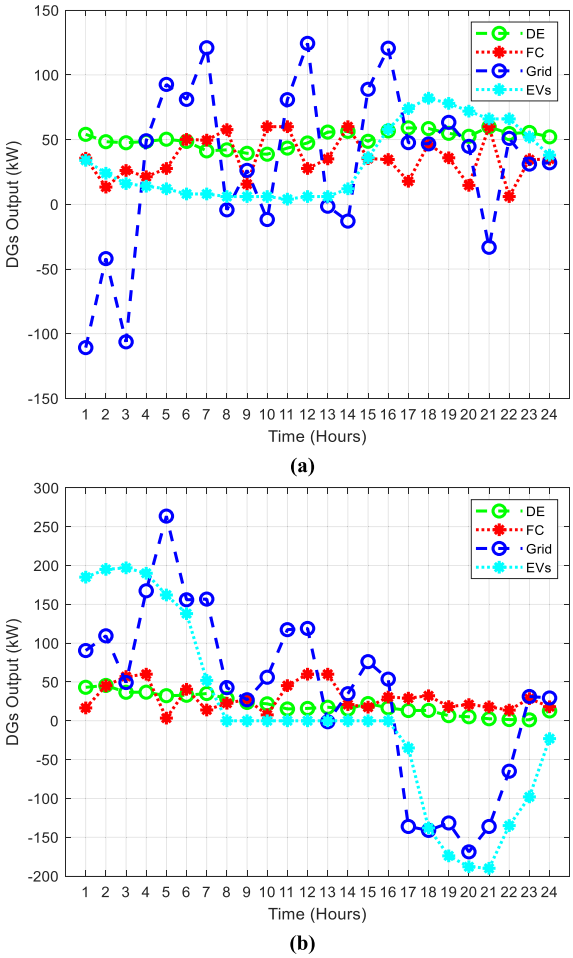

FIGURE 32. ABC-based unscheduled economic dispatch with 80 EVs (a) autonomous mode; (b) coordinated mode.

TABLE 10. RTEP summer dispatch results under scheduling schemes 1 and 2 for 80 EVs.

Algo	Cost	scheme 1	scheme 2	%Δ1	%Δ2
PSO	C1	4490.4929	3570.7595	6.67	-8.08
	C2	616.3269	504.0715	-46.06	55.29
	C3	418.9732	299.067	7.68	-8.71
	C	3063.5077	2436.0878	3.95	-4.70
ABC	C1	5132.2481	4231.2533	17.62	14.26
	C2	964.595	858.2117	10.90	49.91
	C3	506.0443	391.0309	22.88	22.68
	C	3571.3798	2957.9254	17.23	17.05

TABLE 11. RTEP summer dispatch results under scheduling schemes 1 and 2 for 700 EVs.

Algo	Cost	scheme 1	scheme 2	%Δ1	%Δ2
PSO	C1	10582.1336	2844.2494	0.58	-2.66
	C2	1400.4876	563.6082	14.07	-16.20
	C3	1191.0367	209.2019	1.29	-5.77
	C	7227.2666	1979.2703	1.27	-3.69
ABC	C1	10374.0237	2155.6655	-3.07	-33.73
	C2	1194.4344	545.3385	-6.85	-26.13
	C3	1154.2757	123.1598	-3.28	-77.85
	C	7037.6282	1526.9147	-3.24	-33.40

Fig. 45a and Fig. 45b show PSO-based TOU summer load scheduling with 700 EVs in autonomous and coordinated modes. EVs charging load is significant during

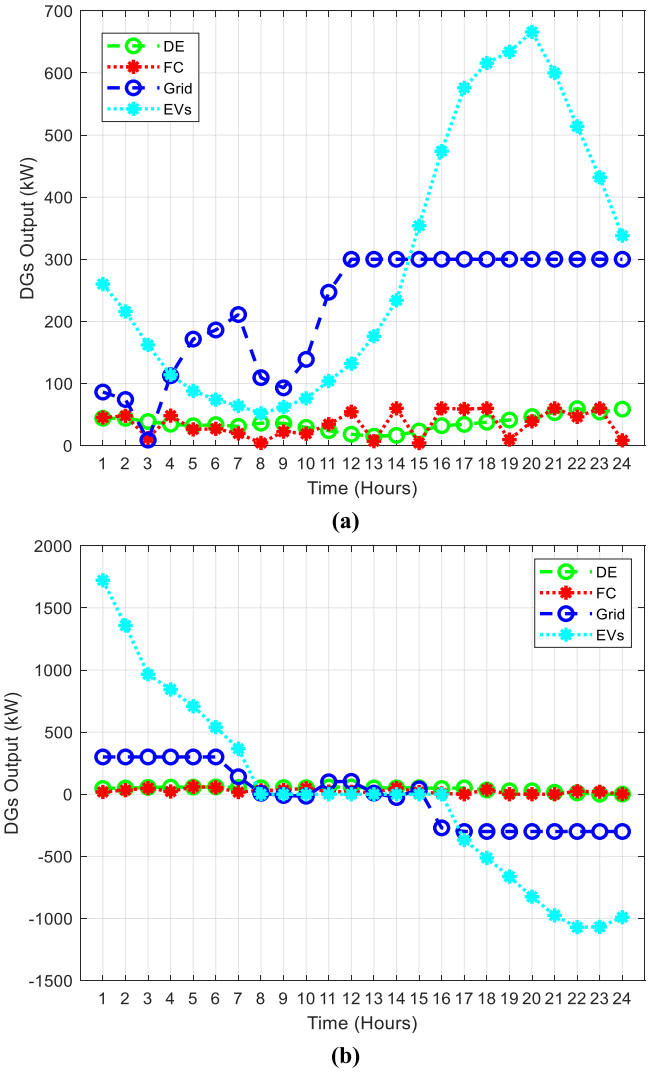

FIGURE 33. PSO-based unscheduled economic dispatch with 700 EVs (a) autonomous mode; (b) coordinated mode.

the autonomous mode throughout the daytime with almost 700 kW peak at night (2000). During coordinated mode, excess energy from DGs is supplied to the grid at night (1600-2400). EVs charging load is more during the starting day (0100-0700), while EVs discharging load is significant at night (1700-2400).

Fig. 46a and Fig. 46b show ABC-based TOU summer load scheduling with 700 EVs in autonomous and coordinated modes. The almost same trend of PSO-based modes is observed during autonomous and coordinated modes.

Table 12 shows TOU summer load scheduling results for 80 EVs during autonomous and coordinated modes. Both PSO and ABC algorithms performed better during autonomous mode by reducing all four costs. A significant reduction in cost C2 is observed during both PSO and ABC algorithms. During coordinated mode, the ABC algorithm performed better by reducing all four costs such as the C1, C2, C3, and C. PSO algorithm performed better by reducing

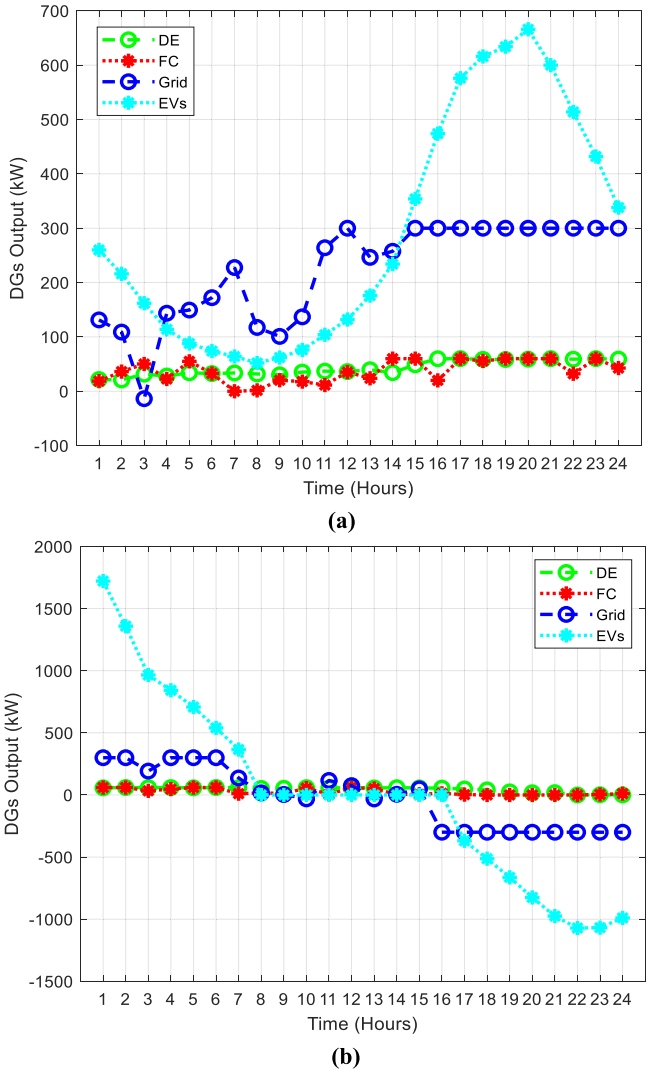

FIGURE 34. ABC-based unscheduled economic dispatch with 700 EVs (a) autonomous mode; (b) coordinated mode.

three costs such as the C1, C3, and C. Significant reduction in cost C3 with PSO and C2 with ABC are observed.

Table 13 shows TOU summer load scheduling results with 700 EVs. The ABC algorithm performed better during autonomous mode with the reduction of all four costs. The PSO algorithm performance is better with a reduction of C1, C3, and C. Both algorithms performed better during coordinated mode by reducing all four costs. A significant reduction in C3 is observed with both algorithms. However, cost reduction with ABC is 1.5 times as compared to PSO.

B. WINTER LOAD

Fig. 47 and Fig. 48 show the unscheduled convergence curves for winter load during autonomous mode for 80 EVs and 700 EVs, respectively. It is observed that the performance of the ABC algorithm is better with 80 EVs, while both performed well with 700 EVs. Table 14 shows the computational burden of unscheduled load under different circumstances.

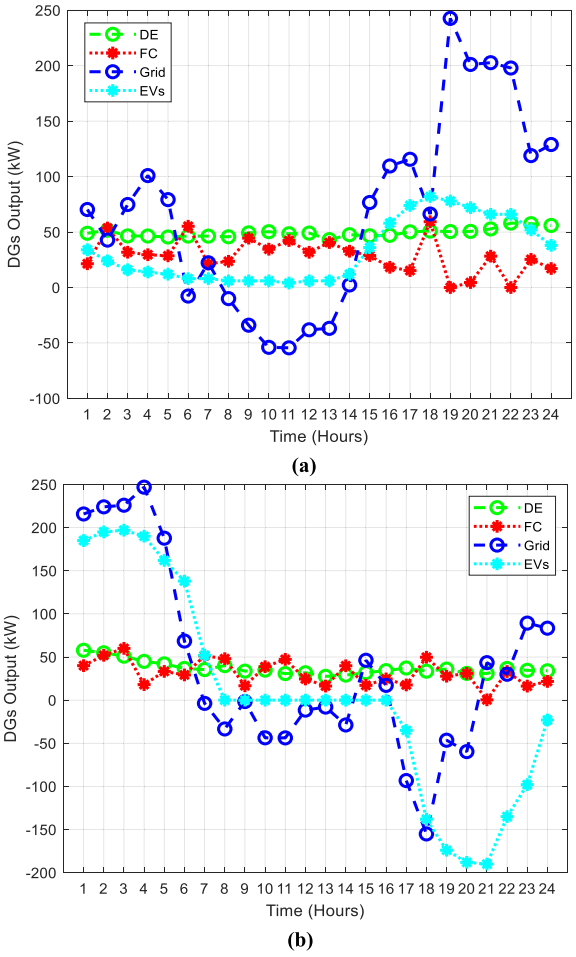

FIGURE 35. PSO-based summer CPP scheduled economic dispatch with 80 EVs (a) autonomous mode; (b) coordinated mode.

TABLE 12. TOU summer dispatch results under scheduling schemes 1 and 2 for 80 EVs.

Algo	Cost	**scheme** 1	**scheme** 2	%Δ1	%Δ2
PSO	C1	3869.1977	2514.3656	-8.32	-53.49
	C2	301.1446	615.4427	-198.92	63.38
	C3	329.2558	166.9843	-17.47	-94.70
	C	2576.9377	1778.103	-14.19	-43.45
ABC	C1	3879.5221	2867.2609	-8.98	-26.53
	C2	282.255	251.0342	-204.50	-71.25
	C3	329.4609	203.0022	-18.46	-48.94
	C	2578.6566	1912.5417	-14.63	-28.30

These table values are used as the base values for the comparison of three DRPs.

Fig. 49 and Fig. 50 show the convergence curves for CPP winter tariff during autonomous mode for 80 EVs and 700 EVs, respectively. It is observed that the performance of the ABC algorithm is better with 80 EVs, while both performed well with 700 EVs. Table 15 shows data for the CPP winter tariff. During the CPP winter tariff, no significant reduction of computational burden is observed. The simulation time reduction is only observed with PSO for 700 EVs in autonomous mode. All remaining scenarios show more computational burden as compared to the base case.

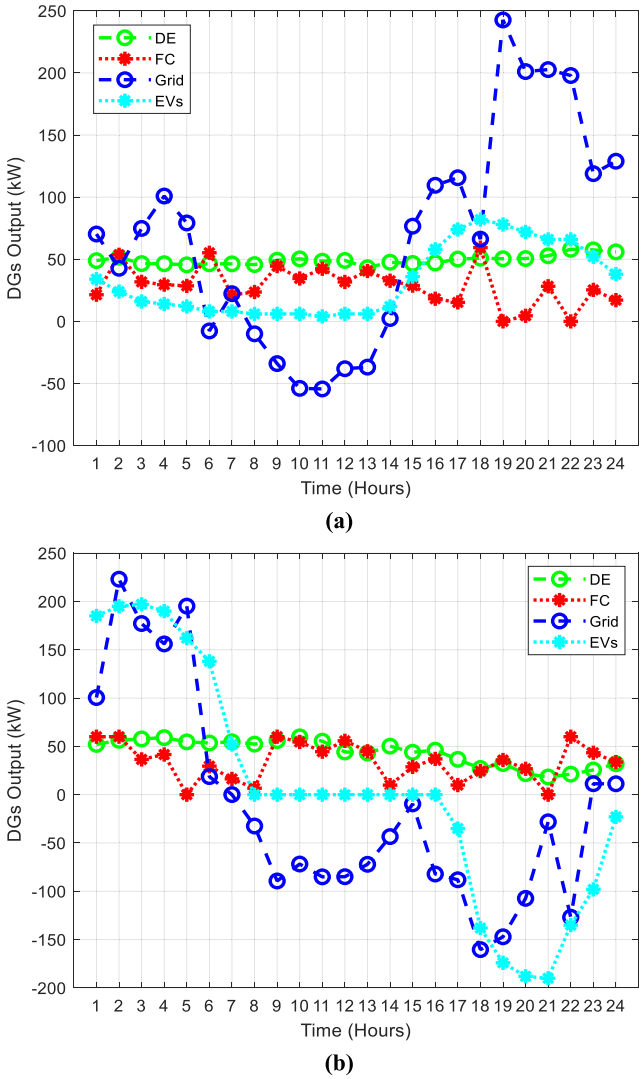

FIGURE 36. ABC-based summer CPP scheduled economic dispatch with 80 EVs (a) autonomous mode; (b) coordinated mode.

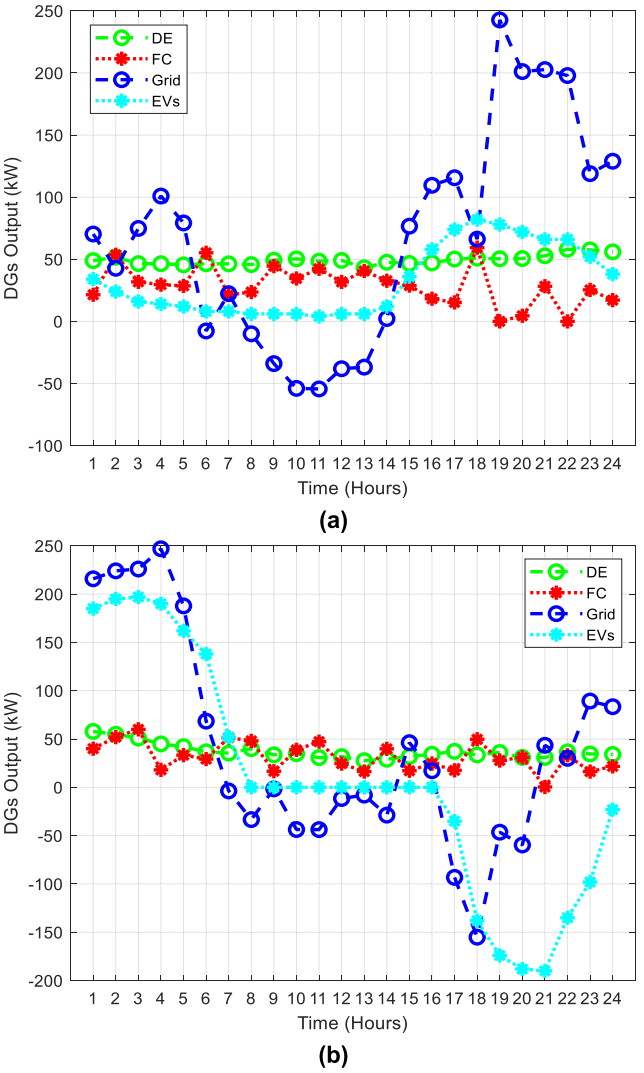

FIGURE 37. PSO-based summer CPP scheduled economic dispatch with 700 EVs (a) autonomous mode; (b) coordinated mode.

TABLE 13. TOU summer dispatch results under scheduling schemes 1 and 2 for 700 EVs.

Algo	Cost	**scheme** 1	**scheme** 2	%Δ1	%Δ2
PSO	C1	10158.3374	1733.6682	-3.57	-68.43
	C2	1330.2227	645.6531	9.53	-1.44
	C3	1136.3743	75.1876	-3.46	-194.29
	C	6933.4358	1278.991	-2.92	-60.46
ABC	C1	10252.1723	1605.2185	-4.30	-79.59
	C2	1155.633	506.1934	-10.44	-35.88
	C3	1135.3931	54.1511	-5.00	-304.49
	C	6948.0094	1158.9436	-4.57	-75.75

Fig. 51 and Fig. 52 show the convergence curves for the RTEP winter tariff. It is observed that the performance of the PSO algorithm is better for both cases, with 80 EVs and 700 EVs in autonomous mode. Table 16 shows the data of simulation time for RTEP winter tariff. During the RTEP winter tariff, no significant reduction in computational burden is observed. All scenarios show more computational burden as compared to the base case.

TABLE 14. Comparative analysis of computational burden between two algorithms for unscheduled load.

Algorithm	EVs	Mode	Simulation time/s
PSO	80	Autonomous	2.225139
ABC	80	Autonomous	3.003032
PSO	80	Coordinated	2.205948
ABC	80	Coordinated	3.023931
PSO	700	Autonomous	2.223305
ABC	700	Autonomous	3.000195
PSO	700	Coordinated	2.177649
ABC	700	Coordinated	3.073849

Fig. 53 shows the convergence curve for the TOU winter tariff. It is observed that the performance of both algorithms is better in coordinated mode with 80 EVs. Table 17 shows the data of simulation time for the TOU winter tariff. During the TOU winter tariff, no significant reduction in computational

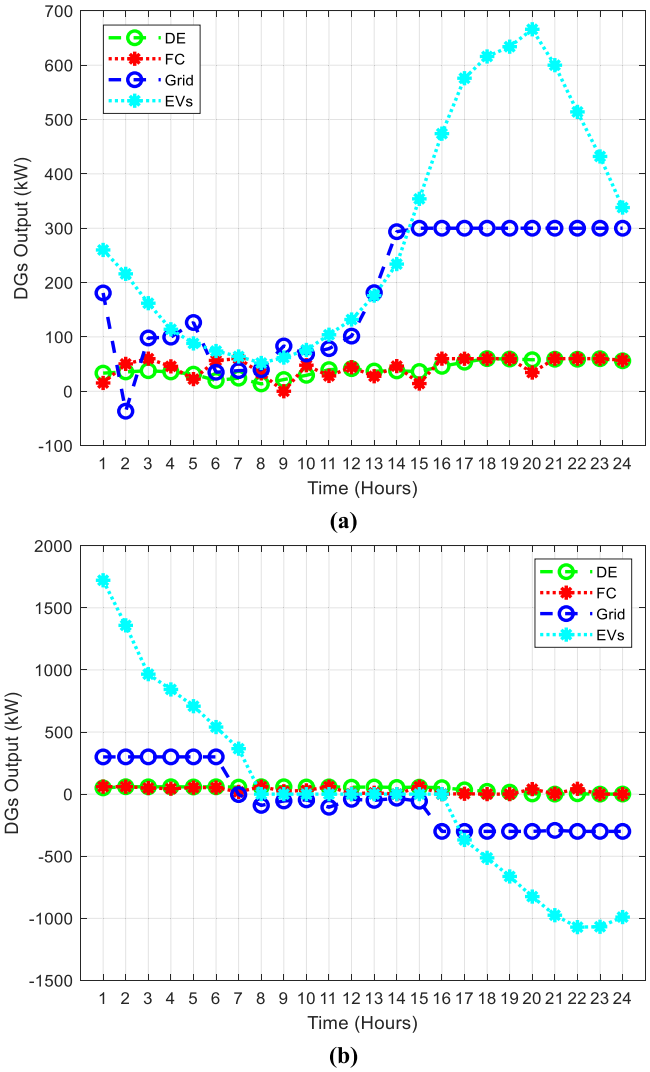

FIGURE 38. ABC-based summer CPP scheduled economic dispatch with 700 EVs (a) autonomous mode; (b) coordinated mode.

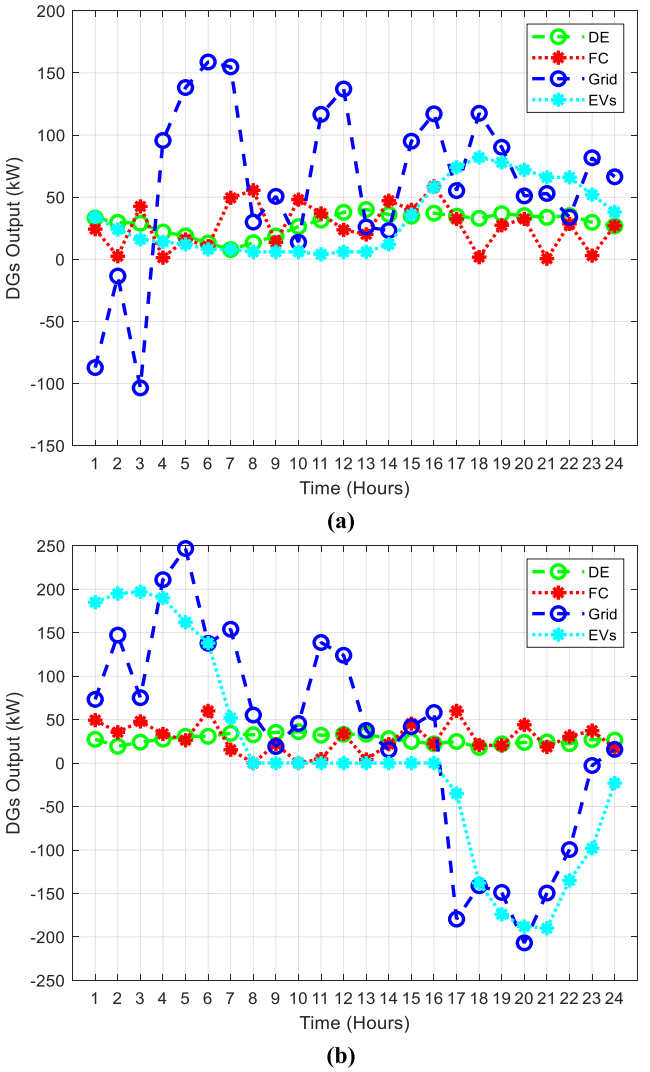

FIGURE 39. PSO-based summer RTEP scheduled economic dispatch with 80 EVs (a) autonomous mode; (b) coordinated mode.

TABLE 15. Comparative analysis of computational burden between two algorithms for winter CPP.

Algorithm	EVs	Mode	Simulation time/s	%Δ
PSO	80	Autonomous	2.245979	0.93
ABC	80	Autonomous	3.066589	2.07
PSO	80	Coordinated	2.222352	0.74
ABC	80	Coordinated	3.027236	0.11
PSO	700	Autonomous	2.185886	-1.71
ABC	700	Autonomous	3.086529	2.80
PSO	700	Coordinated	2.688031	18.99
ABC	700	Coordinated	3.213368	4.34

burden is observed. All scenarios show more computational burden as compared to the base case.

1) UNSCHEDULED WINTER LOAD

Fig. 54a and Fig. 54b show PSO-based unscheduled winter load scheduling with 80 EVs in autonomous and coordinated modes. Excess energy from DGs is supplied to the grid (0100-0700, 0900-1000, 1300-1400, 1900-2400). EVs charging load is negligible during the starting day (0100-1400), while EVs' charging load increases during the second half-day (1500-2400). Excess energy from DGs is supplied to the grid (0600, 0900, 1300-2400). EVs charging load is significant during the start of the day (0100-0700), while EVs discharging load is significantly increased during the second half of the day (1700-2400).

Fig. 55a and Fig. 55b show ABC-based unscheduled winter load scheduling with 80 EVs in autonomous and coordinated modes. Excess energy from DGs is supplied to the grid (0100-0700, 1000, 1300-1400, 2100-2400). EVs charging load is small during the starting day (0100-1400), while EVs' charging load increases during the second half-day (1500-2400). Excess energy from DGs is supplied to the grid (0600-0700, 0900, 1300-2400). EVs charging load is small during the

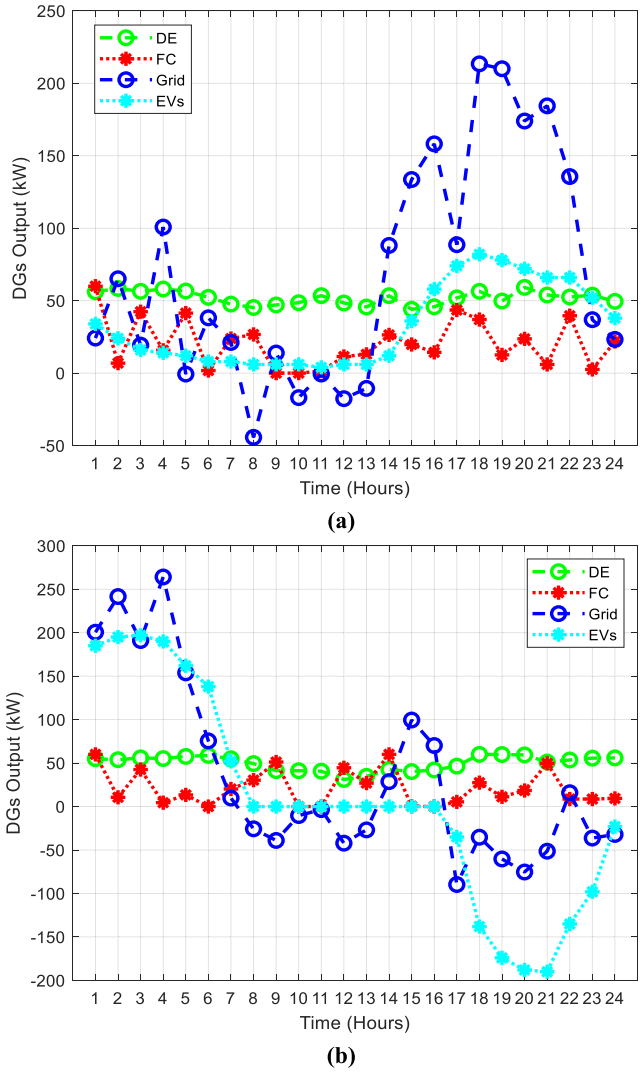

FIGURE 40. ABC-based summer RTEP scheduled economic dispatch with 80 EVs (a) autonomous mode; (b) coordinated mode.

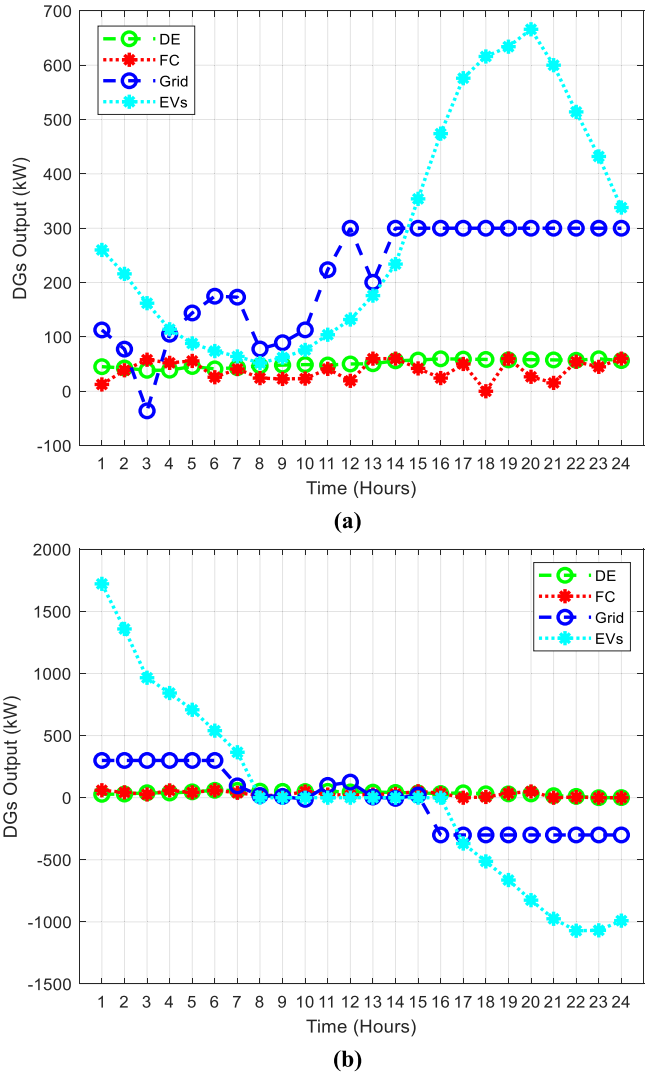

FIGURE 41. PSO-based summer RTEP scheduled economic dispatch with 700 EVs (a) autonomous mode; (b) coordinated mode.

TABLE 16. Comparative analysis of computational burden between two algorithms for winter RTEP.

Algorithm	EVs	Mode	Simulation time/s	%Δ
PSO	80	Autonomous	2.342861	5.02
ABC	80	Autonomous	3.284263	8.56
PSO	80	Coordinated	2.238205	1.44
ABC	80	Coordinated	3.065467	1.35
PSO	700	Autonomous	2.284734	2.69
ABC	700	Autonomous	3.122689	3.92
PSO	700	Coordinated	2.285992	4.74
ABC	700	Coordinated	3.113650	1.28

TABLE 17. Comparative analysis of computational burden between two algorithms for winter TOU.

Algorithm	EVs	Mode	Simulation time/s	%Δ
PSO	80	Autonomous	2.271931	2.06
ABC	80	Autonomous	3.147521	4.59
PSO	80	Coordinated	2.658108	17.01
ABC	80	Coordinated	3.294661	8.22
PSO	700	Autonomous	2.311524	3.82
ABC	700	Autonomous	3.441829	12.83
PSO	700	Coordinated	2.252925	3.34
ABC	700	Coordinated	3.177120	3.25

starting day (0100-1400), while EVs' charging load increases during the second half-day (1500-2400).

Fig. 56a and Fig. 56b show PSO-based unscheduled winter load scheduling with 700 EVs in autonomous and coordinated modes. EVs charging load is significant during the autonomous mode throughout the daytime with almost 700 kW peak at night (2000). During coordinated mode, excess energy from DGs is supplied to the grid at night (1600-2400). EVs charging load is more during the starting day (0100-0700), while EVs discharging load is significant at night (1700-2400).

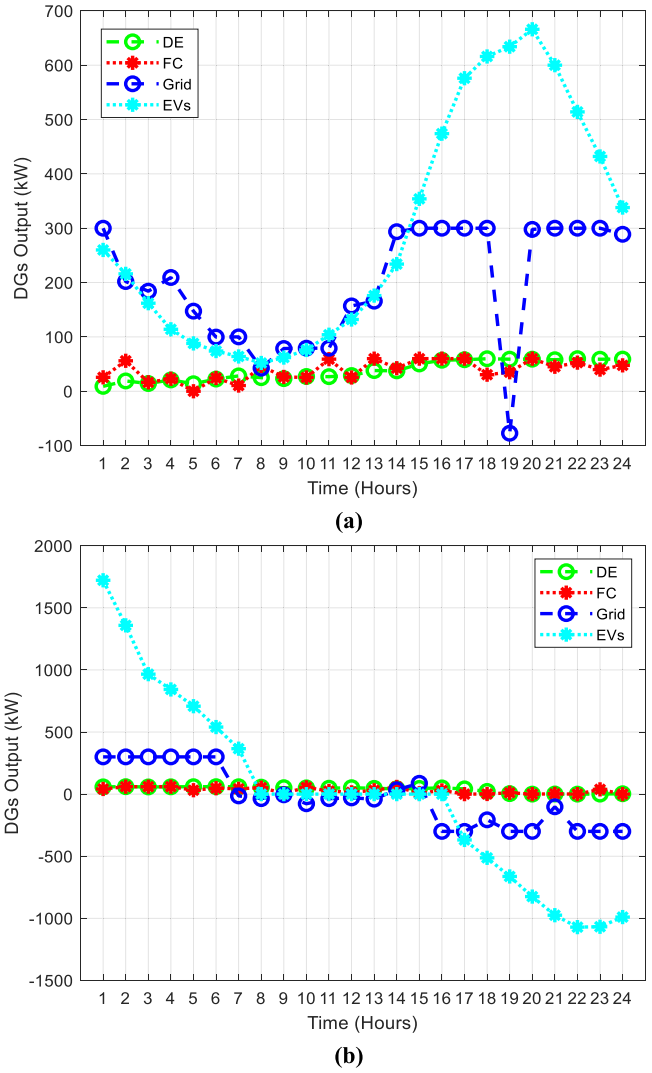

FIGURE 42. ABC-based summer RTEP scheduled economic dispatch with 700 EVs (a) autonomous mode; (b) coordinated mode.

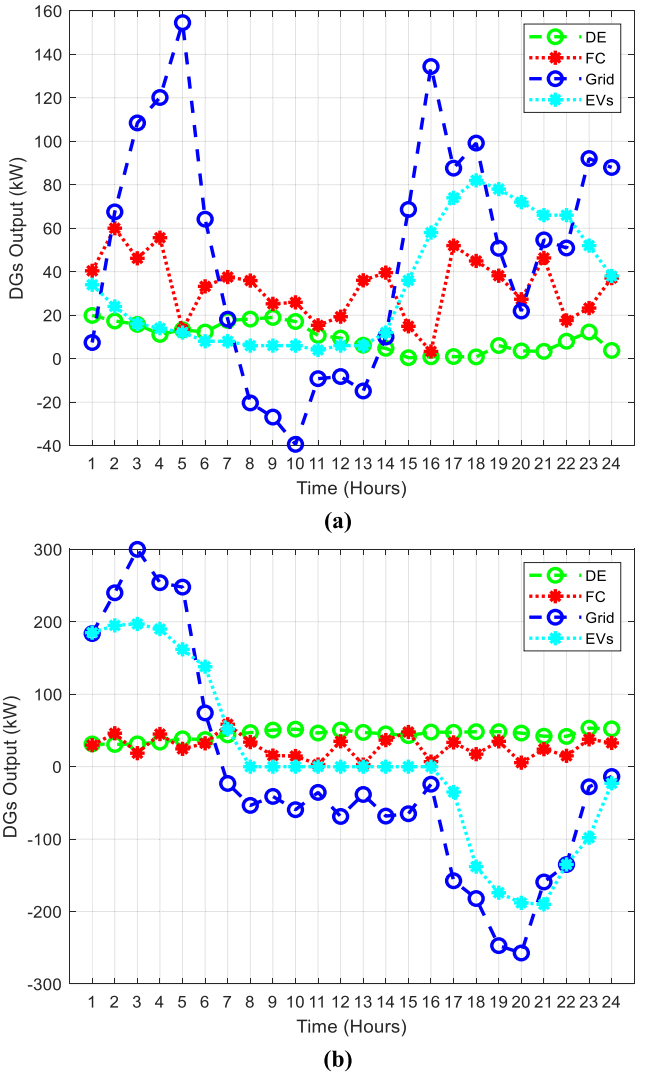

FIGURE 43. PSO-based summer TOU scheduled economic dispatch with 80 EVs (a) autonomous mode; (b) coordinated mode.

TABLE 18. Dispatch results under scheduling schemes 1 and 2 for 80 EVs.

Algorithm	Cost objective	scheme 1	scheme 2
PSO	C1	1521.3236	866.982
	C2	525.3294	164.9139
	C3	42.3393	49.6141
	C	1109.2086	600.0594
ABC	C1	1968.5864	815.6616
	C2	112.8522	236.3278
	C3	86.0131	51.1249
	C	1292.1448	585.9727

TABLE 19. Dispatch results under scheduling schemes 1 and 2 for 700 EVs.

Algorithm	Cost objective	scheme 1	scheme 2
PSO	C1	8659.9236	1841.7634
	C2	1000.2083	616.31
	C3	941.8109	85.7642
	C	5873.3327	1341.3757
ABC	C1	8717.5761	1726.5516
	C2	907.04	529.5349
	C3	938.9377	72.6437
	C	5885.6912	1244.198

Fig. 57a and Fig. 57b show ABC-based, unscheduled winter load scheduling with 700 EVs in autonomous and coordinated modes. Almost the same trend of PSO-based modes is observed during autonomous and coordinated modes.

Table 18 and Table 19 shows unscheduled load results during scheduling scheme 1 (autonomous) and scheduling scheme 2 (coordinated), respectively. The data of these tables are used as the base case for three DRPs.

2) CPP SCHEDULED WINTER LOAD

Fig. 58a and Fig. 58b show PSO-based CPP winter load scheduling with 80 EVs in autonomous and coordinated modes. Excess energy from DGs is supplied to the grid (0100-1400). EVs' charging load is negligible during the starting day (0100-1400), while EVs' charging load increases during the second half-day (1500-2400), and Excess energy

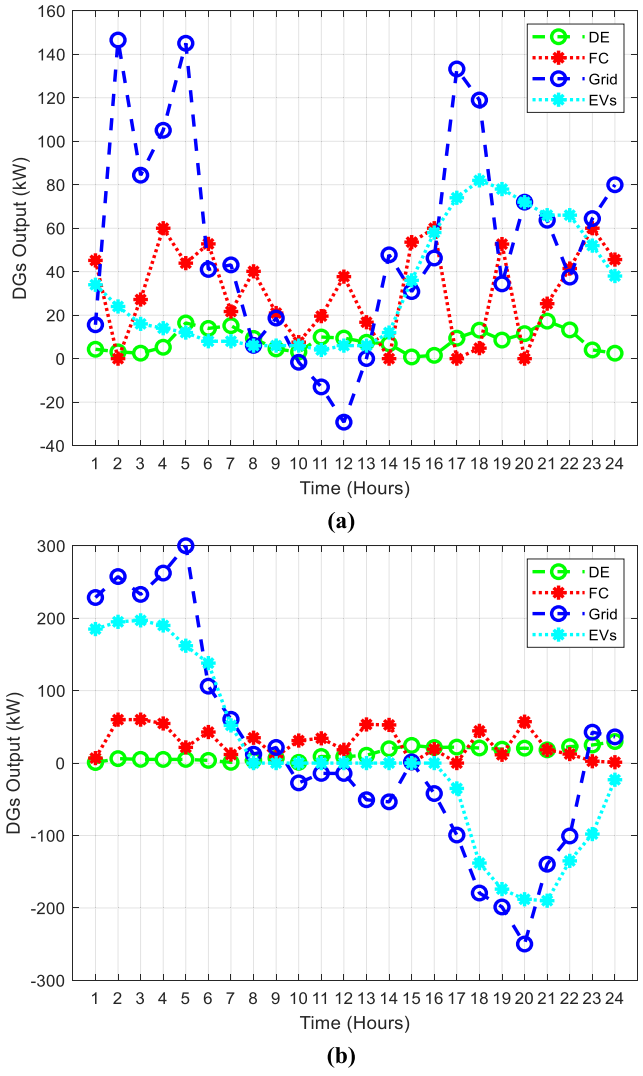

FIGURE 44. ABC-based summer TOU scheduled economic dispatch with 80 EVs (a) autonomous mode; (b) coordinated mode.

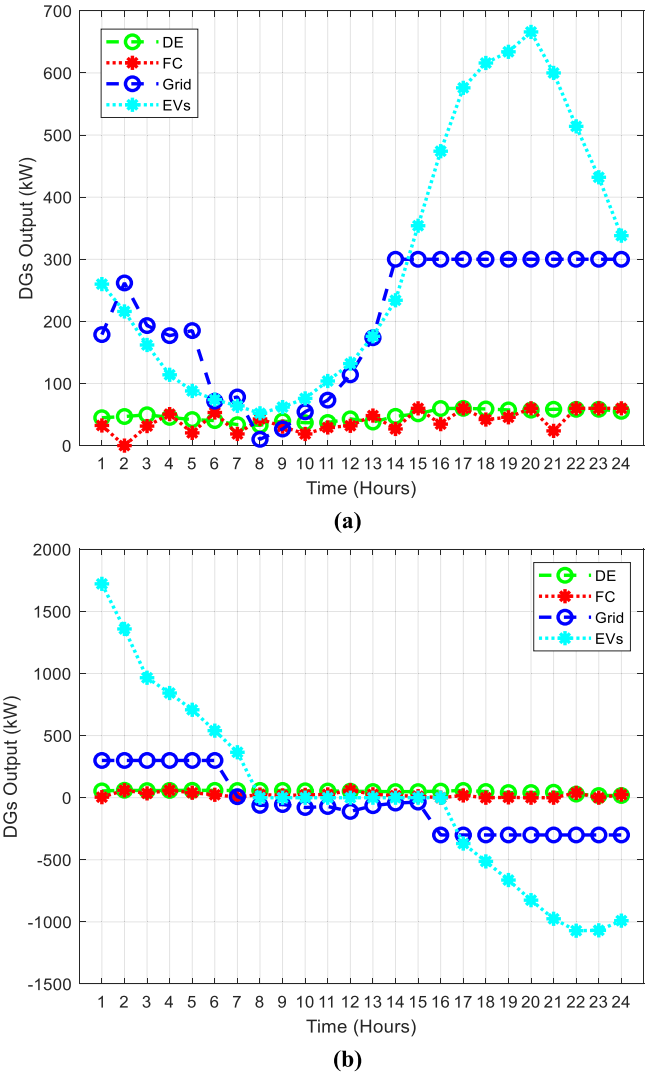

FIGURE 45. PSO-based summer TOU scheduled economic dispatch with 700 EVs (a) autonomous mode; (b) coordinated mode.

from DGs is supplied to the grid (0600-2400). EVs charging load is significant during the start of the day (0100-0700), while EVs discharging load is significantly increased during the second half of the day (1700-2400).

Fig. 59a and Fig. 59b show ABC-based CPP winter load scheduling with 80 EVs in autonomous and coordinated modes, respectively. Excess energy from DGs is supplied to the grid (0100-1700, 2000). EVs' charging load is small during the starting day (0100-1400), while EVs' charging load increases during the second half-day (1500-2400), and Excess energy from DGs is supplied to the grid (0600-2200). EVs charging load is large during the starting day (0100-0700), while EVs' discharging load increases during the second half-day (1700-2400).

Fig. 60a and Fig. 60b show PSO-based CPP winter load scheduling with 700 EVs in autonomous and coordinated modes, respectively. EVs charging load is significant during the autonomous mode throughout the daytime with almost 700 kW peak at night (2000). During coordinated mode, excess energy from DGs is supplied to the grid at night (1600-2400). EVs charging load is more during the starting day (0100-0700), while EVs discharging load is significant at night (1700-2400).

Fig. 61a and Fig. 61b show ABC-based CPP winter load scheduling with 700 EVs in autonomous and coordinated modes. The almost same trend of PSO-based modes is observed during autonomous and coordinated modes.

Table 20 shows CPP winter load scheduling results for 80 EVs during scheduling scheme 1 (autonomous) and scheduling scheme 2 (coordinated). During autonomous mode, the ABC algorithm performed well by reducing three costs, such as C1, C3, and C. PSO algorithm performed well by reducing one cost such as C2. The ABC algorithm performed better during coordinated mode by reducing one cost, such as C3. PSO algorithm performed better by reducing one cost such as C1.

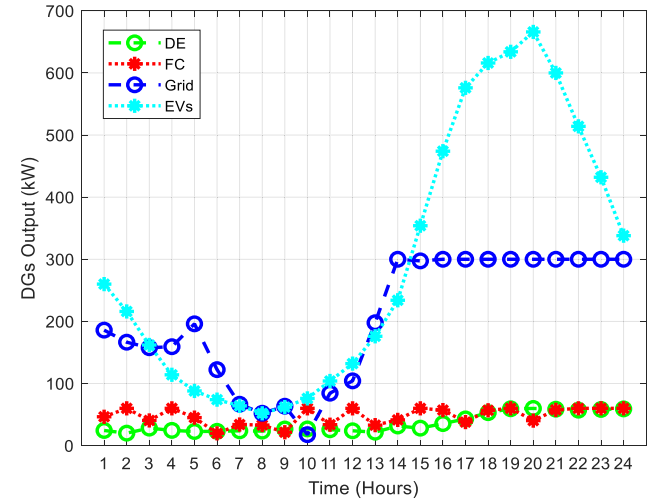

(a)

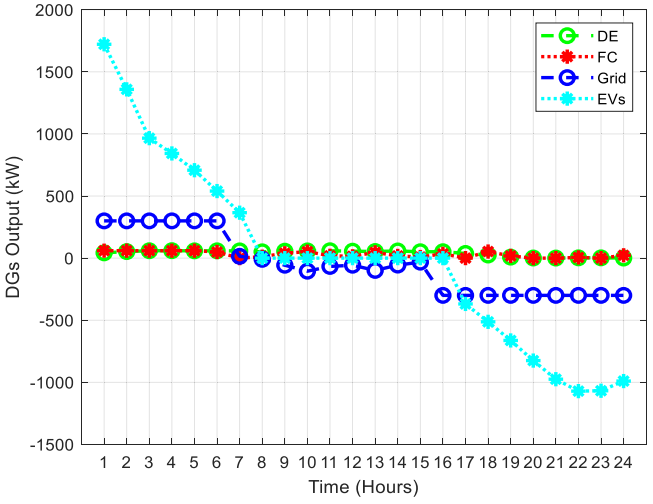

(b)

FIGURE 46. ABC-based summer TOU scheduled economic dispatch with 700 EVs (a) autonomous mode; (b) coordinated mode.

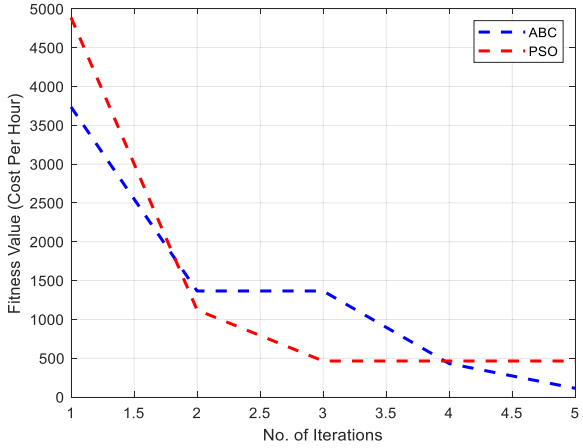

FIGURE 47. Unscheduled convergence value for PSO and ABC with 80 EVs with an autonomous mode.

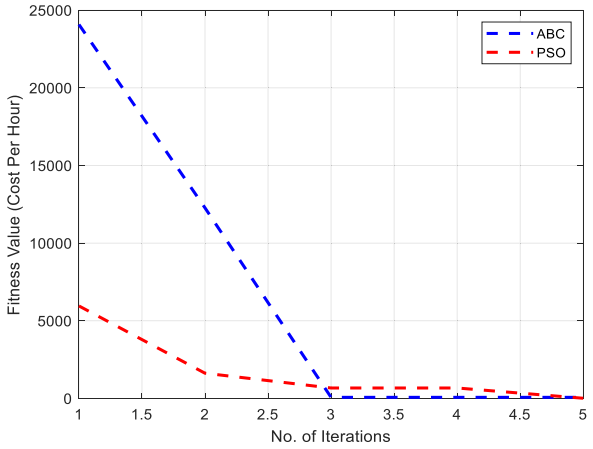

FIGURE 48. Unscheduled convergence value for PSO and ABC with 700 EVs with an autonomous mode.

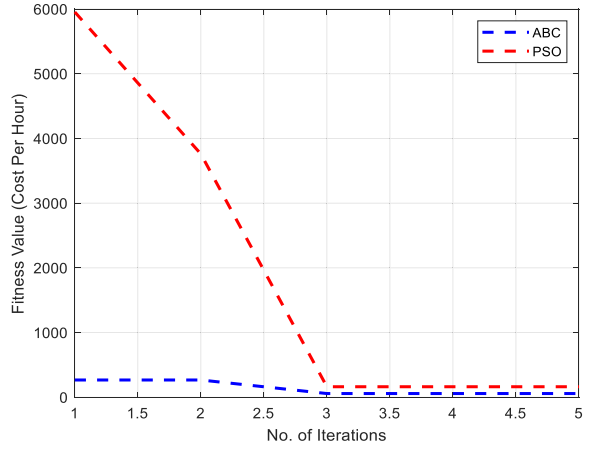

FIGURE 49. Winter CPP convergence value for PSO and ABC with 80 EVs with an autonomous mode.

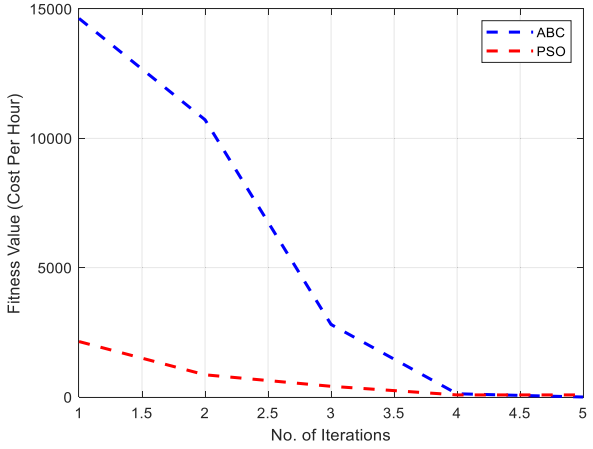

FIGURE 50. Summer CPP convergence value for PSO and ABC with 700 EVs with an autonomous mode.

Table 21 shows the CPP winter load scheduling results for 700 EVs during scheduling scheme 1 (autonomous) and scheduling scheme 2 (coordinated). During autonomous mode, both algorithms performed better by reducing three costs such as C1, C3, and C. During coordinated mode; both algorithms performed better by reducing all four costs.

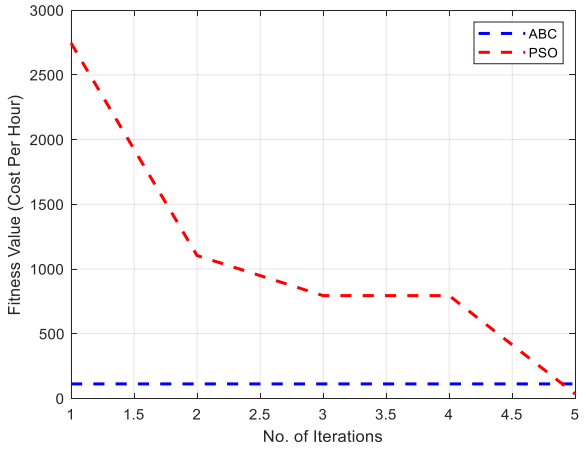

FIGURE 51. Winter RTEP convergence value for PSO and ABC with 80 EVs with an autonomous mode.

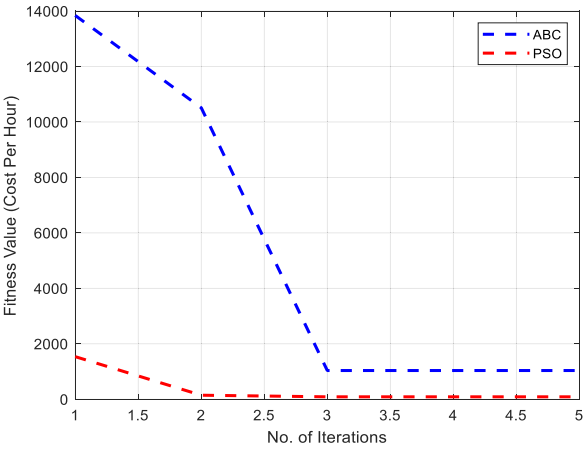

FIGURE 52. Winter RTEP convergence value for PSO and ABC with 700 EVs with an autonomous mode.

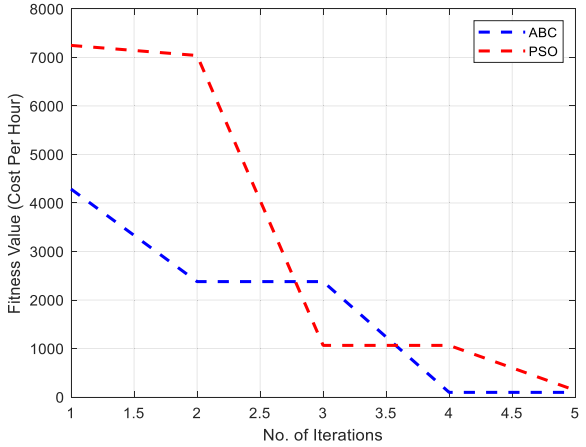

FIGURE 53. Winter TOU convergence value for PSO and ABC with 80 EVs with coordinated mode.

A significant reduction in cost C3 is observed during both algorithms. However, PSO reduced C3 cost twice as compared to ABC.

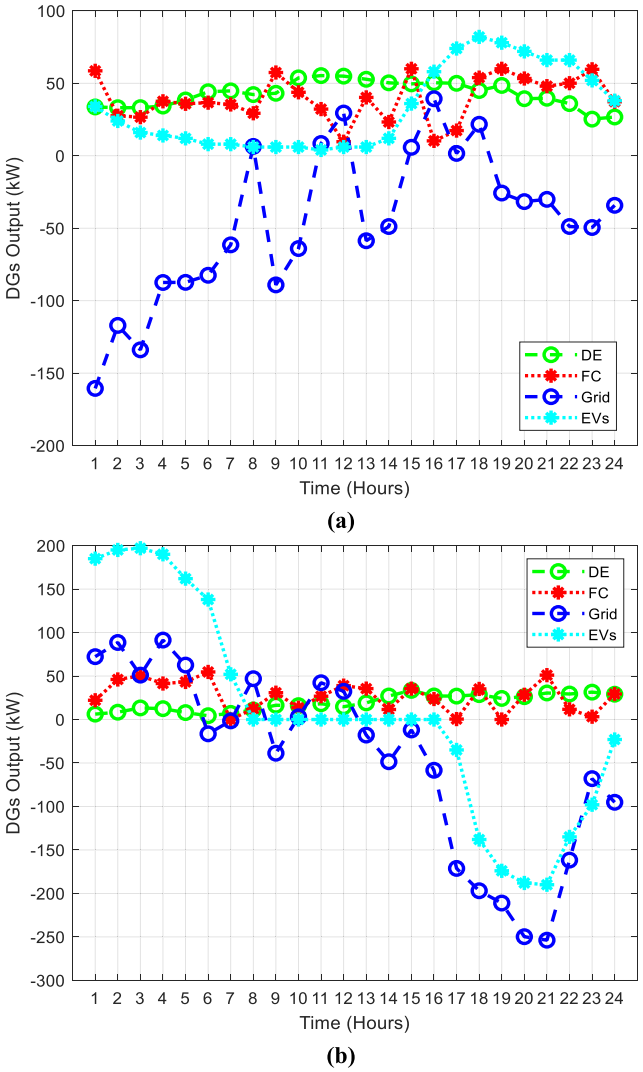

FIGURE 54. PSO-based unscheduled economic dispatch with 80 EVs (a) autonomous mode; (b) coordinated mode.

TABLE 20. CPP winter dispatch results under scheduling schemes 1 and 2 for 80 EVs.

Algo	Cost	scheme 1	scheme 2	%Δ1	%Δ2
PSO	C1	1855.0062	785.3103	17.99	-10.40
	C2	419.5309	458.2646	-25.22	64.01
	C3	80.9113	49.6897	47.67	0.15
	C	1298.4752	623.8149	14.58	3.81
ABC	C1	1730.9831	913.1524	-13.73	10.68
	C2	545.8613	343.898	79.33	31.28
	C3	70.1098	37.3885	-22.68	-36.74
	C	1250.9727	674.4215	-3.29	13.11

3) RTEP SCHEDULED WINTER LOAD

Fig. 62a and Fig. 62b show PSO-based RTEP winter load scheduling with 80 EVs in autonomous and coordinated modes. Excess energy from DGs is supplied to the grid (0100-0700, 0900-1000, 1300-1400, 1700, 2100-2400). EVs charging load is negligible during the starting day (0100-1400), while EVs' charging load increases during

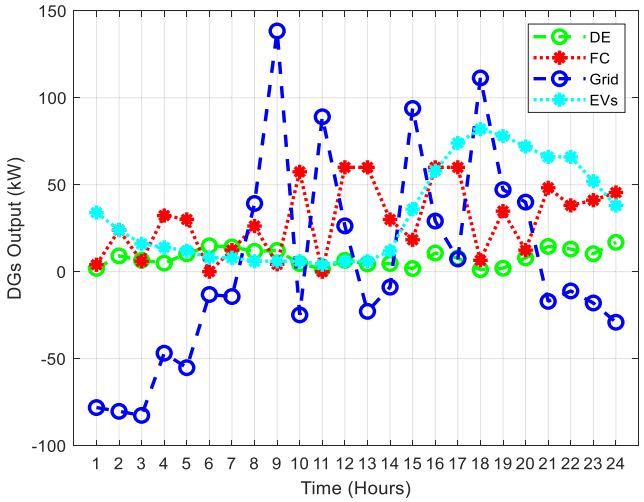

(a)

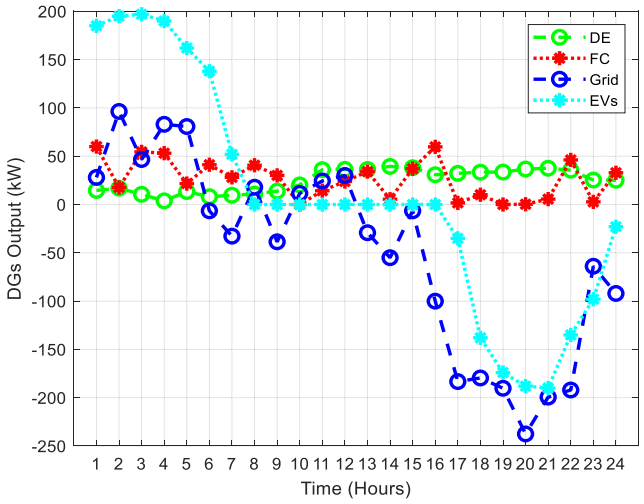

(b)

FIGURE 55. ABC-based unscheduled economic dispatch with 80 EVs (a) autonomous mode; (b) coordinated mode.

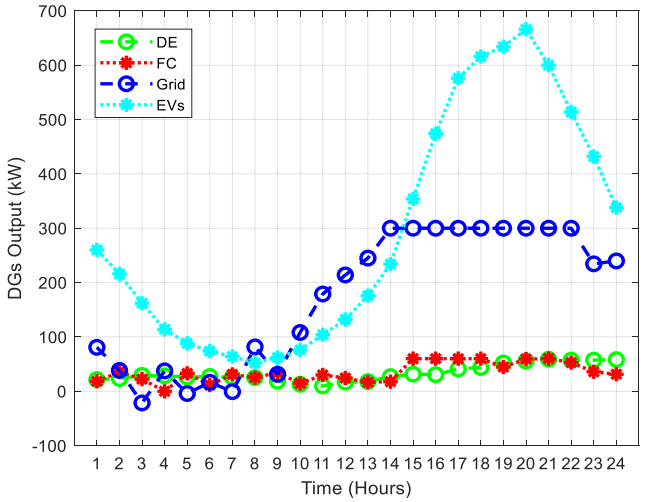

(a)

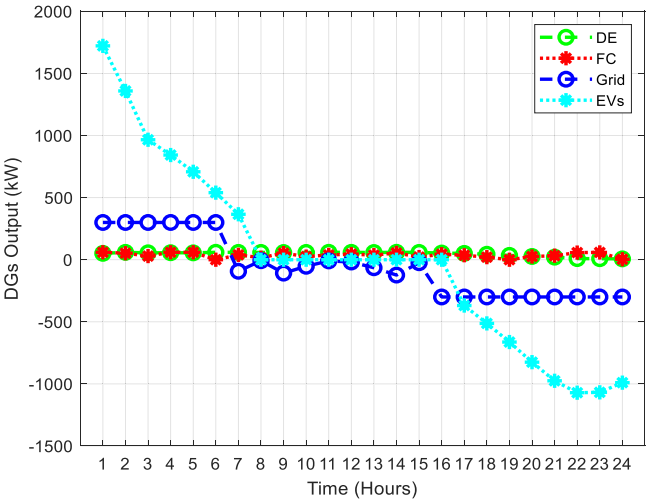

(b)

FIGURE 56. PSO-based unscheduled economic dispatch with 700 EVs (a) autonomous mode; (b) coordinated mode.

TABLE 21. CPP winter dispatch results under scheduling schemes 1 and 2 for 700 EVs.

Algo	Cost	scheme 1	scheme 2	%Δ1	%Δ2
PSO	C1	8403.882	1060.1536	-3.05	-73.73
	C2	1081.9049	454.7972	7.55	-35.51
	C3	910.6476	14.8398	-3.42	-477.93
	C	5728.0737	794.3457	-2.54	-68.87
ABC	C1	8586.4189	1002.682	-1.53	-72.19
	C2	932.1657	422.0123	2.70	-25.48
	C3	923.5546	20.4465	-1.67	-255.29
	C	5807.0234	749.8549	-1.35	-65.93

the second half-day (1500-2400). Excess energy from DGs is supplied to the grid (0700, 0900-1000, 1300-1400, 1600-2400). EVs charging load is significant during the start of the day (0100-0700), while EVs discharging load is significantly increased during the second half of the day (1700-2400).

Fig. 63a and Fig. 63b show ABC-based RTEP winter load scheduling with 80 EVs in autonomous and coordinated modes. Excess energy from DGs is supplied to the grid (0100-1400, 1700). EVs' charging load is small during the starting day (0100-1400), while EVs' charging load increases during the second half-day (1500-2400), and excess energy from DGs is supplied to the grid (0600-1400, 1700-2400). EVs' charging load is large during the starting day (0100-0700), while EVs discharging load is significantly increased during the second half-day (1700-2400).

Fig. 64a and Fig. 64b show PSO-based RTEP winter load scheduling with 700 EVs in autonomous and coordinated modes. EVs charging load is significant during the autonomous mode throughout the daytime with almost 700 kW peak at night (2000). During coordinated mode, excess energy from DGs is supplied to the grid at night (0300-0700, 0900). EVs charging load is more during the

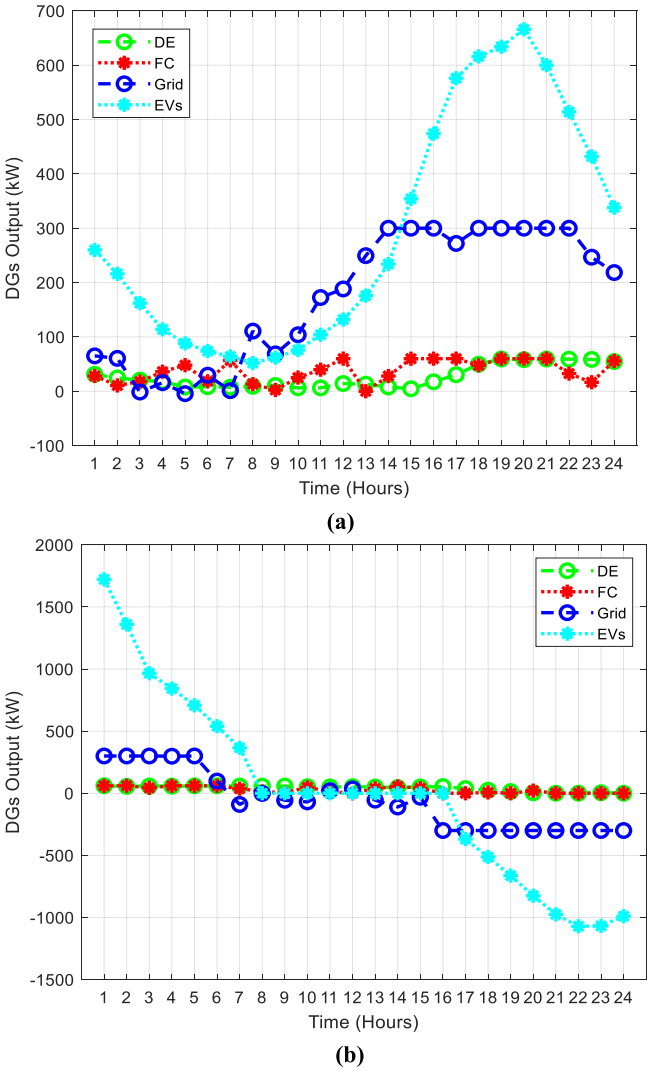

FIGURE 57. ABC-based unscheduled economic dispatch with 700 EVs (a) autonomous mode; (b) coordinated mode.

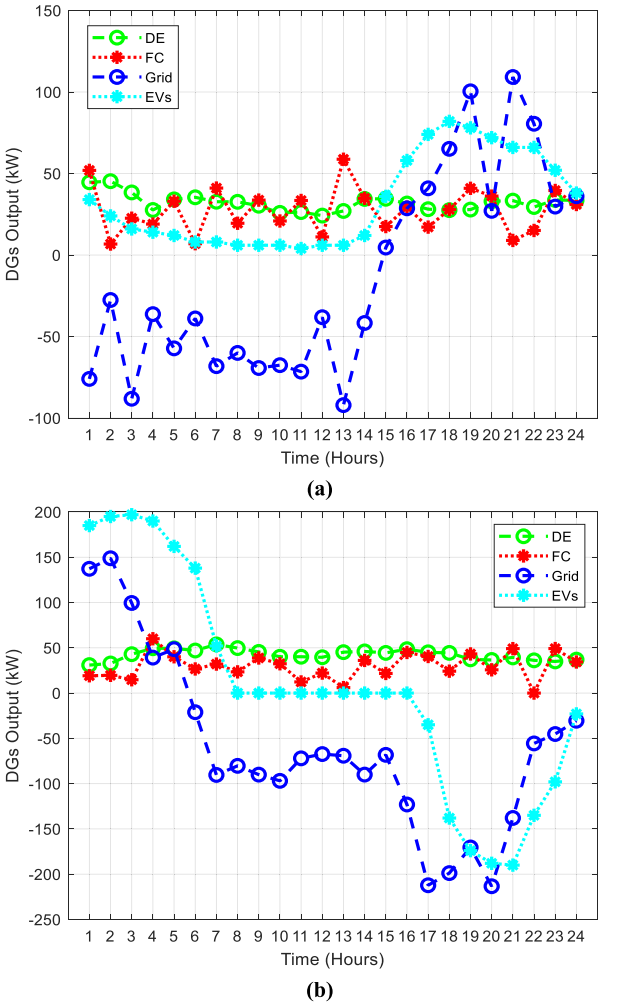

FIGURE 58. PSO-based winter CPP scheduled economic dispatch with 80 EVs (a) autonomous mode; (b) coordinated mode.

starting day (0100-0700), while EVs discharging load is significant at night (1700-2400).

Fig. 65a and Fig. 65b show ABC-based RTEP winter load scheduling with 700 EVs in autonomous and coordinated modes. Almost the same trend of PSO-based modes is observed during autonomous and coordinated modes.

Table 22 shows RTEP winter load scheduling results for 80 EVs during autonomous and coordinated modes. During autonomous mode, the ABC algorithm performed better by reducing three costs, such as C1, C3, and C. PSO algorithm performed better by reducing one cost such as C2. The ABC algorithm performed better during coordinated mode by reducing one cost, such as C3. The PSO algorithm performed better by reducing two costs, C2 and C3. A significant reduction in cost C2 is observed during the PSO algorithm.

Table 23 shows RTEP winter load scheduling results for 700 EVs during autonomous and coordinated. During

TABLE 22. RTEP winter dispatch results under scheduling schemes 1 and 2 for 80 EVs.

Algo	Cost	scheme 1	scheme 2	%Δ1	%Δ2
PSO	C1	1659.7352	1018.4321	8.34	14.87
	C2	396.4596	19.8833	-32.51	-729.41
	C3	55.8665	35.1751	24.21	-41.05
	C	1165.5061	657.5599	4.83	8.74
ABC	C1	1613.1887	839.5415	-22.03	2.84
	C2	489.7223	255.6429	76.96	7.56
	C3	53.1054	49.2939	-61.97	-3.71
	C	1159.6566	605.9816	-11.42	3.30

autonomous mode, both algorithms performed better by reducing three costs such as C1, C3, and C. During coordinated mode; both algorithms performed better by reducing all four costs. A significant reduction in cost C3 is observed during the ABC algorithm.

4) TOU SCHEDULED WINTER LOAD

Fig. 66a and Fig. 66b show PSO-based TOU winter load scheduling with 80 EVs in autonomous and coordinated

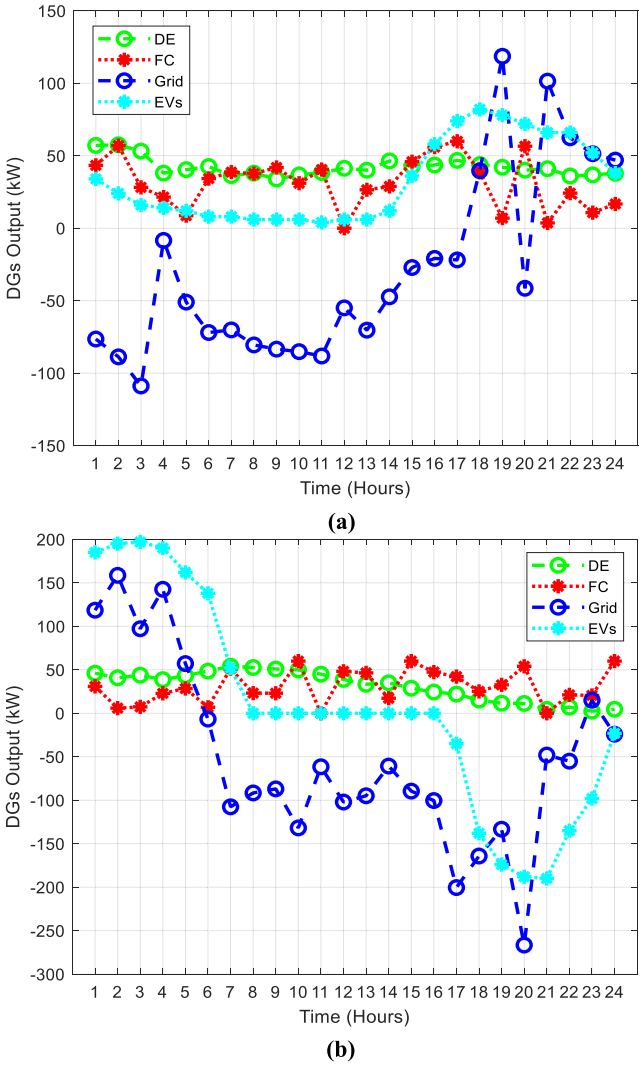

FIGURE 59. ABC-based winter CPP scheduled economic dispatch with 80 EVs (a) autonomous mode; (b) coordinated mode.

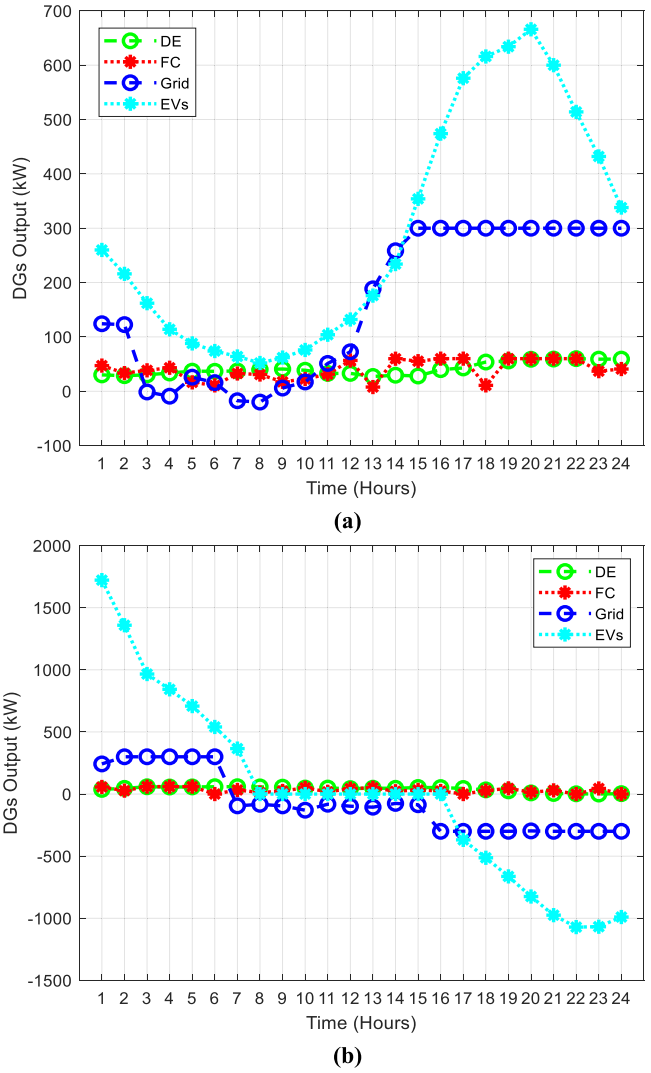

FIGURE 60. PSO-based winter CPP scheduled economic dispatch with 700 EVs (a) autonomous mode; (b) coordinated mode.

TABLE 23. RTEP winter dispatch results under scheduling schemes 1 and 2 for 700 EVs.

Algo	Cost	scheme 1	scheme 2	%Δ1	%Δ2
PSO	C1	8528.5101	1827.2607	-1.54	-0.79
	C2	1243.2803	576.7901	19.55	-6.85
	C3	931.0706	84.3353	-1.15	-1.69
	C	5851.2833	1321.7799	-0.38	-1.48
ABC	C1	8186.7494	1146.7785	-6.48	-50.56
	C2	1135.7766	410.6204	20.14	-28.96
	C3	881.2795	3.713	-6.54	-1856.47
	C	5600.6004	836.9499	-5.09	-48.66

modes. Excess energy from DGs is supplied to the grid (0100-0700, 0900-1000, 1300-1400, 1700, 1900, 2100-2400). EVs charging load is negligible during the starting day (0100-1400), while EVs' charging load increases during the second half-day (1500-2400). Excess energy from DGs is supplied to the grid (0600-0700, 0900, 1400, 1600-2400). EVs charging load is significant during the start of the day (0100-0700), while EVs discharging load is significantly increased during the second half of the day (1700-2400).

Fig. 67a and Fig. 67b show ABC-based TOU winter load scheduling with 80 EVs in autonomous and coordinated modes. Excess energy from DGs is supplied to the grid (0100-1000, 1200-1500, 1700, 1900-2400). EVs' charging load is small during the starting day (0100-1400), while EVs' charging load increases during the second half-day (1500-2400). Excess energy from DGs is supplied to the grid (0900-1000, 1300-2400). EVs charging load is large during the starting day (0100-0700), while EVs' discharging load increases during the second half-day (1700-2400).

Fig. 68a and Fig. 68b show PSO-based TOU winter load scheduling with 700 EVs in autonomous and coordinated modes. EVs charging load is significant during the autonomous mode throughout the daytime with almost 700 kW peak at night (2000). During coordinated mode, excess energy from DGs is supplied to the grid at night

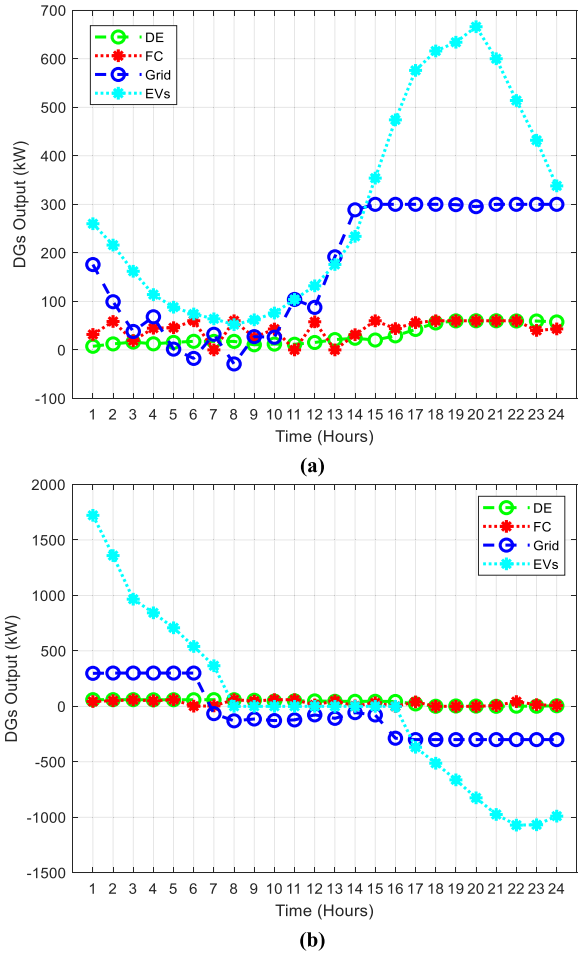

FIGURE 61. ABC-based winter CPP scheduled economic dispatch with 700 EVs (a) autonomous mode; (b) coordinated mode.

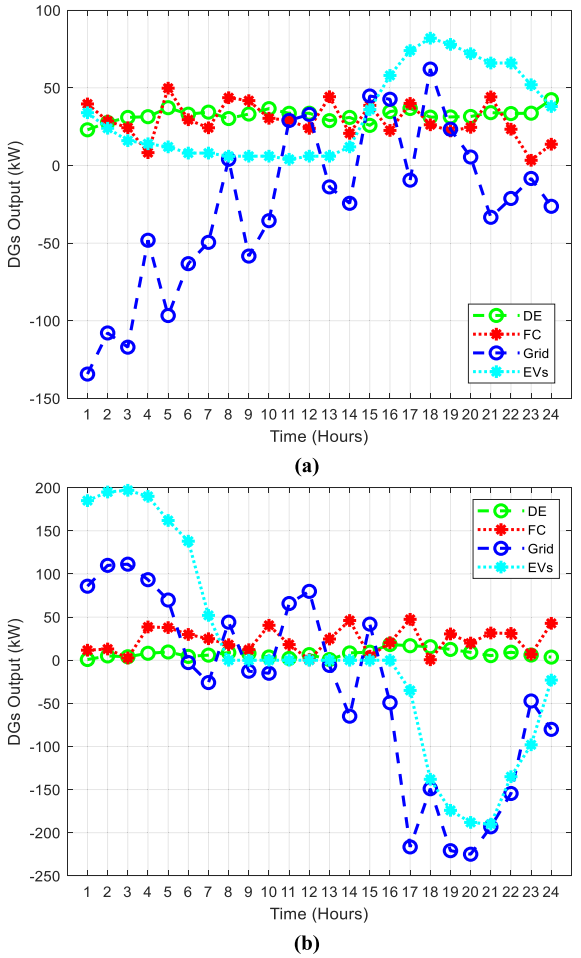

FIGURE 62. PSO-based winter RTEP scheduled economic dispatch with 80 EVs (a) autonomous mode; (b) coordinated mode.

(0700, 0900, 1600-2400). EVs charging load is more during the starting day (0100-0700), while EVs discharging load is significant at night (1700-2400).

Fig. 69a and Fig. 69b show ABC-based TOU winter load scheduling with 700 EVs in autonomous and coordinated modes. The almost same trend of PSO-based modes is observed during autonomous and coordinated modes.

Table 24 shows TOU winter load scheduling results for 80 EVs during autonomous and coordinated modes. Both PSO and ABC algorithms performed better during autonomous mode by reducing three costs such as C1, C3, and C. Significant reduction in cost C3 is observed during the ABC algorithm. Both ABC and PSO algorithms performed better during coordinated mode by reducing two costs: the C2 and C3. Significant reductions in cost C2 with PSO and ABC are observed.

Table 25 shows TOU winter load scheduling results for 700 EVs during autonomous and coordinated. The ABC algorithm performed better during autonomous mode by reducing all four costs. PSO algorithm performed better by reducing three costs such as C2, C3, and C. During coordinated mode, both ABC and PSO algorithms performed better by reducing all four costs such as C1, C2, C3, and C.

TABLE 24. TOU winter dispatch results under scheduling schemes 1 and 2 for 80 EVs.

Algo	Cost	scheme 1	scheme 2	%Δ1	%Δ2
PSO	C1	1508.887	980.4396	-0.82	11.57
	C2	544.6215	67.6713	3.54	-143.70
	C3	41.9053	38.1275	-1.04	-30.13
	C	1106.2242	646.0115	-0.27	7.11
ABC	C1	1405.3441	959.7902	-40.08	15.02
	C2	657.505	99.6847	82.84	-137.08
	C3	33.0517	38.9323	-160.24	-31.32
	C	1068.4983	641.2111	-20.93	8.61

VII. CRITICAL ANALYSIS AND DISCUSSION

- During unscheduled summer load, a significant reduction of computational burden is observed in the case of the PSO algorithm for 80 EVs in autonomous mode. The convergence curves showed that the performance of the ABC algorithm is better in autonomous mode, while PSO performed well in coordinated mode.

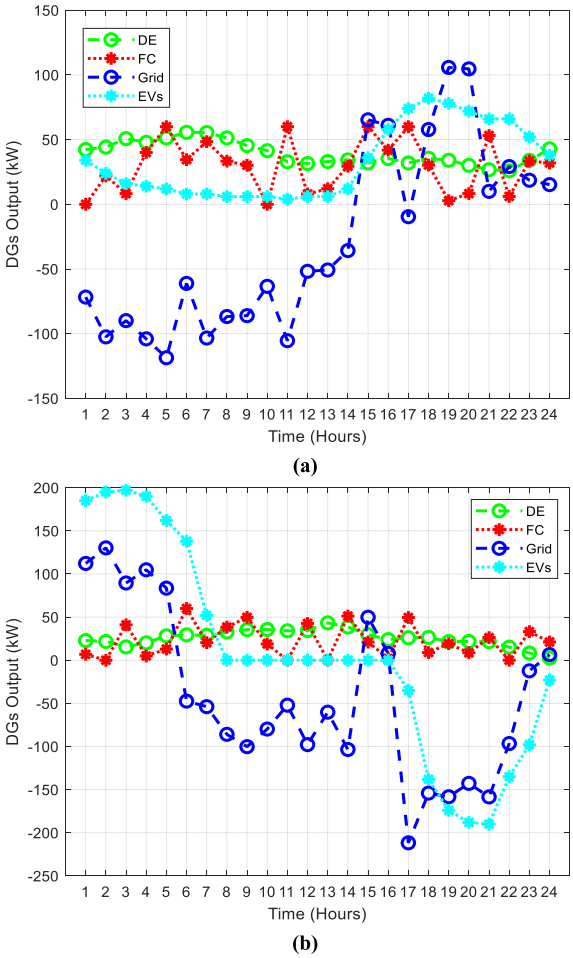

FIGURE 63. ABC-based winter RTEP scheduled economic dispatch with 80 EVs (a) autonomous mode; (b) coordinated mode.

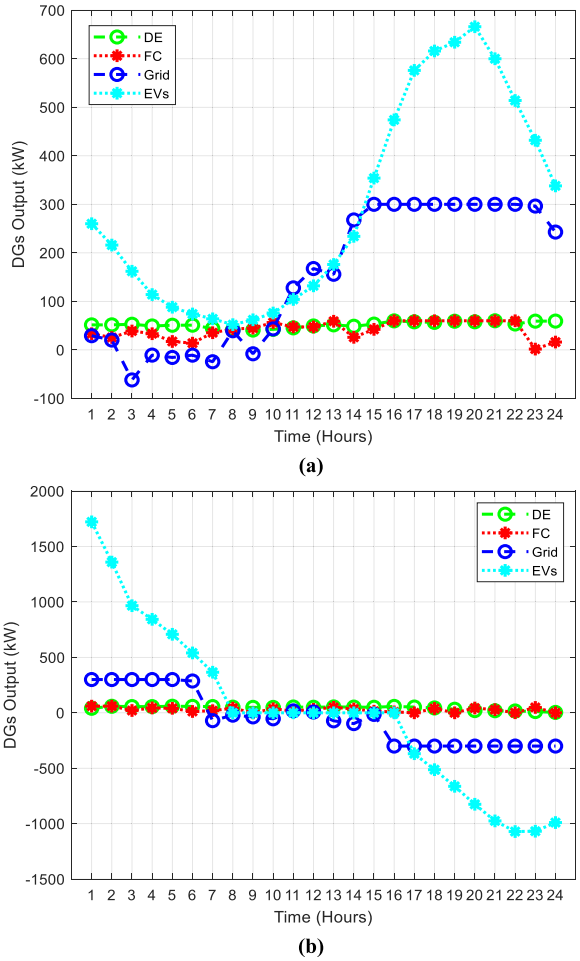

FIGURE 64. PSO-based winter RTEP scheduled economic dispatch with 700 EVs (a) autonomous mode; (b) coordinated mode.

TABLE 25. TOU winter dispatch results under scheduling schemes 1 and 2 for 700 EVs.

Algo	Cost	scheme 1	scheme 2	%Δ1	%Δ2
PSO	C1	8674.9533	1692.5545	0.17	-8.82
	C2	932.9087	500.0297	-7.21	-23.25
	C3	940.8529	67.5326	-0.10	-27.00
	C	5865.4228	1214.3856	-0.13	-10.46
ABC	C1	8538.9301	1611.4795	-2.09	-7.14
	C2	1253.0818	480.2035	27.62	-10.27
	C3	927.606	57.8562	-1.22	-25.56
	C	5860.0898	1156.6066	-0.44	-7.57

- During the CPP summer tariff, a significant reduction of computational burden is observed in the PSO algorithm for 80 EVs in autonomous mode. The simulation time reduction is also observed with ABC and PSO for 80 EVs in autonomous and coordinated modes, respectively. All remaining scenarios show more computational burden as compared to the base case. CPP summer load scheduling results for 80 EVs during scheduling scheme 1 (autonomous) and scheduling scheme 2 (coordinated) are analyzed. During autonomous mode, the ABC algorithm outperformed PSO by reducing all four costs, such as the operating cost (C1), pollutant treatment cost (C2), carbon emissions cost (C3), and the overall cost (C). During coordinated mode, the ABC algorithm also outperformed PSO by reducing three costs as the operating cost (C1), carbon emissions cost (C3), and the overall cost (C). CPP summer load scheduling results for 700 EVs during scheduling scheme 1 (autonomous) and scheduling scheme 2 (coordinated) are analyzed. During autonomous mode, the ABC algorithm performed better by reducing all four costs such as C1, C2, C3, and C. The PSO algorithm performed better by reducing one cost, such as C2. Both ABC and PSO algorithms performed better during coordinated mode by reducing all four costs such as C1, C2, C3, and C. Significant reduction in cost C3 is observed during both ABC and PSO algorithms. However, ABC reduced C3 cost twice as compared to PSO.
- During the RTEP summer tariff, a significant reduction in computational burden is observed with PSO for 80 EVs in autonomous mode. The simulation time reduction is also observed with PSO for 80 EVs and

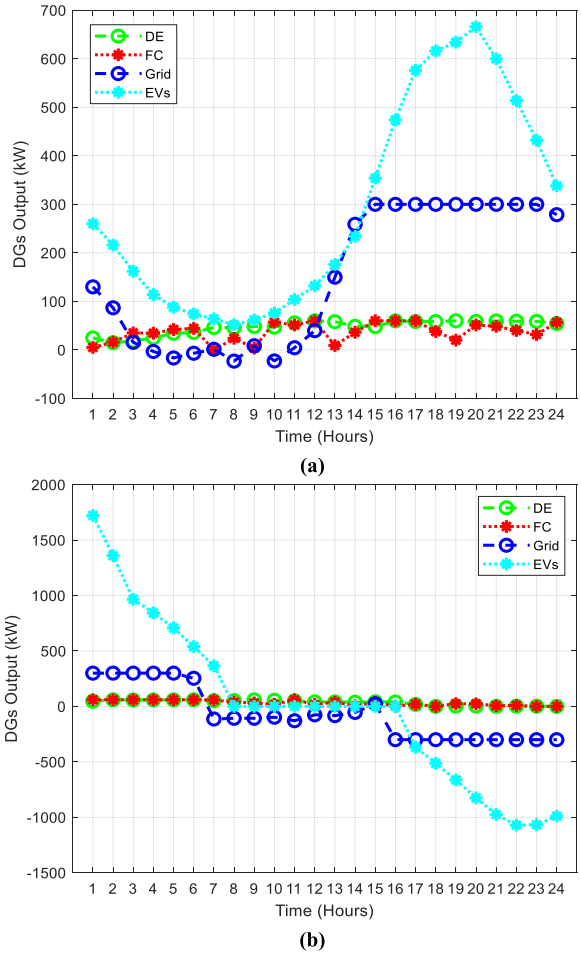

FIGURE 65. ABC-based winter RTEP scheduled economic dispatch with 700 EVs (a) autonomous mode; (b) coordinated mode.

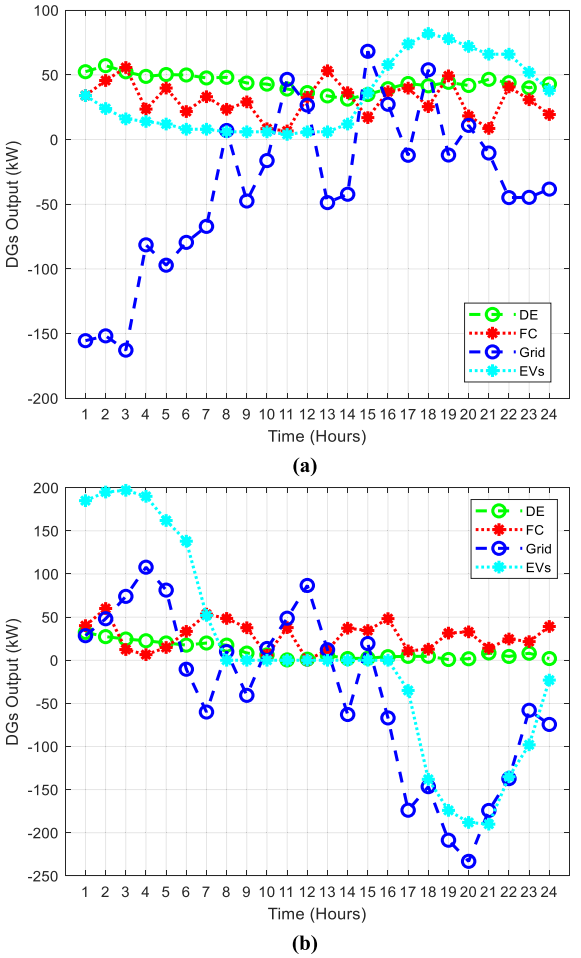

FIGURE 66. PSO-based winter TOU scheduled economic dispatch with 80 EVs (a) autonomous mode; (b) coordinated mode.

700 EVs in coordinated and autonomous modes, respectively. All remaining scenarios show more computational burden as compared to the base case. The almost same trend of final convergence is observed for both algorithms during autonomous and coordinated modes. RTEP summer load scheduling results for 80 EVs during autonomous and coordinated modes are analyzed. The PSO algorithm performed better during autonomous mode by reducing one cost, such as C2. The PSO algorithm performed better during coordinated mode by reducing three costs such as the C1, C3, and C. RTEP summer load scheduling results for 700 EVs during autonomous and coordinated. The ABC algorithm performed better during autonomous mode by reducing all four costs. During coordinated mode, both algorithms performed better by reducing all four costs. A significant reduction in cost C3 is observed during the ABC algorithm.

- During the TOU summer tariff, a significant reduction in computational burden is observed with PSO for 80 EVs in autonomous mode. The simulation time reduction is also observed with PSO and ABC for 80 EVs in coordinated and autonomous modes, respectively. All remaining scenarios show more computational burden as compared to the base case. The convergence curves showed that the performance of the PSO algorithm is better in coordinated mode. TOU summer load scheduling results for 80 EVs during autonomous and coordinated modes are analyzed. Both PSO and ABC algorithms performed better during autonomous mode by reducing all four costs. A significant reduction in cost C2 is observed during both PSO and ABC algorithms. During coordinated mode, the ABC algorithm performed better by reducing all four costs such as the C1, C2, C3, and C. PSO algorithm performed better by reducing three costs such as the C1, C3, and C. Significant reduction in cost C3 with PSO and C2 with ABC are observed. TOU summer load scheduling results for 700 EVs during autonomous and coordinated are analyzed. The ABC algorithm performed better during autonomous mode by reducing all four costs. PSO algorithm performed better by reducing three costs such as C1, C3, and C. During coordinated mode; both algorithms performed better by reducing all four costs.

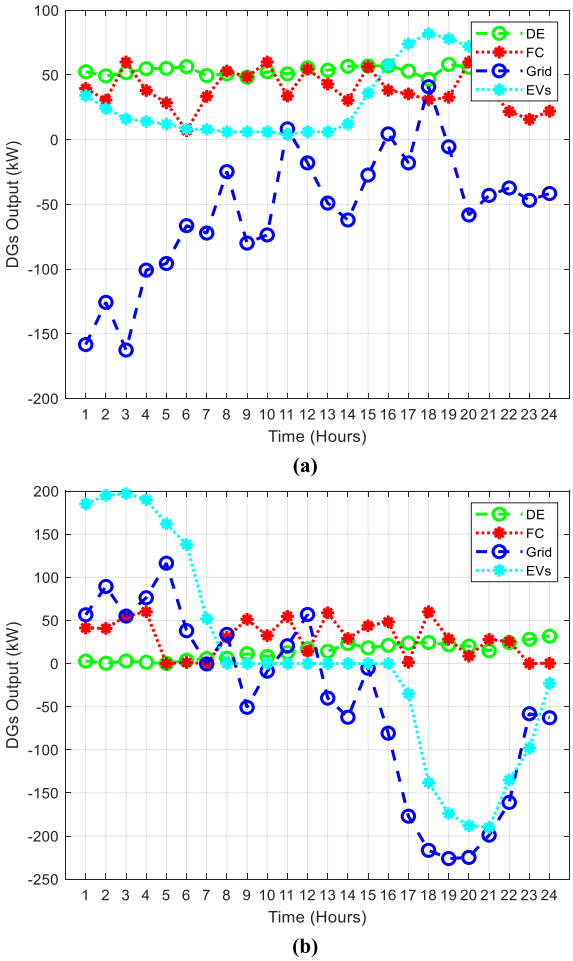

FIGURE 67. ABC-based winter TOU scheduled economic dispatch with 80 EVs (a) autonomous mode; (b) coordinated mode.

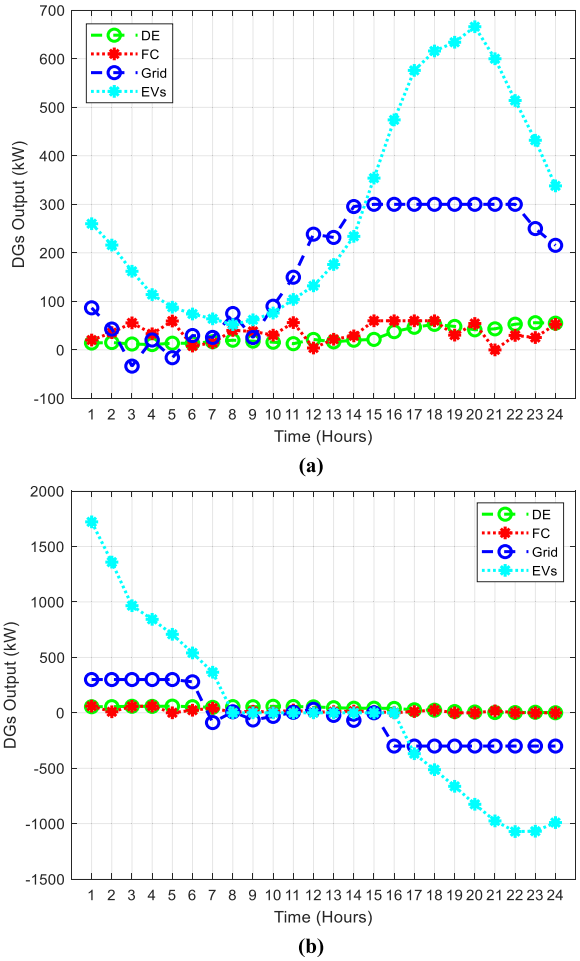

FIGURE 68. PSO-based winter TOU scheduled economic dispatch with 700 EVs (a) autonomous mode; (b) coordinated mode.

A significant reduction in cost C3 is observed during both ABC and PSO algorithms. However, cost reduction with ABC is 1.5 times as compared to PSO.

- During unscheduled winter load, convergence curves showed that the performance of the ABC algorithm is better with 80 EVs, while both performed well with 700 EVs.
- During the CPP winter tariff, the convergence curves showed that the performance of the ABC algorithm is better with 80 EVs, while both algorithms performed well with 700 EVs. No significant reduction of computational burden is observed. The simulation time reduction is only observed with PSO for 700 EVs in autonomous mode. All remaining scenarios showed more computational burden as compared to the base case. CPP winter load scheduling results for 80 EVs during autonomous and coordinated mode are analyzed. During autonomous mode, the ABC algorithm performed well by reducing three costs, such as C1, C3, and C. PSO algorithm performed well by reducing one cost such as C2. The ABC algorithm performed better during coordinated mode by reducing one cost, such as C3. PSO algorithm performed better by reducing one cost such as C1. CPP winter load scheduling results for 700 EVs during autonomous and coordinated are analyzed. During autonomous mode, both algorithms performed better by reducing three costs such as C1, C3, and C. During coordinated mode; both algorithms performed better by reducing all four costs. A significant reduction in cost C3 is observed during both algorithms. However, PSO reduced C3 cost twice as compared to ABC.
- During RTEP winter tariff, the convergence curves showed that the performance of the PSO algorithm is better for both cases with 80 EVs and 700 EVs in autonomous mode. No significant reduction in computational burden is observed. All scenarios showed more computational burden as compared to the base case. RTEP winter load scheduling results for 80 EVs during autonomous and coordinated modes are analyzed. During autonomous mode, the ABC algorithm performed better by reducing three costs, such as C1, C3, and C. PSO algorithm performed better by reducing one cost

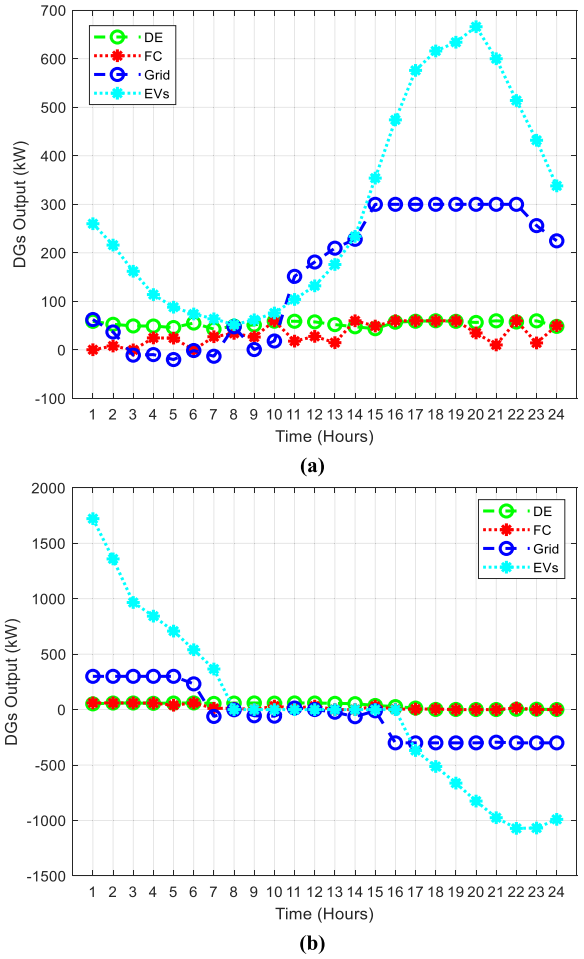

FIGURE 69. ABC-based winter TOU scheduled economic dispatch with 700 EVs (a) autonomous mode; (b) coordinated mod.

such as C2. The ABC algorithm performed better during coordinated mode by reducing one cost, such as C3. The PSO algorithm performed better by reducing two costs, C2 and C3. A significant reduction in cost C2 is observed during the PSO algorithm. RTEP winter load scheduling results for 700 EVs during autonomous and coordinated. During autonomous mode, both algorithms performed better by reducing three costs such as C1, C3, and C. During coordinated mode; both algorithms performed better by reducing all four costs. A significant reduction in cost C3 is observed during the ABC algorithm.

- During the TOU winter tariff, the convergence curve showed that the performance of both algorithms is better in coordinated mode with 80 EVs. No significant reduction in computational burden is observed. All scenarios showed more computational burden as compared to the base case. TOU winter load scheduling results for 80 EVs during autonomous and coordinated modes are analyzed. Both algorithms performed better during autonomous mode by reducing three costs such as C1, C3, and C. Significant reduction in cost C3 is observed during the ABC algorithm. During coordinated mode, both algorithms performed better by reducing two costs, such as the C2 and C3. Significant reductions in cost C2 with PSO and ABC are observed. TOU winter load scheduling results for 700 EVs during autonomous and coordinated are analyzed. The ABC algorithm performed better during autonomous mode by reducing all four costs. PSO algorithm performed better by reducing three costs such as C2, C3, and C. During coordinated mode, both algorithms performed better by reducing all four costs.

VIII. CONCLUSION

In this paper, the joint optimization modeling approach is proposed for the planning and operation of grid-connected residential MGs with the help of demand response programs (DRPs). The constraints complexity of many smart residential appliances is included in the DRPs load shifting process. Proposed model performance is investigated with and without DRPs under summer and winter load data. MG planning and operation optimization models are validated while comparing different results with two algorithms, i.e., ABC and PSO. Overall assessment of results showed that the proposed MG planning and operation modeling approach can provide good solutions while maximizing RERs and EVs integration with the support of DRPs.

REFERENCES

[1] O. Hafez and K. Bhattacharya, "Optimal planning and design of a renewable energy based supply system for microgrids," *Renew. Energy*, vol. 45, pp. 7–15, Sep. 2012.

[2] Q. Fu, L. F. Montoya, A. Solanki, A. Nasiri, V. Bhavaraju, T. Abdallah, and D. C. Yu, "Microgrid generation capacity design with renewables and energy storage addressing power quality and surety," *IEEE Trans. Smart Grid*, vol. 3, no. 4, pp. 2019–2027, Dec. 2012.

[3] P. Palensky and D. Dietrich, "Demand side management: Demand response, intelligent energy systems, and smart loads," *IEEE Trans. Ind. Informat.*, vol. 7, no. 3, pp. 381–388, Aug. 2011.

[4] K. Zhou, S. Yang, Z. Chen, and S. Ding, "Optimal load distribution model of microgrid in the smart grid environment," *Renew. Sustain. Energy Rev.*, vol. 35, pp. 304–310, Jul. 2014.

[5] N. I. Nwulu and X. Xia, "Optimal dispatch for a microgrid incorporating renewables and demand response," *Renew. Energy*, vol. 101, pp. 16–28, Feb. 2017.

[6] M. H. Imani, P. Niknejad, and M. R. Barzegaran, "The impact of customers' participation level and various incentive values on implementing emergency demand response program in microgrid operation," *Electr. Power Energy Syst.*, vol. 96, pp. 114–125, Mar. 2018.

[7] J. Shen, C. Jiang, Y. Liu, and J. Qian, "A microgrid energy management system with demand response for providing grid peak shaving," *Electr. Power Compon. Syst.*, vol. 44, no. 8, pp. 843–852, 2016.

[8] A. Khodaei, S. Bahramirad, and M. Shahidehpour, "Microgrid planning under uncertainty," *IEEE Trans. Power Syst.*, vol. 30, no. 5, pp. 2417–2425, Sep. 2015.

[9] *Kammen: Renewable Energy Options for the Emerging-Google Scholar*. Accessed: Sep. 26, 2021. [Online]. Available: https://scholar.google.com/scholar?cluster=2465164507733390681&hl=en&as_sdt=0

[10] A. Saif, V. Ravikumar Pandi, H. H. Zeineldin, and S. Kennedy, "Optimal allocation of distributed energy resources through simulation-based optimization," *Electr. Power Syst. Res.*, vol. 104, pp. 1–8, Nov. 2013.

[11] M. Manbachi and M. Ordonez, "AMI-based energy management for islanded AC/DC microgrids utilizing energy conservation and optimization," *IEEE Trans. Smart Grid*, vol. 10, no. 1, pp. 293–304, Jan. 2019.

[12] A. Askarzadeh, "A memory-based genetic algorithm for optimization of power generation in a microgrid," *IEEE Trans. Sustain. Energy*, vol. 9, no. 3, pp. 1081–1089, Jul. 2018.

[13] M. Marzband, M. Ghadimi, A. Sumper, and J. L. Domínguez-García, "Experimental validation of a real-time energy management system using multi-period gravitational search algorithm for microgrids in islanded mode," *Appl. Energy*, vol. 128, pp. 164–174, Sep. 2014.

[14] L. Luo, S. S. Abdulkareem, A. Rezvani, M. R. Miveh, S. Samad, N. Aljojo, and M. Pazhoohesh, "Optimal scheduling of a renewable based microgrid considering photovoltaic system and battery energy storage under uncertainty," *J. Energy Storage*, vol. 28, Apr. 2020, Art. no. 101306.

[15] F. H. Aghdam, N. T. Kalantari, and B. Mohammadi-Ivatloo, "A chance-constrained energy management in multi-microgrid systems considering degradation cost of energy storage elements," *J. Energy Storage*, vol. 29, Jun. 2020, Art. no. 101416.

[16] K. Gholami and E. Dehnavi, "A modified particle swarm optimization algorithm for scheduling renewable generation in a micro-grid under load uncertainty," *Appl. Soft Comput.*, vol. 78, pp. 496–514, May 2019.

[17] M. G. M. Abdolrasol, M. A. Hannan, A. Mohamed, U. A. U. Amiruldin, I. B. Z. Abidin, and M. N. Uddin, "An optimal scheduling controller for virtual power plant and microgrid integration using the binary backtracking search algorithm," *IEEE Trans. Ind. Appl.*, vol. 54, no. 3, pp. 2834–2844, May 2018.

[18] M. K. K. Darabi, H. G. G. Ganjehlou, A. Jafari, M. Nazari-Heris, G. B. B. Gharehpetian, and M. Abedi, "Evaluating the effect of demand response programs (DRPs) on robust optimal sizing of islanded microgrids," *Energies*, vol. 14, no. 18, p. 5750, Sep. 2021.

[19] M. F. Roslan, M. A. Hannan, P. Jern Ker, R. A. Begum, T. I. Mahlia, and Z. Y. Dong, "Scheduling controller for microgrids energy management system using optimization algorithm in achieving cost saving and emission reduction," *Appl. Energy*, vol. 292, Jun. 2021, Art. no. 116883.

[20] A. Maleki and A. Askarzadeh, "Optimal sizing of a PV/wind/diesel system with battery storage for electrification to an off-grid remote region: A case study of Rafsanjan, Iran," *Sustain. Energy Technol. Assessments*, vol. 7, pp. 147–153, Sep. 2014.

[21] Y. A. Katsigiannis, P. S. Georgilakis, and E. S. Karapidakis, "Hybrid simulated annealing-tabu search method for optimal sizing of autonomous power systems with renewables," *IEEE Trans. Sustain. Energy*, vol. 3, no. 3, pp. 330–338, Jul. 2012.

[22] A. Maleki, M. Ameri, and F. Keynia, "Scrutiny of multifarious particle swarm optimization for finding the optimal size of a PV/wind/battery hybrid system," *Renew. Energy*, vol. 80, pp. 552–563, Aug. 2015.

[23] U. Akram, M. Khalid, and S. Shafiq, "Optimal sizing of a wind/solar/battery hybrid grid-connected microgrid system," *IET Renew. Power Gener.*, vol. 12, no. 1, pp. 72–80, Aug. 2018.

[24] L. Moretti, L. Meraldi, A. Niccolai, G. Manzolini, and S. Leva, "An innovative tunable rule-based strategy for the predictive management of hybrid microgrids," *Electronics*, vol. 10, no. 10, p. 1162, May 2021.

[25] A. Jafari, H. G. Ganjehlou, T. Khalili, B. Mohammadi-Ivatloo, A. Bidram, and P. Siano, "A two-loop hybrid method for optimal placement and scheduling of switched capacitors in distribution networks," *IEEE Access*, vol. 8, pp. 38892–38906, 2020.

[26] M. A. M. Ramli, H. R. E. H. Bouchekara, and A. S. Alghamdi, "Optimal sizing of PV/wind/diesel hybrid microgrid system using multi-objective self-adaptive differential evolution algorithm," *Renew. Energy*, vol. 121, pp. 400–411, Jan. 2018.

[27] A. Jafari, H. Ganjeh Ganjehlou, F. Baghal Darbandi, B. Mohammadi-Ivatloo, and M. Abapour, "Dynamic and multi-objective reconfiguration of distribution network using a novel hybrid algorithm with parallel processing capability," *Appl. Soft Comput.*, vol. 90, May 2020, Art. no. 106146.

[28] H. Ganjeh Ganjehlou, H. Niaei, A. Jafari, D. O. Aroko, M. Marzband, and T. Fernando, "A novel techno-economic multi-level optimization in home-microgrids with coalition formation capability," *Sustain. Cities Soc.*, vol. 60, Sep. 2020, Art. no. 102241.

[29] F. Ahmad and M. S. Alam, "Optimal sizing and analysis of solar PV, wind, and energy storage hybrid system for campus microgrid," *Smart Sci.*, vol. 6, no. 2, pp. 150–157, Apr. 2018.

[30] M. H. Amrollahi and S. M. T. Bathaee, "Techno-economic optimization of hybrid photovoltaic/wind generation together with energy storage system in a stand-alone micro-grid subjected to demand response," *Appl. Energy*, vol. 202, pp. 66–77, Sep. 2017.

[31] R. Belfkira, Z. Lu, and G. Barakat, "Optimal sizing study of hybrid wind/PV/diesel power generation unit," *Solar Energy*, vol. 85, no. 1, pp. 100–110, Jan. 2011.

[32] T. Khalili, H. G. Ganjehlou, A. Bidram, S. Nojavan, and S. Asadi, "Financial risk-based scheduling of micro grids accompanied by surveying the influence of the demand response program," in *Proc. IEEE/IAS 57th Ind. Commercial Power Syst. Tech. Conf. (I&CPS)*, Apr. 2021, pp. 1–9.

[33] S. Diaf, D. Diaf, M. Belhamel, M. Haddadi, and A. Louche, "A methodology for optimal sizing of autonomous hybrid PV/wind system," *Energy Policy*, vol. 35, no. 11, pp. 5708–5718, Nov. 2007.

[34] L. Moretti, S. Polimeni, L. Meraldi, P. Raboni, S. Leva, and G. Manzolini, "Assessing the impact of a two-layer predictive dispatch algorithm on design and operation of off-grid hybrid microgrids," *Renew. Energy*, vol. 143, pp. 1439–1453, Dec. 2019.

[35] A. Jafari, H. Ganjeh Ganjehlou, T. Khalili, and A. Bidram, "A fair electricity market strategy for energy management and reliability enhancement of islanded multi-microgrids," *Appl. Energy*, vol. 270, Jul. 2020, Art. no. 115170.

[36] F. A. Bhuiyan, A. Yazdani, and S. L. Primak, "Optimal sizing approach for islanded microgrids," *IET Renew. Power Generation*, vol. 9, no. 2, pp. 166–175, 2015.

[37] Z. Wang, B. Chen, J. Wang, J. Kim, and M. M. Begovic, "Robust optimization based optimal DG placement in microgrids," *IEEE Trans. Smart Grid*, vol. 5, no. 5, pp. 2173–2182, Sep. 2014.

[38] A. M. Eltamaly, M. A. Mohamed, and A. I. Alolah, "A novel smart grid theory for optimal sizing of hybrid renewable energy systems," *Sol. Energy*, vol. 124, pp. 26–38, Feb. 2016.

[39] A. Jafari, T. Khalili, H. G. Ganjehlou, and A. Bidram, "Optimal integration of renewable energy sources, diesel generators, and demand response program from pollution, financial, and reliability viewpoints: A multi-objective approach," *J. Cleaner Prod.*, vol. 247, Feb. 2020, Art. no. 119100.

[40] S. Surender Reddy, P. R. Bijwe, and A. R. Abhyankar, "Real-time economic dispatch considering renewable power generation variability and uncertainty over scheduling period," *IEEE Syst. J.*, vol. 9, no. 4, pp. 1440–1451, Dec. 2015.

[41] S. S. Reddy, P. R. Bijwe, and A. R. Abhyankar, "Joint energy and spinning reserve market clearing incorporating wind power and load forecast uncertainties," *IEEE Syst. J.*, vol. 9, no. 1, pp. 152–164, Mar. 2015.

[42] J. A. Momoh, S. S. Reddy, and Y. Baxi, "Stochastic Voltage/VAR control with load variation," in *Proc. IEEE Power Energy Soc. Gen. Meeting*, Oct. 2014, pp. 1–5.

[43] S. S. Reddy, P. R. Bijwe, and A. R. Abhyankar, "Optimal dynamic emergency reserve activation using spinning, hydro and demand-side reserves," *Frontiers Energy*, vol. 10, no. 4, pp. 409–423, Nov. 2016.

[44] H. E. H. Shalaby, "A review on demand side management applications, techniques, and potential energy and cost saving," *ELEKTRIKA-J. Electr. Eng.*, vol. 20, no. 1, pp. 21–33, Apr. 2021.

[45] H. Wasim Khan, M. Usman, G. Hafeez, F. R. Albogamy, I. Khan, Z. Shafiq, M. U. A. Khan, and H. I. Alkhammash, "Intelligent optimization framework for efficient demand-side management in renewable energy integrated smart grid," *IEEE Access*, vol. 9, pp. 124235–124252, 2021.

[46] T. Nasir, S. S. H. Bukhari, S. Raza, H. M. Munir, M. Abrar, H. A. U. Muqeet, K. L. Bhatti, J.-S. Ro, and R. Masroor, "Recent challenges and methodologies in smart grid demand side management: State-of-the-art literature review," *Math. Problems Eng.*, vol. 2021, pp. 1–16, Aug. 2021.

[47] K. Chaurasia and H. R. Kamath, "Artificial intelligence and machine learning based: Advances in demand-side response of renewable energy-integrated smart grid," in *Smart Systems: Innovations in Computing* (Smart Innovation, Systems and Technologies), vol. 235, A. K. Somani, A. Mundra, R. Doss, and S. Bhattacharya, Eds. Singapore: Springer, 2022, doi: 10.1007/978-981-16-2877-1_18.

[48] L. Li, L. Ling, Y. Yang, and R. Poursoleiman, "Modeling and optimal energy operation considering probabilistic and sustainable renewable energy models and demand side management," *Energy Buildings*, vol. 231, Jan. 2021, Art. no. 110557.

[49] S. Xu, Y. Zhao, Y. Li, and Y. Zhou, "An iterative uniform-price auction mechanism for peer-to-peer energy trading in a community microgrid," *Appl. Energy*, vol. 298, Sep. 2021, Art. no. 117088.

[50] M. Hemmati, M. A. Mirzaei, M. Abapour, K. Zare, B. Mohammadi-Ivatloo, H. Mehrjerdi, and M. Marzband, "Economic-environmental analysis of combined heat and power-based reconfigurable microgrid integrated with multiple energy storage and demand response program," *Sustain. Cities Soc.*, vol. 69, Jun. 2021, Art. no. 102790.

[51] M. A. Taghikhani, "Renewable resources and storage systems stochastic multi-objective optimal energy scheduling considering load and generation uncertainties," *J. Energy Storage*, vol. 43, Nov. 2021, Art. no. 103293.
[52] M. S. Rawat and S. Vadhera, "Heuristic optimization techniques for voltage stability enhancement of radial distribution network with simultaneous consideration of network reconfiguration and DG sizing and allocations," *TURKISH J. Electr. Eng. Comput. Sci.*, vol. 27, no. 1, pp. 330–345, Jan. 2019.
[53] M. G. Hemeida, A. A. Ibrahim, A.-A.-A. Mohamed, S. Alkhalaf, and A. M. B. El-Dine, "Optimal allocation of distributed generators DG based manta ray foraging optimization algorithm (MRFO)," *Ain Shams Eng. J.*, vol. 12, no. 1, pp. 609–619, Mar. 2021.
[54] A. Selim, S. Kamel, and F. Jurado, "Efficient optimization technique for multiple DG allocation in distribution networks," *Appl. Soft Comput.*, vol. 86, Jan. 2020, Art. no. 105938.
[55] H. B. Tolabi, A. L. Ara, and R. Hosseini, "A new thief and police algorithm and its application in simultaneous reconfiguration with optimal allocation of capacitor and distributed generation units," *Energy*, vol. 203, Jul. 2020, Art. no. 117911.
[56] H. U. R. Habib, S. Wang, A. Waqar, B. S. Farhan, K. M. Kotb, and Y.-S. Kim, "Combined heat and power units sizing and energy cost optimization of a residential building by using an artificial bee colony algorithm," *IEEE Access*, vol. 8, pp. 218289–218303, 2020.
[57] H. U. R. Habib, U. Subramaniam, A. Waqar, B. S. Farhan, K. M. Kotb, and S. Wang, "Energy cost optimization of hybrid renewables based V2G microgrid considering multi objective function by using artificial bee colony optimization," *IEEE Access*, vol. 8, pp. 62076–62093, 2020.
[58] H. Liu, Y. Ji, H. Zhuang, and H. Wu, "Multi-objective dynamic economic dispatch of microgrid systems including vehicle-to-grid," *Energies*, vol. 8, no. 5, pp. 4476–4495, May 2015.
[59] L. Bhamidi and S. Sivasubramani, "Optimal planning and operational strategy of a residential microgrid with demand side management," *IEEE Syst. J.*, vol. 14, no. 2, pp. 2624–2632, Jun. 2020.
[60] S. Lenhart and K. Araújo, "Microgrid decision-making by public power utilities in the united states: A critical assessment of adoption and technological profiles," *Renew. Sustain. Energy Rev.*, vol. 139, Apr. 2021, Art. no. 110692.
[61] M. Nazari-Heris, S. Asadi, and B. Mohammadi-Ivatloo, Eds., *Planning and Operation of Multi-Carrier Energy Networks*. Switzerland: Springer, 2021.
[62] M. Nazari-Heris, S. Asadi, and B. Mohammadi-Ivatloo. (2021). *Planning and Operation of Multi-carrier Energy Networks*. Accessed: Oct. 19, 2021. [Online]. Available: https://www.researchgate.net/profile/Morteza-Nazari-Heris/publication/350643036_Planning_and_Operation_of_Multi-Carrier_Energy_Networks/links/60bced10a6fdcc22eae3c2e0/Planning-and-Operation-of-Multi-Carrier-Energy-Networks.pdf
[63] B. Zhao, X. Zhang, J. Chen, C. Wang, and L. Guo, "Operation optimization of standalone microgrids considering lifetime characteristics of battery energy storage system," *IEEE Trans. Sustain. Energy*, vol. 4, no. 4, pp. 934–943, Oct. 2013.
[64] J. Chen, W. Zhang, J. Li, W. Zhang, Y. Liu, B. Zhao, and Y. Zhang, "Optimal sizing for grid-tied microgrids with consideration of joint optimization of planning and operation," *IEEE Trans. Sustain. Energy*, vol. 9, no. 1, pp. 237–248, Jan. 2018.
[65] M. H. Moradi, M. Eskandari, and S. M. Hosseinian, "Operational strategy optimization in an optimal sized smart microgrid," *IEEE Trans. Smart Grid*, vol. 6, no. 3, pp. 1087–1095, May 2015.
[66] L. Guo, W. Liu, J. Cai, B. Hong, and C. Wang, "A two-stage optimal planning and design method for combined cooling, heat and power microgrid system," *Energy Convers. Manage.*, vol. 74, pp. 433–445, Oct. 2013.
[67] *Shah Allah Ditta-Wikipedia*. Accessed: Sep. 30, 2021. [Online]. Available: https://en.wikipedia.org/wiki/Shah_Allah_Ditta
[68] F. A. Mohamed and H. N. Koivo, "Multiobjective optimization using modified game theory for online management of microgrid," *Eur. Trans. Electr. Power*, vol. 21, no. 1, pp. 839–854, Jan. 2011.
[69] G. R. Aghajani, H. A. Shayanfar, and H. Shayeghi, "Demand side management in a smart micro-grid in the presence of renewable generation and demand response," *Energy*, vol. 126, pp. 622–637, May 2017.
[70] K. Qian, C. Zhou, Y. Yuan, X. Shi, and M. Allan, "Analysis of the environmental benefits of distributed generation," in *Proc. 21st IEEE Power Energy Soc. Gen. Meeting-Convers. Del. Elect. Energy*, Jul. 2008, pp. 1–5.
[71] D. Setlhaolo and X. Xia, "Optimal scheduling of household appliances with a battery storage system and coordination," *Energy Buildings*, vol. 94, pp. 61–70, May 2015.
[72] A. Tascikaraoglu, A. R. Boynuegri, and M. Uzunoglu, "A demand side management strategy based on forecasting of residential renewable sources: A smart home system in Turkey," *Energy Buildings*, vol. 80, pp. 309–320, Sep. 2014.
[73] S. L. Arun and M. P. Selvan, "Intelligent residential energy management system for dynamic demand response in smart buildings," *IEEE Syst. J.*, vol. 12, no. 2, pp. 1329–1340, Jun. 2018.
[74] H. Shakouri and A. Kazemi, "Multi-objective cost-load optimization for demand side management of a residential area in smart grids," *Sustain. Cities Soc.*, vol. 32, pp. 171–180, Jul. 2017.
[75] P. Mesarić and S. Krajcar, "Home demand side management integrated with electric vehicles and renewable energy sources," *Energy Buildings*, vol. 108, pp. 1–9, Dec. 2015.
[76] F. Y. Melhem, O. Grunder, Z. Hammoudan, and N. Moubayed, "Energy management in electrical smart grid environment using robust optimization algorithm," *IEEE Trans. Ind. Appl.*, vol. 54, no. 3, pp. 2714–2726, May 2018.
[77] H. Hussain, N. Javaid, S. Iqbal, Q. Hasan, K. Aurangzeb, and M. Alhussein, "An efficient demand side management system with a new optimized home energy management controller in smart grid," *Energies*, vol. 11, no. 1, p. 190, Jan. 2018.

HABIB UR RAHMAN HABIB (Member, IEEE) received the B.Sc. degree in electrical engineering and the M.Sc. degree in electrical power engineering from the University of Engineering and Technology Taxila, Pakistan, in 2009 and 2015, respectively, and the Ph.D. degree from the State Key Laboratory of Advanced Electromagnetic Engineering, School of Electrical and Electronic Engineering, Huazhong University of Science and Technology, Wuhan, China, in 2021.

Since 2009, he has been with the COMSATS Institute of Information Technology, Pakistan, and the Wah Engineering College, University of Wah, Pakistan. He has been a Management Trainee Officer (Maintenance Department) with Dynamic Packaging Pvt. Ltd., Lahore, Pakistan. He is currently with the Department of Electrical Engineering, University of Engineering and Technology Taxila. His research interests include smart grid, energy economics, and control applications in power systems, renewable resources integration, power electronics applications to power systems, and distributed generation. He is a member of many Technical and Professional Committees including IEEE. He has participated in different international conferences including Singapore; China; USA; Pakistan; Dubai, UAE; and Australia. He has been serving as a Reviewer for many journals including IEEE Systems Journal, *International Transactions on Electrical Energy Systems*, IEEE Access, and *International Journal of Power Electronics and Drive Systems*.

ASAD WAQAR received the Electrical Engineering degree from the UET Taxila, in 2002, the master's degree in electrical power engineering from RWTH, Aachen, Germany, in 2011, and the Ph.D. degree in electrical engineering from the Huazhong University of Science and Technology, China, in 2016. After graduation, he worked for different industries for several years. He is currently working as a Professor with the Department of Electrical Engineering, Bahria University, Islamabad, Pakistan. He has successfully supervised more than 30 master thesis students. He is also supervising three Ph.D. students at Bahria University as well. He has published research articles in many reputed international journals. His research interests include smart grids, microgrids operation and control, power quality, power electronics, network reinforcement planning, demand side management, and big data analysis in power systems. He serves as an Active Reviewer for *Applied Energy*, *International Transactions on Electrical Energy Systems*, IEEE Access, *Renewable and Sustainable Energy Reviews*, and *International Journal for Engineering Science and Technology*.

MOHAMED G. HUSSIEN (Member, IEEE) was born in Zefta, Gharbeya, Egypt, in 1988. He received the B.Sc. and M.Sc. degrees in electrical engineering from the Department of Electrical Power and Machines Engineering, Faculty of Engineering, Tanta University, Tanta, Egypt, in 2011 and 2016, respectively, and the Ph.D. degree from the School of Electrical and Electronic Engineering, Huazhong University of Science and Technology, Wuhan, China, in 2020.

He is currently an Assistant Professor with the Department of Electrical Power and Machines Engineering, Faculty of Engineering, Tanta University. He has published scientific papers in both international conferences and high-quality SCI journals. His research interests include electrical machines analysis, electrical drives, electric vehicles, sensorless control, doubly-fed machines, power electronics, and renewable energy systems.

Dr. Hussien is a member of the IEEE-IES Electric Machines Technical Committee and the IEEE-IES Technical Committee on Renewable Energy Systems. His paper has been selected as one of the best papers published in the period (2019–2020) in the IEEE TRANSACTIONS ON ENERGY CONVERSION in the ''Power Generations Systems and Grid Interfaces'' area. He received the Best Paper Award from IEEE IAS. He is serving as an Editorial Board Member for the *Distributed Generation and Alternative Energy Journal* and an Associate Editor for the *IET Renewable Power Generation* journal. He has been serving as a Reviewer for both IEEE conferences and many IEEE journals, including IEEE ACCESS, the IEEE TRANSACTIONS ON INDUSTRIAL ELECTRONICS, and the IEEE TRANSACTIONS ON POWER ELECTRONICS.

ABDUL KHALIQUE JUNEJO (Member, IEEE) was born in Larkana, Sindh, Pakistan, in 1989. He received the bachelor's and master's degrees in electrical engineering from the Quaid-e-Awam UEST Nawabshah, Sindh, in 2011 and 2015, respectively, and the Ph.D. degree from the State Key Laboratory of Advanced Electromagnetic Engineering, School of Electrical and Electronics Engineering, Huazhong University of Science and Technology, Wuhan, China. He is currently employed as an Assistant Professor with the Quaid-e-Awam UEST Nawabshah. His research interests include the sliding mode control, direct torque control (DTC), model predictive control (MPC), sensorless control methods for permanent magnet synchronous machines (PMSM), induction machines (IM), and linear IM and drives. He has served as a Reviewer for IEEE journals, including the IEEE TRANSACTIONS ON INDUSTRIAL ELECTRONICS, the IEEE TRANSACTIONS ON POWER ELECTRONICS, the IEEE TRANSACTIONS ON TRANSPORTATION ELECTRIFICATION, *Assembly Automation*, Article in Journal, (Emerald Group Publishing Ltd.), and the IEEE JOURNAL OF EMERGING AND SELECTED TOPICS IN INDUSTRIAL ELECTRONICS.

MEHDI JAHANGIRI received the Ph.D. degree in mechanical engineering from the Isfahan University of Technology (IUT), Isfahan, Iran, in 2016. He is currently an Assistant Professor of mechanical engineering with Shahrekord Branch, Islamic Azad University, Shahrekord, Iran. He is a Referee in IEEE, Springer, Elsevier, and other international journals. He is the author of several publications on mechanical engineering, including about 130 papers published in scientific journals and conferences. His current research interests include biomechanics and renewable energy. He is the winner of the Shahrekord Branch, Islamic Azad University ''Top Researcher Award'' in 2014 and 2019.

RASOOL M. IMRAN received the B.Sc. degree in electrical engineering from Al-Furat Al-Awsat Technical University, Iraq, in 2011, the M.Tech. degree from the Sam Higginbottom University of Agriculture, Technology and Sciences, India, in 2014, and the Ph.D. degree from the Huazhong University of Science and Technology, China, in 2018. He is currently an Assistant Professor with the School of Artificial Intelligence, Wuchang University of Technology, China. His research interests include microgrid control and stability, management of renewable energy sources, battery management systems, and predictive control of electric vehicles.

YUN-SU KIM (Senior Member, IEEE) received the B.S. and Ph.D. degrees in electrical engineering from Seoul National University, Seoul, South Korea, in 2010 and 2016, respectively.

From 2015 to 2017, he worked as a Senior Researcher with the Korea Electrotechnology Research Institute (KERI). He joined the Faculty of the Gwangju Institute of Science and Technology (GIST), in 2018, where he is currently an Associate Professor with the Graduate School of Energy Convergence. He was the Director of the Korean Society for New and Renewable Energy and the Korean Institute of Electrical Engineers. His research interests include distribution networks, distributed energy resources, microgrid, artificial intelligence, and wireless power transfer.

JUN-HYEOK KIM (Student Member, IEEE) received the B.S. degree in electronic engineering from Handong University, Pohang, South Korea, in 2019. He is currently pursuing the Ph.D. degree with the Graduate School of Energy Convergence, Gwangju Institute of Science and Technology (GIST), Gwangju, South Korea. His research interests include distribution network analysis, distributed energy resources, microgrid control, and artificial intelligence.